

UNIVERSITA' DEGLI STUDI DI PARMA

Dottorato di ricerca in Scienze e Tecnologie
dei Materiali Innovativi

Ciclo XXIV

2009-2011

Self-assembled Networks
via Molecular Recognition

Coordinatore:
Prof. Enrico Dalcanale

Tutor:
Prof. Enrico Dalcanale

Dottorando: Marco Dionisio

Anno 2012

Contents

CHAPTER 1

General Introduction

1.1 Introduction	1
1.2 Molecular Receptor Design	5
1.3 References and Notes	12

CHAPTER 2

Guest-controlled aggregation of cavitand gold nanoparticles and N-methyl pyridinium-terminated PEG

2.1 State of the Art	15
2.1.1 3D Assembly Issue	18
2.2 Introduction	21
2.3 Results and Discussion	22
2.4 Conclusions	33
2.5 Acknowledgments	33
2.6 Experimental Section	34
2.7 References and Notes	38

CHAPTER 3

Polymer – nanoparticles network: assembly kinetics and solvent dependence

3.1 Introduction	42
3.2 Results and Discussion	43
3.2.1 Assembly Dynamics	43
3.2.2 Solvent Effect on Network Formation	50
3.3 Conclusions	54
3.4 Acknowledgments	54
3.5 Experimental Section	55
3.6 References and Notes	56

CHAPTER 4

Cavitand-functionalized SWCNTs for N-methylammonium of molecular recognition salts sensing in water

4.1 State of the Art	58
4.2 Introduction	65
4.3 Results and Discussion	66
4.4 Conclusions	74
4.5 Acknowledgments	74
4.6 Experimental Section	75
4.7 References and Notes	81

CHAPTER 5

Polymer blending as macroscopic expression

5.1 State of the Art	85
5.2 Results and Discussion	96
5.2.1 Design, synthesis, characterization of monomers and Copolymers	96
5.2.2 Complexation properties of copolymer in solution	103
5.2.3 DSC analysis	104
5.2.4 Solid state mixing	107
5.2.4.1 Control Experiments	108
5.2.5 Host-guest polymers as interphase compatibilizers	109
5.3 Reversible supramolecular cross-linking via molecular recognition	113
5.4 Conclusions	121
5.5 Acknowledgments	121
5.6 Experimental Section	122
5.7 References and Notes	131

APPENDIX A

Materials and Methods	134
-----------------------	-----

The Author	139
-------------------	-----

1.1 Introduction.

Over the last 150 years, molecular chemistry has developed a large set of tools for making or breaking covalent bonds between atoms in a controlled and precise fashion and has implemented them for constructing sophisticated molecules and materials.

Supramolecular chemistry aims the development of highly complex chemical systems, mastering the interactions among molecular components.¹ Such interactions are non-covalent forces, namely electrostatic and van der Waals forces or hydrophobic effects, π - π stacking interactions, metal coordination, hydrogen bonding and host-guest interactions.²

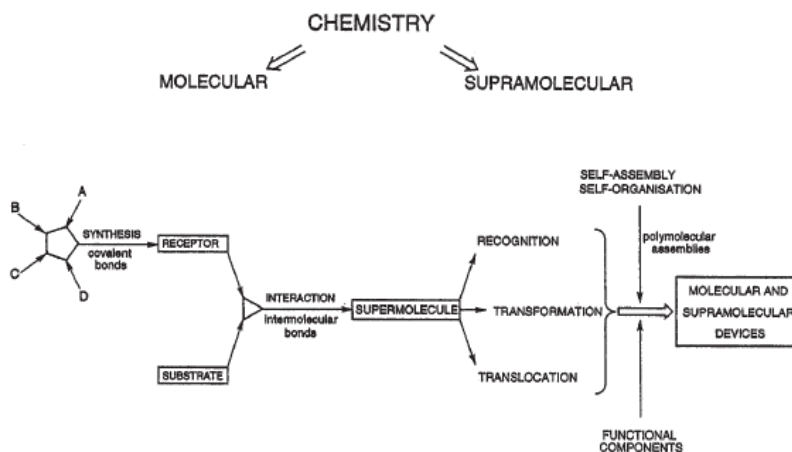


Figure 1.1 From molecular to supramolecular chemistry: molecules, supermolecules, molecular and supramolecular devices (Reproduced from Lehn, J.M., *Rep. Prog. Phys.*, 2004, 67, 249-265).

Being the connection between the constituents reversible, the supramolecular objects are by nature reversible, that means they can undergo assembly/disassembly/exchange processes, because they are formed under thermodynamic conditions, so trial-and-error corrections are essential.¹ They are constitutionally dynamic materials (CDMs),³ in principle able to select their constituents in response to external stimuli or environmental factors, behaving as adaptive materials.

Supramolecular architectures are build up by self-assembly process, molecular recognition or self organization. In any case the result is the formation of ordered assemblies from disordered mixtures of molecules. Thus, self-assembly is scientifically interesting and technologically important for several reasons a) it is well established and used by Nature; b) it provides routes to a range of material with regular structures; c) it seems to offer one of the most general strategies now available for generating nanostructures.⁴

Supramolecular chemistry has a strong impact on material science⁵ via the manipulation of the non-covalent forces that hold the constituents together, leading up to the design of smart, functional supramolecular materials and the precise control of their build up and of their properties.

Indeed, the introduction of specific groups enhances active functions such as the recognition of guests or to switch surface properties.⁵

Among all, the most attractive materials are those where the assembly/disassembly processes are coupled with switching protocols that allow reversible control over the building processes.⁵

In this regard particularly interesting is the example reported by Kaifer and coworkers.⁶ They assembled a network using fullerenes as small noncovalent linking units to bridge γ -cyclodextrines (γ -CDs) capped gold nanoparticles in a three dimensional fashion and create large assemblies of hybrid nanoparticles with diameter of about 300 nm (Figure 1.2). The motivation was the induction of aggregation by supramolecular recognition to create nanoparticles assemblies for electronic circuit components with extraordinarily high degree of integration.

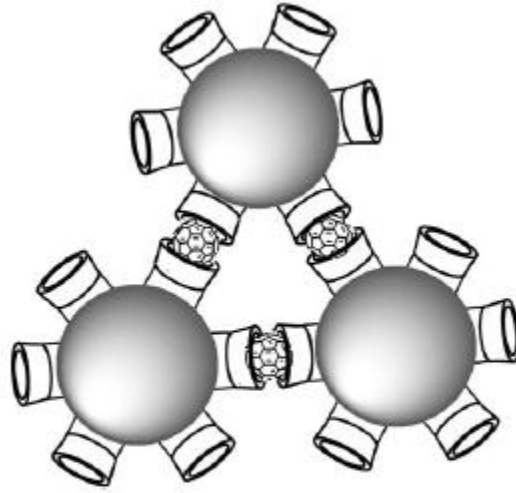


Figure 1.2 Fullerene induced aggregation of CD-capped AuNPs.

In the 2005 Reinhoudt *et al.* demonstrated how the concept of multivalency can play an important role in the harnessing of “smart” materials (Figure 1.3).⁷ They prepared a complex structure using a layer-by-layer techniques. They took an advantage from the strong cyclodextrin-adamantane interactions: CDs decorated gold nanoparticles were connected with 5th generation dendrimers ended with adamantyl moieties. Using this approach, a well-defined multilayer thin films up to 18 nanometer-thick were created in a controlled manner.

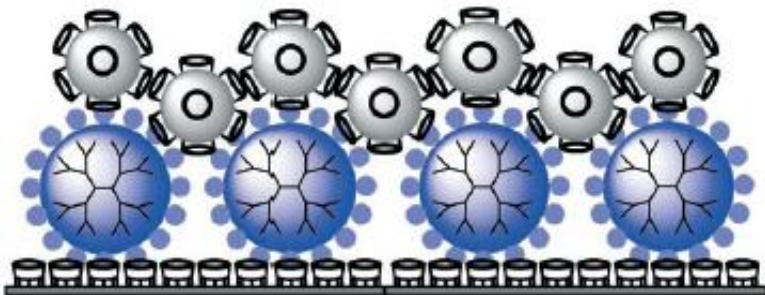


Figure 1.3 Layer by layer assembly of adamantyl-terminated dendrimers and AuNPs functionalized with cyclodextrines.

The preparation of polymers, in particular supramolecular polymers, is an important field in which self assembly is very attractive. Supramolecular polymers are polymers based on monomeric units held together with directional and reversible secondary interactions.⁸

The high directionality of the bonds and their reversibility are very appealing to solve technical and practical problems, since their unique mechanical, electronic, biological and self-healing properties.⁹

The field was started by Meijer in 1997 when he exploited the use of self-complementary DDAA (donor-donor-acceptor-acceptor) array of four hydrogen bonds of 2-ureido-4-pyrimidone derivatives to realize supramolecular polymers, featuring great stability at elevated temperatures and under high levels of strain.¹⁰

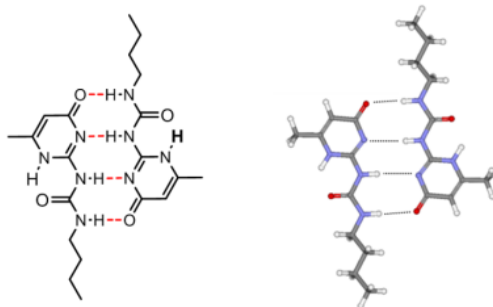


Figure 1.4 Homodimer of ureido-pyrimidone units.

From the previous examples, it appears clear that the properties of material depend both on the nature of its constituents and on the interactions between them, thus supramolecular chemistry is a powerful strategy to impart and tune new active functions.

Following this principle, in this thesis we will harness new architectures by mean of self-assembly.

1.2 Molecular Receptor Design.

In the late 1960s, Pedersen, Lehn, Cram and others published the synthesis of macrocyclic molecules that are able to selective binds ions or small organic molecules via non covalent interactions.¹¹ Although the synthesis of these molecular receptors involve the formation of covalent bonds, the objective of the synthesis is the specific recognition function that these receptors display.

In particular, in this thesis we will deal with a specific class of receptors, namely tetraphosphonate cavitands.

A cavitand is defined as synthetic organic compounds with enforced cavities large enough to complex complementary organic molecules or ions.¹² Usually, they are based on resorcin[4]arene (Figure 1.5).

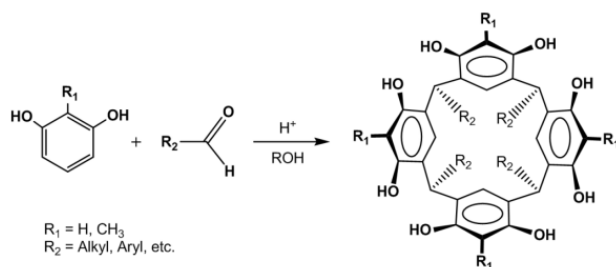


Figure 1.5 Resorcin[4]arene synthesis.

They are prepared by acid catalyzed condensation of an aldehyde with resorcinol.¹³ Choosing the right aldehyde allows to install further functional groups at the lower rim that increase the versatility of the scaffold.

However, the flexibility of the resorcin[4]arene is too high for direct use in host-guest chemistry. Thus, binding the phenolic oxygen with suitable group lead to a rigid cavity, improving complexation capability. Among the possible bridging group available, phosphonates impart special complexation properties toward alcohols,¹⁴ alkaline-earth ions¹⁵ and N-methyl ammonium species, rather than N-methyl pyridinium moieties.¹⁶

The main specific interactions responsible for recognition processes are H-bonding, CH- π , and cation-dipole forces.¹⁷ Namely, a multiple ion-

dipole interaction occurs between the inward facing P=O groups and the positively charged guest moieties; directional H-bonding involve two adjacent P=O groups in presence of H-donor species; CH- π interaction acts between guest acidic protons (e.g. CH₃ group in N-methylpyridinium salts) and the π -basic cavity (Figure 1.6). All these forces operate in a synergistic fashion, assuring high association constant¹⁷ of the complex formation (for example, in the order of 10⁵ M⁻¹ in methanol for N-methylpyridinium guests).

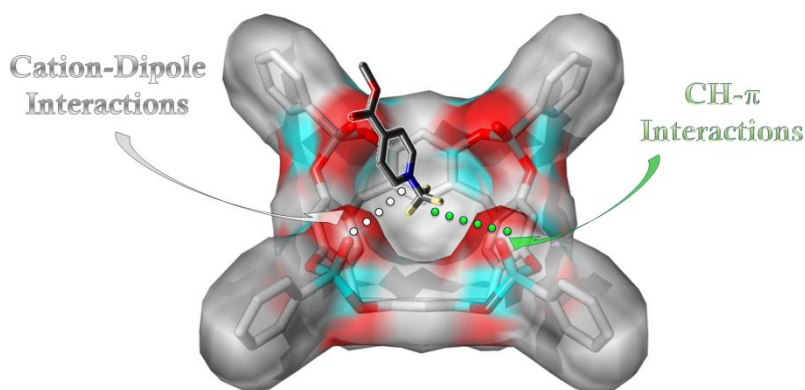


Figure 1.6 *Main interactions responsible for N-methylpyridinium – Tetraphosphonate cavitand complex.*

The higher binding has been observed for the isomer featuring four P=O groups converging toward the center of the cavity. It is clear that stereochemistry is pivotal to determine the cavitand complexing capability, requiring a synthetic route leading to the desired stereoisomer.

The presence of four stereogenic centers in the tetraphosphonate cavitands gives rise to six possible diastereoisomers, differing each from the other for the orientation of the P=O moieties, inward (i) or outward (o) the cavity (for complete nomenclature see ref. 18).

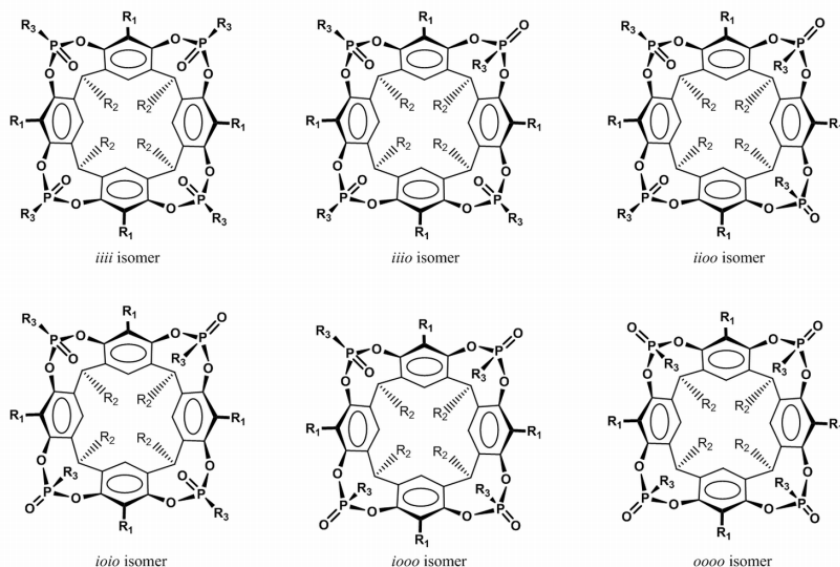
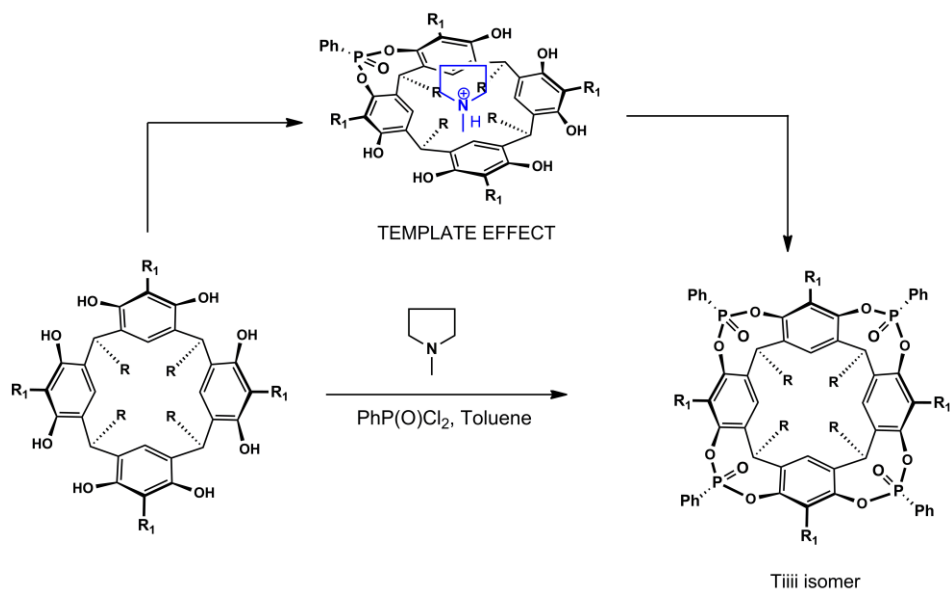


Figure 1.7 Tetraphosphonate cavitand isomers.

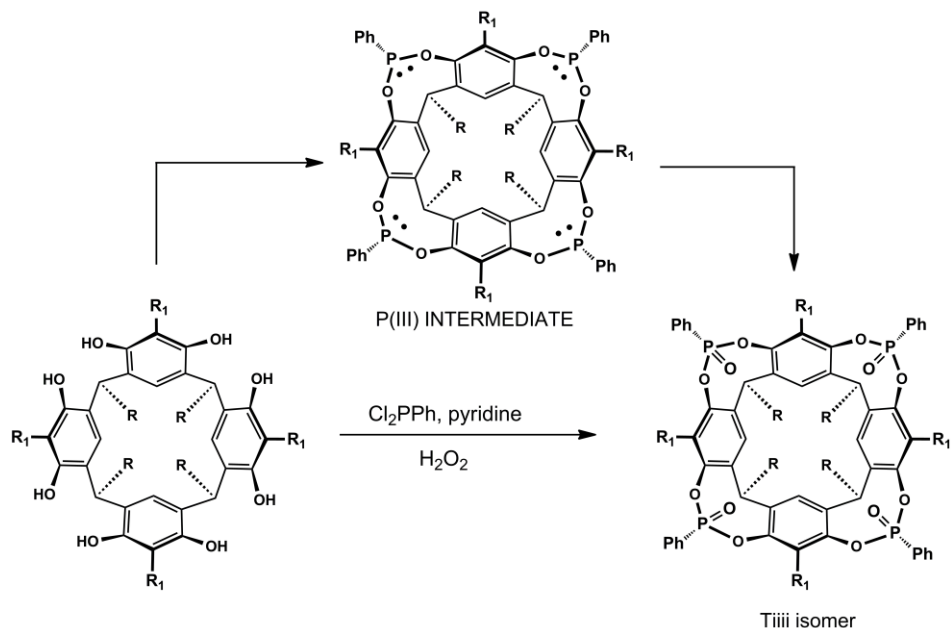
In the 1995, Dutasta *et al.* reported on the synthesis of the T_{iiii} stereoisomer (Scheme 1.1).¹⁹ He nicely showed that carrying out the reaction in toluene with dichlorophenyl phosphine oxide, in presence of N-methylpyrrolidine, led to the formation of desired isomer as major product. This was attributed to the template effect exerted by the base, which is hosted in the forming cavity affecting the outcome of the reaction.

However, this intriguing route suffers of three main drawbacks: i) it is highly dependent on the reaction conditions; ii) the use of less reactive P(V) reagents led to low yield of the desired isomer and iii) also the T_{iiio} is formed, albeit in a low amount.



Scheme 1.1 Tiii isomer synthesis via template effect.

In the 2008, Dalcanale *et al.* reported on the stereoselective synthesis of the Tiii cavitand (Scheme 1.2).²⁰ A resorcin[4]arene is bridged, in pyridine, with a P(III) reagent. The intermediate of the reaction is not isolated, but oxidized *in situ* by hydrogen peroxide. The outcome of the one-pot two steps reaction is the desired product in high yield (up to 90%). The stereoselectivity of the reaction is related to the formation of an intermediate based on P(III), where all the electrons lone pairs point inside the cavity.²¹



Scheme 1.2 *Tiii isomer synthesis via P(III) intermediate.*

The versatility of these molecular receptors has been well established.

Earlier, the interactions of tetraphosphonate cavitand and alcohols were fully explored leading to the construction of a vapor sensing device based on quartz micro balance (QCM).²² The system is based on a Mi isomer, facing inward the cavity, interact with short linear alcohols by CH- π interaction and hydrogen bonding. This approach was further improved moving from mass detection system to fluorescence.²³ A cavitand containing only one PO pointing inside the cavity, bearing a fluorescent probe, is sufficient for the detection of a short linear alcohols with fast response.

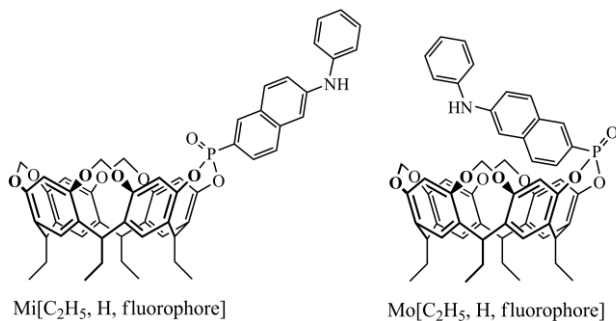


Figure 1.8 Monophosphonate cavitand for fluorescence sensors.

Moreover, the use of tetraphosphonate cavitands were exploited in the hierarchical self-assembly of smart material on silicon surface.²⁴

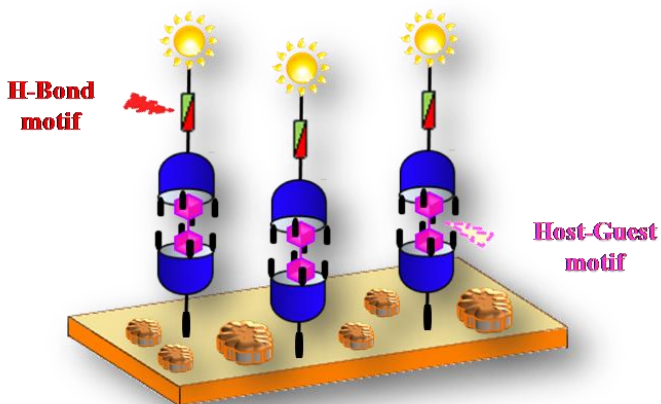


Figure 1.8 Sketch of hierarchical self-assembly on silicon mediated by tetraphosphonate cavitand.

Studies in solution showed the ease of supramolecular polymer formation by self-assembly of tetraphosphonate cavitand based monomers.²⁰

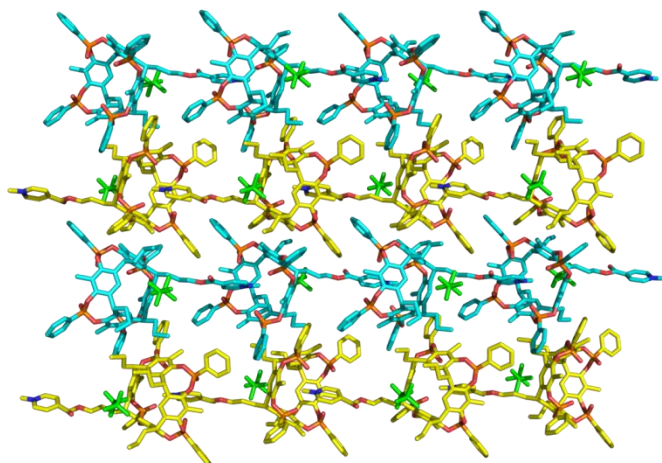


Figure 1.9 *X-ray structure of supramolecular homopolymer based on tetraphosphonate cavitand.*

In this thesis we try to expand the use of tetraphosphonate cavitands to mediate the aggregation of gold nanoparticles and polymer in solution, to functionalize single walled carbon nanotubes (SWCNTs), and to obtain polymer blending as macroscopic expression of molecular recognition in the solid state.

1.3 References and Notes.

- 1 Lehn, J.M. *Rep. Prog. Phys.* **2004**, 67, 249-265.
- 2 Reinhoudt, D.N.; Crego-Calama, M. *Science* **2002**, 295, 2403-2407.
- 3 Lehn, J.M. *Chem. Eur. J.* **2000**, 6, 2097-2102.
- 4 Whitesides, G.M.; Boncheva, M. *Proc. Natl. Acad. Sci. U.S.A.* **2002**, 99, 4796-4774.
- 5 Martinez-Manez, R.; Sancenon, F.; Hoffmann, K.; Rurack, K.; Descalzo, A.B. *Angew. Chem. Int. Ed.* **2006**, 45, 5924-5948.
- 6 Liu, J.; Alvarez, J.; Ong, W.; Kaifer A.E. *Nano Lett.* **2001**, 1, 57-60.
- 7 Crespo-Biel, O.; Dordi, B.; Reinhoudt, D.N.; Huskens, J. *J. Am. Chem. Soc.* **2005**, 127, 7594-7600.
- 8 Brunseveld, L.; Folmer, B.J.B.; Meijer, E.W.; Sijbesma, R.P. *Chem. Rev.* **2001**, 101, 4071-4097.
- 9 *Supramolecular Polymer Chemistry* Edt. Harada A., Wiley-VCH, **2011**.
- 10 Sijbesma R. P., Beijer F. H., Brunsveld L., Folmer B. J. B., Hirschberg J. H. K. K., Lange R. F. M., Lowe J. K. L., Meijer E. W. *Science* **1997**, 278, 1601-1604.
- 11 *Encyclopedia of Supramolecular Chemistry*, Vols. 1,2; Ed.: J.L. Atwood, J.W. Steed, Taylor & Francis Group, New York, 2004, 2005.
- 12 *Container Molecules and Their Guests* (Ed.: J. F. Stoddart), D.J. Cram, J.M. Cram, The Royal Society of Chemistry, Cambridge, **1994**.
- 13 Tunstad L. M., Tucker J. A., Dalcanale E., Weiser J., Bryant J. A., Sherman J. C., Helgeson R. C., Knobler C. B., Cram D. J. *J. Org. Chem.* **1989**, 54,1305-1312.
- 14 Pirondini, L.; Dalcanle, E. *Chem. Soc. Rev.* 2007, 36, 695-706
- 15 Delangle P., Mulatier J.-C., Tinant B., Declercq J.-P., Dutasta J.-P. *Eur. J. Org. Chem.* **2001**, 3695-3704; (b) Dutasta J.-P. *Top. Curr. Chem.* **2004**, 232, 55-91
- 16 Biavardi, E.; Favazza, M.; Motta, A.; Fragalà, I.L.; Massera, C., Prodi, L.; Montalti, M.; Melegari, M.; Condorelli, G.C.; Dalcanale, E. *J. Am. Chem. Soc.* **2009**, 131, 7447-7455.
- 17 Menozzi D., Biavardi E., Massera C., Schmidtchen F.-P., Cornia A., Dalcanale E. *Supramol. Chem.* **2010**, 22, 768.

- 18 Pinalli, R.; Suman, M.; Dalcanale E. *Eur. J. Org. Chem.* **2004**, 3, 451-462.
- 19 Delangle P., Dutasta J.P., *Tetrahedron Lett.* **1995**, 36, 9325-9328.
- 20 R. M. Yebeutchou, F. Tancini, N. Demitri, S. Geremia, R. Mendichi, E. Dalcanale *Angew. Chem., Int. Ed.* **2008**, 47, 4504-4508.
- 21 Xu, W.; Rourke, J. P.; Puddephatt, R. J. R. *J. Chem. Soc., Chem. Commun.* **1993**, 145-147.
- 22 Pinalli, R.; Nachtigall, F.F.; Uguzzoli, F.; Dalcanale, E. *Angew. Chem. Int. Ed.* **1999**, 38, 2377-2380.
- 23 Maffei, F.; Betti, P.; Genovese, D.; Montalti, M.; Prodi, L.; De Zorzi, R.; Geremia, s.; Dalcanale, E. *Angew. Chem. Int. Ed.* **2001**, 50, 4654-4657.
- 24 Tancini, F.; Genovese, D.; Montalti, M.; Cristofolini, L.; Nasi, L.; Prodi, L.; Dalcanale, E. *J. Am. Chem. Soc.* **2010**, 132, 4781-4789.

Guest controlled aggregation of cavitand gold nanoparticles and *N*-methylpyridinium-terminated PEG[§]

2

2.1 State of the Art.

Colloids or nanoparticles are giant metal clusters with dimensions range from 2 to 100 nm, with precise geometries resulting from the packing of the atoms.¹ Among all, gold nanoparticles (AuNPs) are the most stable and they present size-related properties, thus they are involved in material sciences, catalysis and biology.²

The physical properties of AuNPs are neither those of bulk metal, nor those of molecular compounds, but they are strongly size-dependent, subjected to quantum-mechanical rules, namely *quantum size effects*.³ One of these is the so-called plasmon band resonance (PBR). Freely mobile electrons are very close to the surface and show a characteristic collective oscillation frequency in the visible region (for AuNPs of 5-20 nm a band at 530 nm is observed). Interestingly, PBR is affected by the size of the particles and by the surrounding.⁴

[§] Part of the work described in this chapter has been published: for the PEG-AuNPs network see Dionisio, M.; Maffei, F.; Rampazzo, E.; Prodi, L.; Pucci, A.; Ruggeri, G.; Dalcanale E. *Chem. Commun.* **2011**, 47, 6596 – 6598; for the alternative use of cavitand **Ti_{iii}[disulfide,CH₃,Ph]** in sensing see Dionisio, M.; Oliviero, G.; Menozzi, D.; Federici, S.; Yebeutchou, R.M.; Schmidtchen, F.P.; Dalcanale, E.; Bergese P. *J. Am. Chem. Soc.*, **2012**, 134, in press.

Although very attractive, gold nanoparticles are only kinetically stable, that means once they are formed, they tend to aggregate and precipitate, losing the optical properties.⁵

In order to overcome this problem they are capped with suitable protecting groups. In 1994 Brust and Schiffrin reported, for the first time, the facile synthesis of thermally and air stable AuNPs of reduced dispersity and controlled size.⁶ A suitable gold precursor (i.e. tetrachloroauric acid, HAuCl_4) is transferred to toluene using tetraoctylammonium bromide as a phase transfer agent and reduced by NaBH_4 in the presence of dodecanethiol (Figure 2.1).

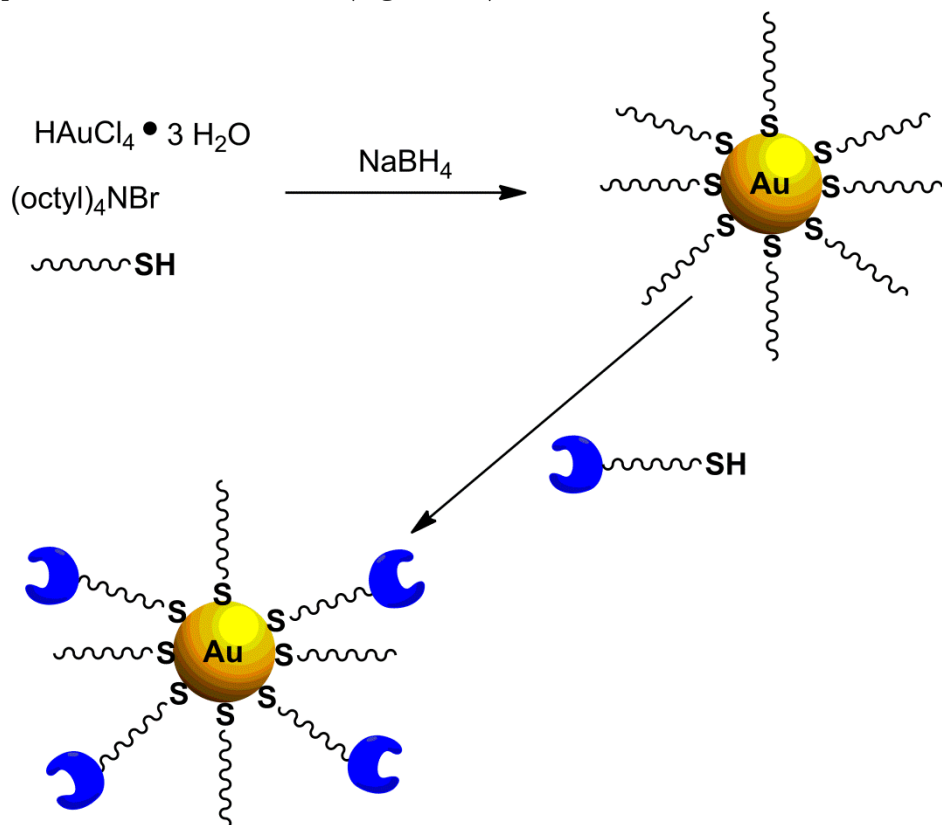


Figure 2.2 Brust-Schiffrinn method for AuNPs synthesis and subsequent modification strategy.

Interestingly, varying the thiol/gold mole ratios it is possible to modify the size of the AuNPs, instead faster addition of reductant give rise to smaller and more monodisperse particles.

The Brust-Schiffrin method is generally considered the best synthetic route because the formed AuNPs can be repeatedly isolated and redissolved in common organic solvent without irreversible aggregation or decomposition; then, they can be easily handled and functionalized just as stable organic and molecular components. Indeed, it is possible to displace, totally or partially, the dodecanthiol protecting group with other ligands in a S_N2 fashion, by the so-called place exchange reaction.⁷

Nanoparticles can simultaneously provide scaffolds for devices and serve as building blocks for the creation of extended two-three dimensional systems.⁸

The former is based on the ability of functionalized nanoparticles to show strong optical change upon guest-induced aggregation processes.⁹ When the interparticle-distance is modified, a shift of the PBR is recorded. The color change, based on analyte-induced aggregation/deaggregation protocols, has been used for the colorimetric sensing of ions (Figure 2.2).

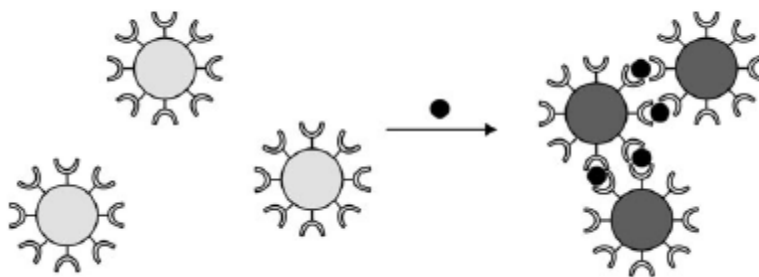


Figure 1.2 AuNPs aggregation upon guest addition.

Functionalization of gold nanoparticles with metalloporphyrins allows the recognition of Cl^- and $H_2PO_4^-$ anion with high association constant,¹⁰ whereas the modification with calix[4]arene selective recognizes cationic

pyridinium moieties.¹¹ In both cases a strong red shift of PRB was observed, and the increase of the association constant is due to the preorganization induced by the organic scaffolds.

2.1.1 The 3D Assembly Issue.

Highly structured, three dimensions nanocomposite have unique magnetic, electronic and optical properties providing new systems for the creation of device and sensors.¹² However, facile control over the spatial distribution of nanoscopic building blocks, such as nanoparticles, from nanoscopic to macroscopic length scales, has been a major impediment in the “bottom-up” fabrication of functional materials.¹³

One way to reach this hard goal is using complementary recognition units as driving force for the assembly, in the so called “bricks and mortar method”; which is functionalized AuNPs (bricks) self-assembled in and with modified polymers, dendrimers etc. (mortars).¹⁴

For example, Rotello *et al.* reported on the formation of complex 3D networks.¹⁵ They employed diaminotriazine-thymine three point hydrogen-bonding interactions to obtain H-bond complementarity between thymine tailored AuNPs and diaminotriazine-functionalized polystyrene. (Figure 2.3).

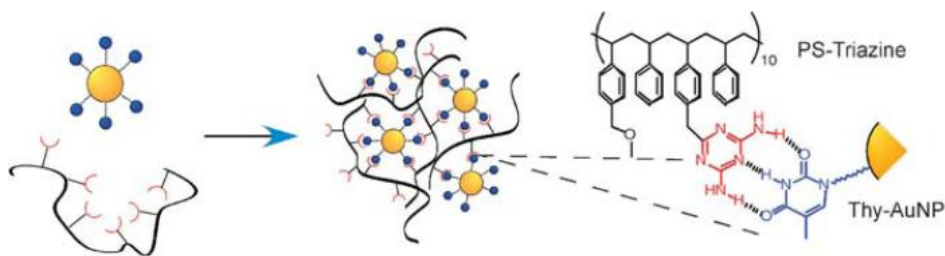


Figure 2.2 Hydrogen-bonding mediates network formation between thymine-AuNPs and diamine-triazine polystyrene.

A black solid was formed immediately after addition of functionalized polystyrene to gold nanoparticles solution. Highly regular structures were formed, of about 100 nm, as a consequence of the specific hydrogen-bonding interactions. At 10 °C, larger aggregates were obtained, forming interconnected networks, and at -20 °C discrete giant spheres were observed, measuring 0.5–1 μm in diameter. The system was further improved by using a diblock copolymer.¹⁶ In fact, the use of recognition functionalized diblock copolymer provided not only the formation of nanometer aggregates, but also precise control of the interparticle distance of AuNP aggregates by changing the length of the diblock copolymer.

Reinhoudt and coworkers explored the possibility of creating complex 3D structures using cyclodextrins (CDs) decorated AuNPs and different kind of adamantane terminated guests.¹⁷ They found that if the degree of favorable host-guest interactions, as in the case of CD-AuNPs and the adamantane modified dendrimer, is too high, precipitation of the network occurred. In the case of shorter linker the nanostructure is partly achieved, because the probability of docking two sites of the same nanoparticles increases, resulting in more soluble structures (Figure 2.4).

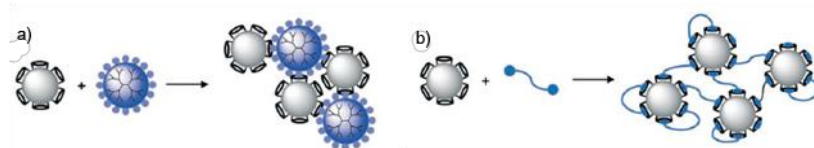


Figure 2.3 Different aggregation mode of CD-AuNPs with a) adamantyl-containing dendrimer; b) adamantyl-containing linear guest.

The Rotello group demonstrated that the interparticle distance can be modulated by varying the length of the spacer, for example varying the generation of the dendrimer employed.¹⁸ Salt bridge formation between poly(amidoamine) (PAMAM) dendrimers of different dimensions and carboxylic acid functionalized AuNPs provides thin films of AuNPs spaced by PAMAM dendrimers, controlling the interparticles distance. Indeed, PBR showed a steady state shift as the AuNPs were assembled with dendrimer G0 through G4 (0th generation to 4th), demonstrating the use of self-assembly to tune plasmonic properties (Figure 2.5).

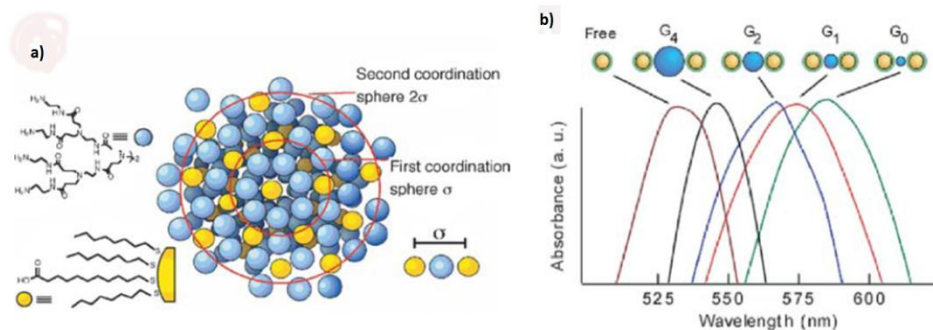


Figure 2.5 a) AuNPs assembly using PAMAM dendrimers; b) PBR changes of AuNPs-PAMAM dendrimers networks from 0th generation to 4th generation.

In this chapter, we describe the aggregation/disaggregation of gold nanoparticles and polyethylene glycol (PEG), driven by complementary host-guest interactions between tetraphosphonate cavitand and *N*-methylpyridinium terminated PEG polymer.

In the following chapter 3, we report the kinetics of PEG-AuNPs network formation as function of temperature and solvent.

2.2 Introduction.

Novel chemical strategies to control the assembly of nanoparticles with polymers are of great interest because they allow the manipulation of the derived hybrid materials and fine-tune their properties.¹⁹ Self-assembly based on selective host-guest interactions provides a powerful tool for the control of structured systems at the molecular level.⁹ The host toolkit used so far in nanoparticle aggregation include mainly cyclodextrins²⁰ and calixarenes.^{11,21} Their guests counterparts are either small molecules or dendrimers.^{3,22} However, very few cases of complementary polymeric guests are described.^{15,8}

Herein we report a guest-controlled aggregation of nanoparticles bearing disulfide functionalized tetraphosphonate cavitand **Tiiii[disulfide,CH₃,Ph]**,²³ using methylpyridinium-terminated **PEG 1** (Chart 2.1) as noncovalent molecular linker between the nanoparticles. Tetraphosphonate cavitands present outstanding molecular recognition properties toward charged N-methylpyridinium guests both in the solid state²⁴ and in solution.²⁵ The large *K_{ass}* values measured for the Tiiii N-methylpyridinium complexes,²⁶ was the starting point to exploit their complexation properties in gold nanoparticle-polymer networking. The introduction of four lipoic acid units at the lower rim of these cavitands allows the functionalization of gold nanoparticles with a stability comparable to thiols.²⁷

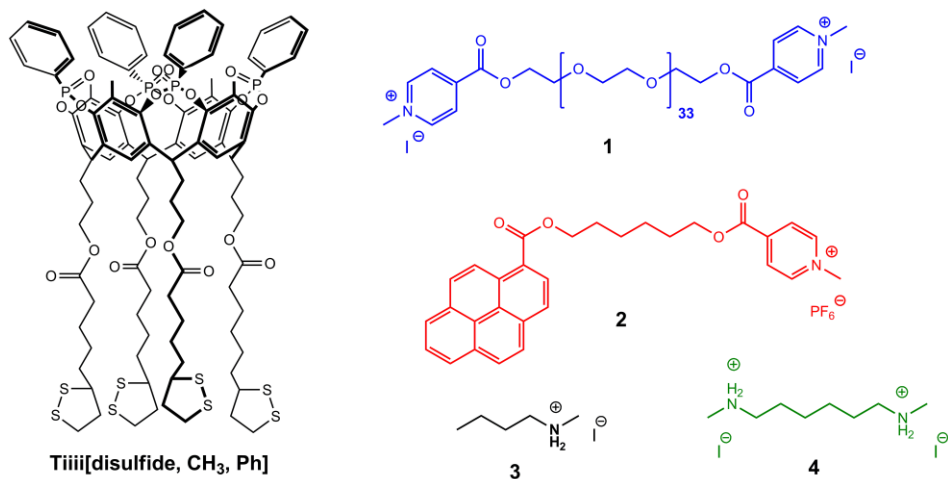
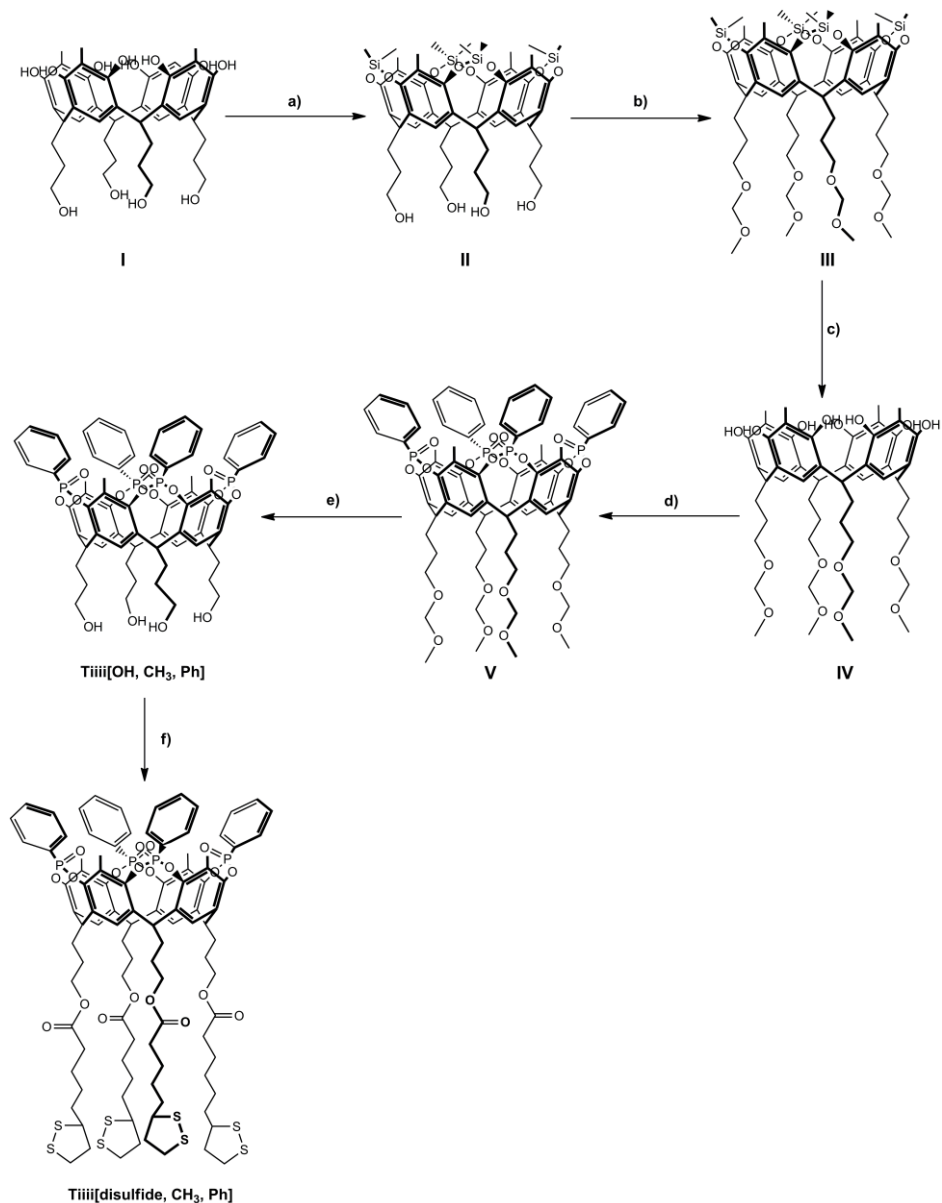


Chart 2.1. Synthesized molecules.

2.3 Results and Discussion

The target cavitand **Tiii[disulfide,CH₃,Ph]**, from now onward referred to as **Tiii** (Scheme 2.1), was prepared in seven steps starting from tetrahydroxy footed resorcinarene.²⁸ The key steps of the synthesis were the stereospecific introduction of four inward phosphonate bridges at the upper rim of the resorcinarene^{25a} and the insertion of the disulfide moieties by adding four equivalents of lipoic acid to a dichloromethane solution of the tetrahydroxy-footed **Tiii** cavitand under Steglich conditions (Scheme 2.1).²⁹



Scheme 2.1. Synthesis of **Tiii[disulfide, CH₃, Ph]**: (a) $\text{Si}(\text{CH}_3)_2\text{Cl}_2$, *Py*, 55 °C 12 h, 85%; (b) *MomCl*, *DIPEA*, *DMF*, 50 °C, 24h, 85%; (c) *HFAq* 36%, *DMF*, O.N., quantitative; (d) 1) PhPCl_2 , *Py*, 70 °C, 3h; 2) $\text{H}_2\text{O}_2/\text{CHCl}_3$ 1:1, 30min 87% (over two steps); (e) *MeOH/CHCl}_3*, HCl_{aq} 36%, 50 °C, O.N.; (f) *Lipoic acid*, *DCC/DMAP*, *DCM*, 40 °C, O.N., 20%.

Dodecanthiol-stabilized gold nanoparticles (**DT-AuNPs**) were synthesized via the *Brust* method,⁶ followed by extensive purification via soxhlet extraction with acetone.³⁰ The average diameter of **DT-AuNPs** was estimated to be 8 nm by DLS analysis (Figure 2.6) with a 6 nm diameter gold nucleus (TEM analysis, Figure 2.7).

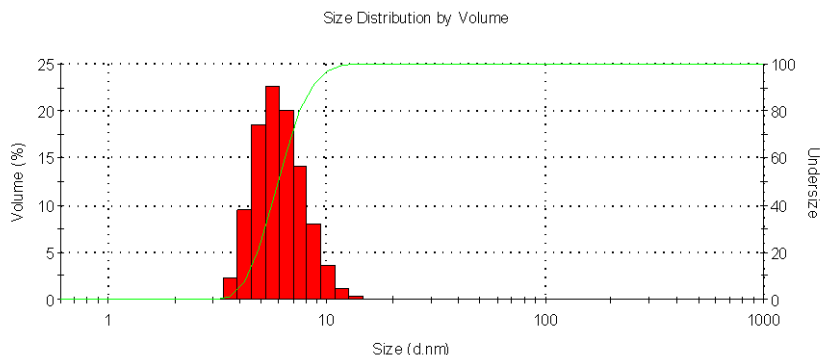


Figure 2.6 Size volume distribution of dodecanthiol coated Au nanoparticles, $d_H = (8 \pm 1)$ nm, (chloroform, 20°C).

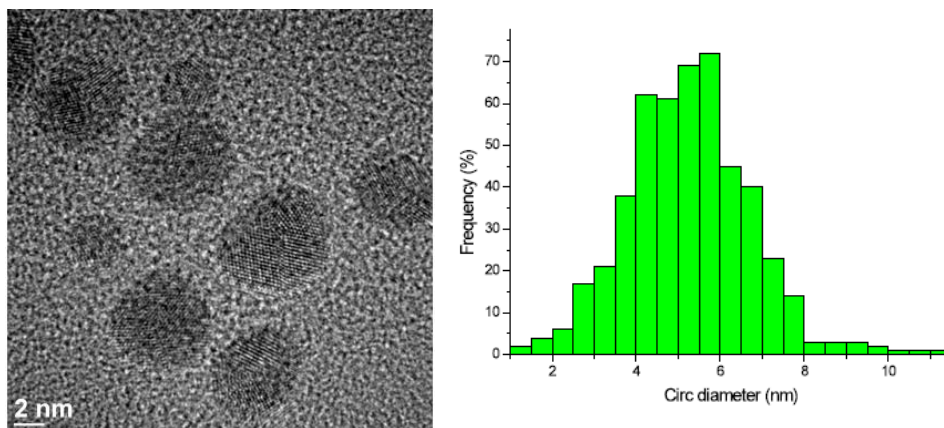
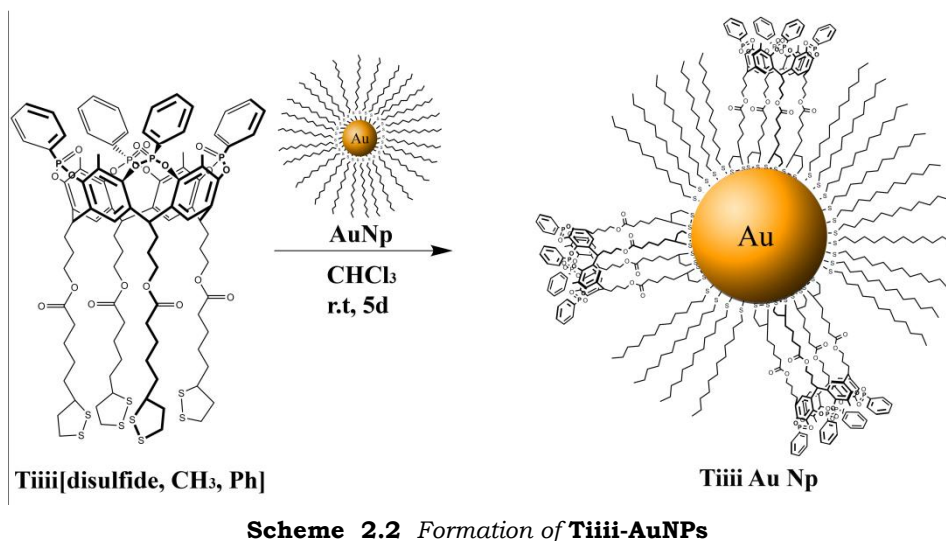


Figure 2.7 HR TEM image of the dodecanthiol AuNPs.

Tiii-AuNPs were obtained by ligand substitution, adding **Tiii** to a chloroform solution of AuNPs and stirring for 5 days (Scheme 2.2).¹⁰



The insertion of **Tiii** in the monolayer was confirmed by ^1H and ^{31}P NMR (Figure 2.8). As expected, the ^1H NMR spectra of **Tiii-AuNPs** is broadened relative to the free ligand **1**.³¹

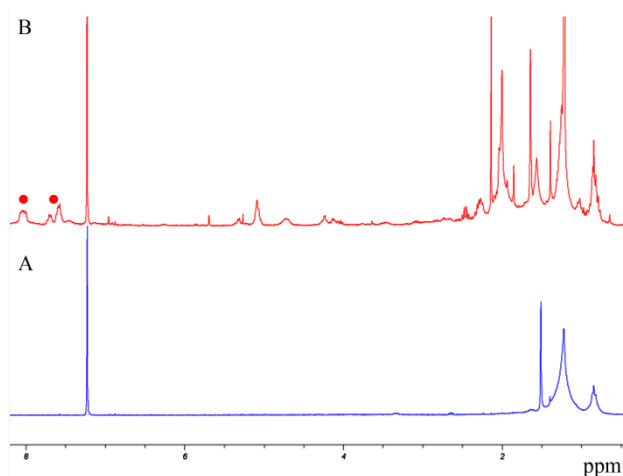


Figure 2.8 A) ^1H -NMR of dodecanthiol-stabilized AuNPs in CDCl_3 ; B) ^1H -NMR of **Tiii-AuNPs** in CDCl_3 (• diagnostic cavitand signals).

Particularly diagnostic is the ^{31}P NMR spectrum, showing the typical peak of the four equivalent P=O groups at 8.59 ppm (Figure 2.9).

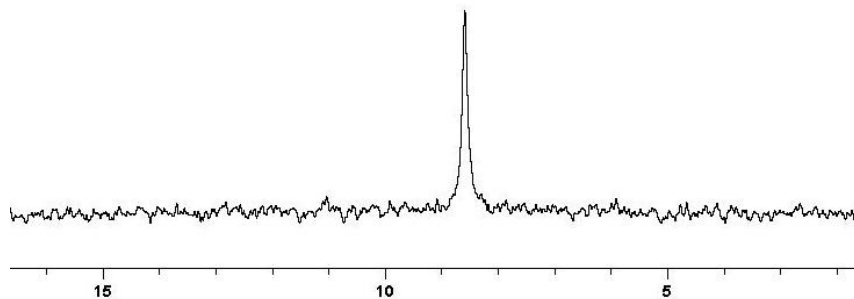


Figure 2.9 ^{31}P NMR of **Tiii-AuNPs** in CDCl_3

The red-shift of the plasmon resonance band (PRB) of about 10 nm confirmed the exchange on the gold nanoparticle (Figure 2.10).

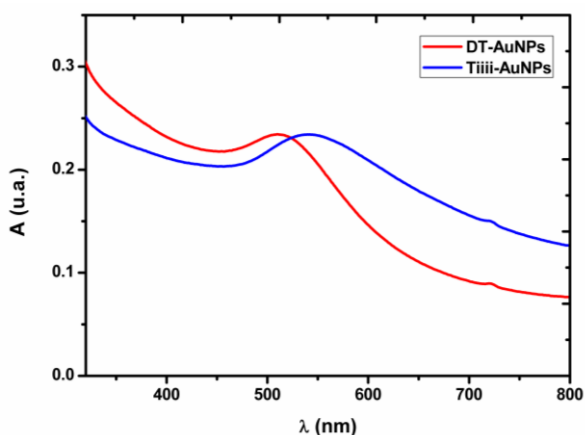
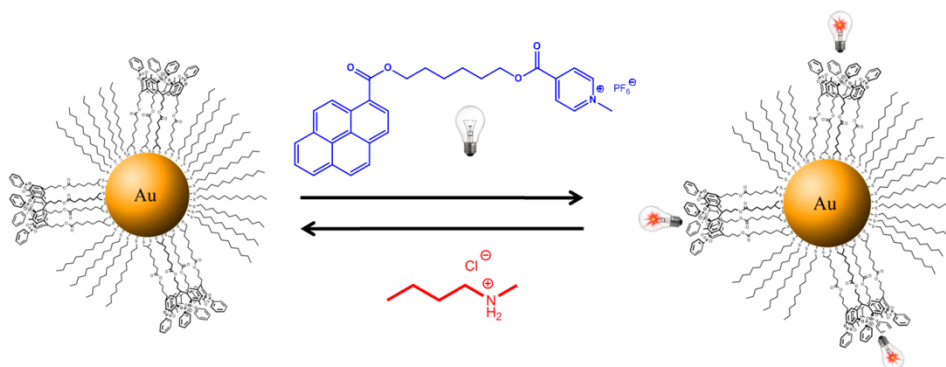


Figure 2.10 Plasmon Band Resonance shift of Dodecanthiol AuNPs (red line); **Tiii-AuNPs** (blue line).

The amount of **Tiii** receptors grafted onto the nanoparticles surface was estimated to be about 3% (w/w) of nanoparticle weight by fluorescent spectroscopy. A dichloromethane solution of the fluorescent pyrene-derivatized guest **2** was titrated with **Tiii-AuNPs** monitoring the variation of the intensity in the emission spectra (Scheme 2.3).



Scheme 2.3 Reversible fluorescent complex formation.

As expected, as the amount of the host increased, an enhancement of the fluorescence was observed, since the inclusion of the pyridinium inside the cavity decreases the efficiency of the electron-transfer process that quenches the fluorescence of the pyrene (Figure 2.11).^{26b} It is noteworthy that, in contrast to what typically happens when pyrene derivatives are directly bound to AuNPs, no quenching nor spectral shifts were observed.³²

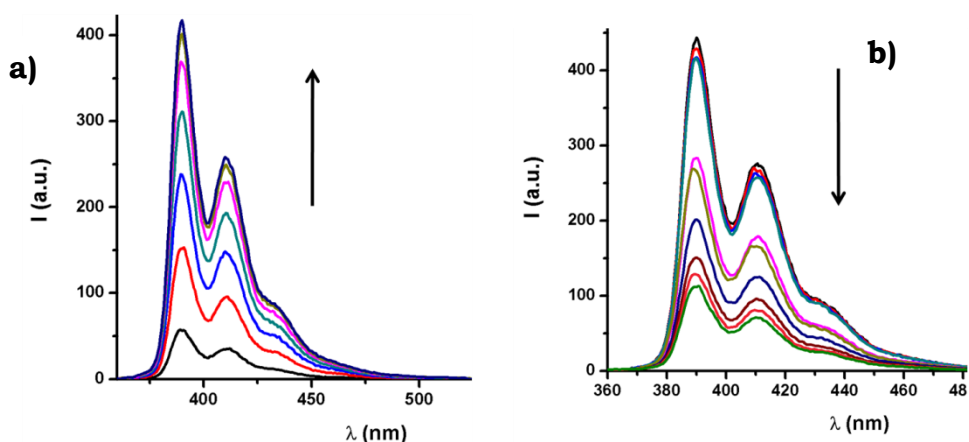


Figure 3.11 a) Fluorescent titration ($\lambda_{exc} = 345 \text{ nm}$) of a CH_2Cl_2 solution of **2** with Tiii-AuNPs; b) Fluorescence titration ($\lambda_{exc} = 345 \text{ nm}$) of a CH_2Cl_2 solution of Tiii-AuNPs•**2** with competitive guest **3** (0 – 1.3 eq).

This method provides an innovative way to evaluate the composition of the ligand shell of a mixed functionalized AuNPs. Moreover it allows the checking of the reversibility of the guest inclusion. Indeed, the addition of increasing amounts of methylbutylammonium iodide **3** to the

solution of **TiIII-AuNPs**•**2** complex resulted in a gradual decrease of the fluorescence. The intensity reached the original value of **2** alone when one equivalent of **3** was added, clearly demonstrating that **2** is completely replaced by the more competitive guest **3** (Scheme 2.3 and Figure 2.11).

The guest controlled aggregation of **TiIII-AuNPs** was achieved using N-methylpyridinium terminated poly(ethylene glycol) (PEG) **1**³³ as a ditopic guest. This guest was prepared starting from a low MW PEG ($M_w = 1500$ Da) because of its monodispersity and ease of functionalization. The **TiIII-AuNPs**-polymer **1** host-guest interaction was demonstrated via ³¹P NMR (Figure 2.12).

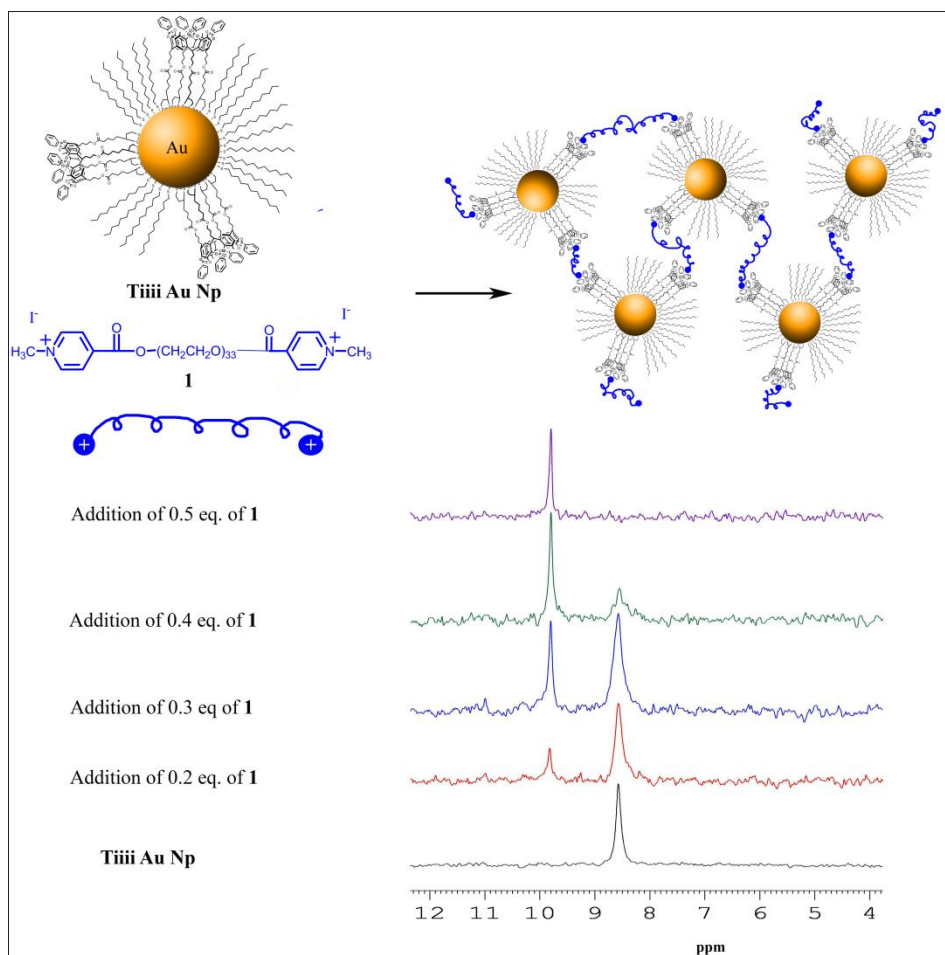


Figure 2.12 ³¹P NMR titration in CDCl₃ of **TiIII-AuNPs** with **1** (concentration of nanoparticles bound **TiIII** $\approx 7 \cdot 10^{-4}$ M). The presence of two signals results from the slow exchange on the NMR time scale.

Addition of ditopic guest **1** to a nanoparticle solution led to the appearance of a new resonance at 9.79 ppm, diagnostic of the guest inclusion within the cavity. All **Tiiii-AuNPs** host sites were saturated after addition of 0.5 equivalents of **1**, indicating that all polymer end groups are fully engaged in complexation. The complexation is kinetically slow, since, after each addition, the equilibration of the two peaks requires several hours.

The reversibility of the host-guest aggregation was tested using methylbutylammonium salt **3** as competitive guest. **3** was added to the solution of the aggregated system **Tiiii-AuNPs•1** described above. The higher affinity of **Tiiii** cavitand towards methylammonium with respect to methylpyridinium ions resulted in the breaking of the network, as evidenced by a further downfield shift of the signal (Figure. 2.13b). The subsequent addition of an excess of a non competitive base such as DBU led to the deprotonation of the ammonium ion and to its release from the cavity (Figure. 2.13c). At this point polymer **1**, still present in solution, slowly complexes again network (Figure 2.13d).

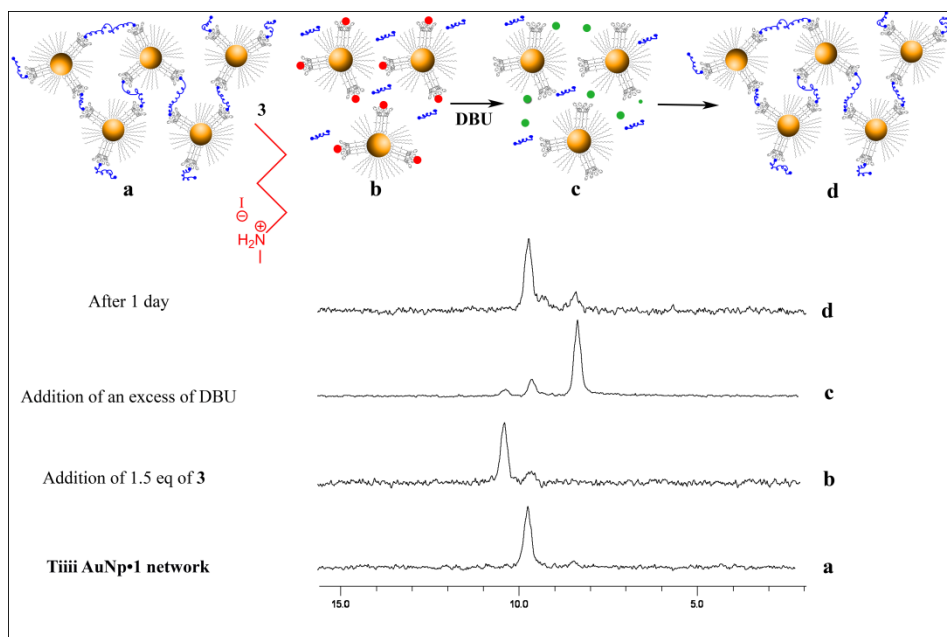


Figure 2.13 ^{31}P NMR monitoring of network assembly/disassembly in CDCl_3 . Red dots: complexed guest **3**, green dots: released *N*-butylmethylamine.

Network assembly/disassembly of the system was followed also by means of DLS measurements. A suspension of **Ti_{iii}-AuNPs** in chloroform with a target cavitand concentration [**Ti_{iii}**] of about 5×10^{-5} M was titrated using a concentrated solution of the ditopic guest **1** (2 mM, CHCl₃). The mean peak area volume distribution was used to have a more realistic insight on the aggregation phenomena promoted by guest **1**, and on the relative concentration of the aggregates during the titration. Starting from a pristine situation in which almost only the distribution ascribable to the system **Ti_{iii}-AuNPs** (25 ± 3) was present, we measured the growing of a second bigger population, due to the formation of the **Ti_{iii}-AuNPs•1** network (75 ± 15 nm). The trend of the peak area volume % vs. [**1**] is reported in Figure 2.14, which also shows the disassembly of the network upon the addition of an excess of **1**, a process ascribable to the saturation of the cavitands on the nanoparticles. The concentration of **1** needed to reach the maximum assembly is proportional with a good agreement to the amount of **Ti_{iii}** present in solution. The reported values of PDI (Polydispersion Index) also indicate that the poly-dispersion of the system during the entire titration is suitable for DLS measurements. In a parallel fashion to NMR experiments, the reversibility of the host-guest aggregation process was tested also with DLS measurements. By adding the competitive guest **3** in the condition where the maximum assembly is observed, the network is reversibly destroyed, as indicated by the disappearance of the peak at 75 nm. (Figure 2.14).

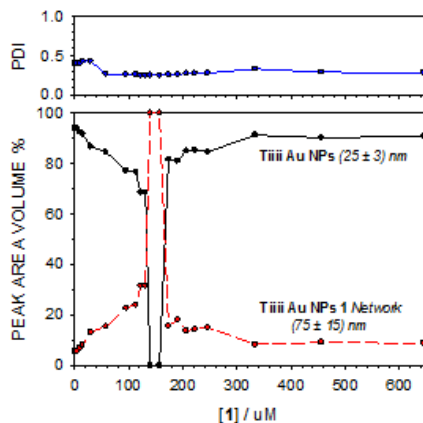


Figure 2.14 DLS titration of a **Ti_{iii}-AuNPs** solution (concentration of nanoparticles bounds $\approx 5 \cdot 10^{-5}$ M, CHCl₃, 20 °C) with ditopic guest **1** (2 mM, CHCl₃). Peak area volume % represents the relative amount ascribable to the main two different distributions measured in solution (black dots **Ti_{iii}-AuNPs**; red dots: **Ti_{iii}-AuNPs•1**).

The formation of the **Ti_{iii}-AuNPs•1** network caused a red-shift of the PRB of about 10 nm (Figure 2.15). This rather small red-shift suggests that the intermolecular network formation is not the only interaction mode available to ditopic polymer guest 1. Indeed, the polymeric nature of 1 allows also intramolecular interactions with two cavitands of a single nanoparticle to occur.³⁴ The intramolecular complexation mode in association with the reduced number of coated cavitands on each AuNP limits the final size of the network.

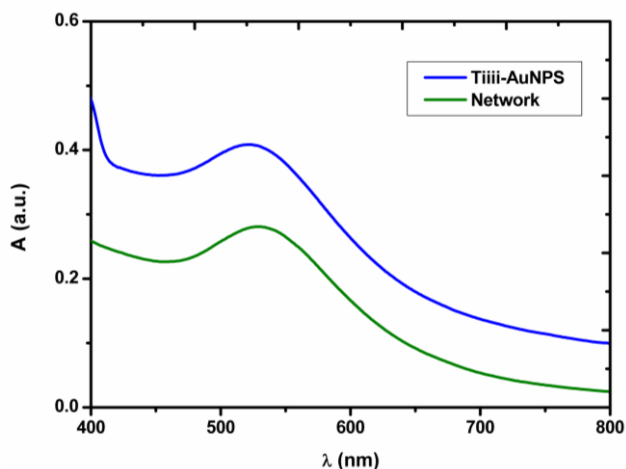


Figure 2.15 Plasmon Band Resonance shift of *Ti_{iii}-AuNP* (blue line), *Ti_{iii}-AuNPs•1* network.

The occurrence of intramolecular versus intermolecular binding in the **AuNPs•1** system has been verified by recurring to the much shorter ditopic guest *N,N'*-dimethyl-1,8-octanediammonium diiodide **4**, too short to undergo intramolecular complexation on a single nanoparticle. A suspension of **Ti_{iii}-AuNPs** was titrated with a methanol solution of guest **4** (Figure 2.16). The **AuNPs•4** network formation was evidenced by the color alteration of the suspension, that turned from dark red to deep blue-purple, as evidenced by the 42 nm red shift of the PRB.

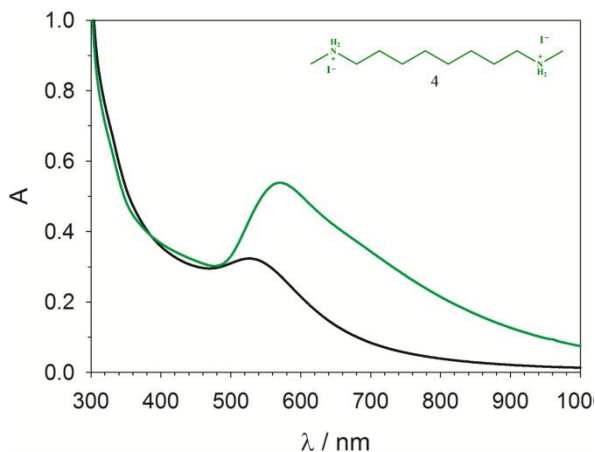


Figure 2.16 Absorption spectra of Ti^{III} -AuNPs (black line) and Ti^{III} -AuNPs with ditopic guest **4** (green line) showing a 42 nm Plasmon band resonance red shift caused by the formation on NPs network.

The shorter length of guest **4** compared to **1**, causes a much closer interaction between nanoparticles in the network, that leads to a marked red shift of their PRB. The formation of larger $\text{AuNPs}\cdot\mathbf{4}$ aggregates with respect to their $\text{AuNPs}\cdot\mathbf{1}$ analogues was confirmed by DLS experiments, which revealed a bimodal distribution of particles with an average diameter of 170 nm (Figure 2.17).

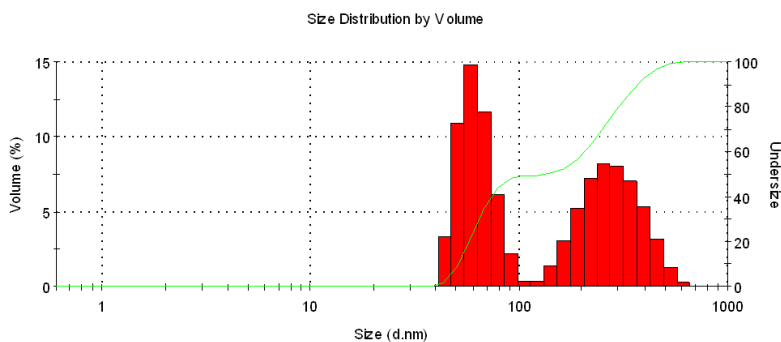


Figure 2.17 Sample size volume distribution during the assembly experiment of Ti^{III} -AuNPs in CHCl_3 with guest **4**. Hydrodinamic diameter: d_H (average) = 170 nm (PDI = 0.29), single distributions d_H small = (64 ± 10) nm, d_H large = (270 ± 80) nm.

2.4 Conclusions.

In conclusion, a new, effective and reversible aggregation mode between AuNPs and PEG which takes advantage of the peculiar complexation properties of tetrakisphosphonate cavitands is reported. The insertion of **Tiiii** on **AuNPs** introduced several appealing features to the system: (a) an innovative way to determine the amount of coated receptors via fluorescence spectroscopy; (b) the use of ^{31}P NMR as diagnostic tool to monitor network assembly/ disassembly and (c) the possibility to turn on/off the AuNPs-polymer assembly via competitive guest replacement. Moreover, the presence of a limited number of cavitand units on each AuNP produced the unusual phenomenon of host saturation driven disassembly, where the presence of an excess of the polymeric ditopic guest led to the preferential complexation of a single N-methylpyridinium end group.

2.5 Acknowledgments.

Special thanks to Francesca Maffei of University of Parma, Enrico Rampazzo and Luca Prodi from University of Bologna; Andrea Pucci and Giacomo Ruggeri from University of Pisa.

2.6 Experimental section.

Tetrahydroxy silylcavitand (II)

To a solution of **I** (2.5g, 3.27mmol) in pyridine (20mL) dimethyldichlorosilane was added (4.13g, 3.85 mL, 32.7 mmol) at once. The resulting mixture was heated to 55°C for 12 hours. The solvent was removed under vacuum and the resulting residue was suspended in water. After filtration compound **II** was obtained in pure form as a white solid (2.46g, 2.45mmol, 84% yield). **¹H NMR (CDCl₃, CD₃OD, 400 MHz):** δ (ppm) 7.11 (s, 4H, ArH); 4.45 (t, 4H, ArCH, ³J = 7.8 Hz); 3.51 (t, 8H, CH₂CH₂OH, ³J = 5.7 Hz); 3.21 (s, 4H, CH₂CH₂CH₂OH); 2.14 (bs, 8H, ArCHCH₂); 1.77 (s, 12H, ArCH₃); 1.38 (bs, 8H, CH₂CH₂CH₂OH); 0.37 (s, 12H, SiCH_{3out}); -0.70 (s, 12H, SiCH_{3in}); **ESI-MS:** *m/z* calcd. for C₅₂H₇₂O₁₂Si₄ (1001.46) [M+Na]⁺: 1024.46. **Found:** 1024.50 [M+Na]⁺.

MOM-protected silylcavitand (III)

To a solution of **II** (2.021 g, 2.02 mmol) in DMF (20 mL), diisopropylethylamine (5.30 mL, 30.3 mmol) and chloromethyl methyl ether (1.54 mL, 20.2 mmol) were added. The resulting mixture was heated a 50°C for 24 hours. The solvent was removed under vacuum and the resulting residue was suspended in water. After filtration compound **III** was obtained in pure form as white solid (2.01 g, 1.70 mmol, 85% yield). **¹H NMR (CDCl₃ , 300 MHz):** δ (ppm) 7.17 (s, 4H, ArH); 4.59 (s, 8H, OCH₂O); 4.58 (t, 4H, ArCH, ³J = 7.8 Hz); 3.51 (t, 8H, CH₂CH₂CH₂O, ³J = 5.7 Hz); 3.34 (s, 12H, OCH₃); 2.30 (q, 8H, CH₂CH₂CH₂O, ³J = 7.5 Hz); 1.87 (s, 12H, ArCH₃); 1.58 (q, 8H, CH₂CH₂CH₂OH, ³J = 7.5 Hz); 0.47 (s, 12H, SiCH_{3out}); -0.72 (s, 12H, SiCH_{3in}). **ESI-MS:** *m/z* calcd. for C₆₀H₈₈O₁₆Si₄: (1177.67) [M+Na]⁺: 1200.67. **Found:** 1200.12 [M+Na]⁺.

MOM-protected resorcinare (IV)

An aqueous 36% HF solution (0.65 mL) was added to **III** (1.6 gr., 1.36 mmol) dissolved in DMF (20 mL). The mixture was heated at 50°C overnight. The solvent was removed in vacuo and the product was washed with water. Vacuum filtration afforded pure **IV** (1.30 g, 1.36 mmol, quantitative yield). **¹H NMR (DMSO-D₆ , 300 MHz):** δ (ppm) 8.68 (s, 8H, ArOH); 7.29 (s, 4H, ArH); 4.53 (s, 8H, OCH₂O); 4.22 (t, 4H, ArCH, ³J = 7.8 Hz); 3.48 (t, 8H, CH₂CH₂CH₂O, ³J = 6.0 Hz); 3.24 (s, 12H, OCH₃); 2.27 (m, 8H, CH₂CH₂CH₂O); 1.94 (s, 12H, ArCH₃); 1.58 (m, 8H, CH₂CH₂CH₂OH). **ESI-MS:** *m/z* calcd. for C₅₂H₇₂O₁₆: (953.12) [M+Na]⁺: 976.20. **Found:** 976.20 [M+Na]⁺.

MOM-protected tetraphosphonate cavitand (V)

To a solution of **IV** (1.345 g, 1.41 mmol) in freshly distilled pyridine (15 mL), dichlorophenylphosphine (0.8 mL, 5.9 mmol) was added slowly, at room temperature. After 3 hours of stirring at 70 °C, the solution was allowed to cool at room temperature and 10 mL of a mixture of aqueous 35% H₂O₂ and CHCl₃ (1:1) was added. The resulting mixture was stirred for 30 minutes at room temperature, then the solvent was removed in vacuo. Addition of water resulted in the precipitation of a white powder, which is filtered to give pure **V** (1.77 g, 1.23 mmol, 87% yield). **¹H NMR (CDCl₃, 300 MHz):** δ (ppm) 8.06 (m, 8H, P(O)ArH_{ORTO}); 7.56 (m, 4H+8H, P(O)ArH_{PARA} + P(O)ArH_{META}); 7.17(s, 2H, ArH_{DOWN}); 4.82 (bt, 4H, ArCH₃); 4.62 (s, 8H, OCH₂O); 3.62 (t, 8H, CH₂CH₂CH₂O, ³J = 6.0 Hz); 3.35 (s, 12H, OCH₃); 2.56 (m, 8H, CH₂CH₂CH₂O); 2.10 (s, 12H, ArCH₃); 1.60 (m, 8H, CH₂CH₂CH₂OH); **³¹P{¹H} NMR (CDCl₃, 161 MHz):** δ (ppm) 8.58 (s, P(O)); **ESI-MS:** *m/z* calcd. for C₇₀H₇₂O₁₄P₄: (1441.36) [M+Na]⁺: 1464.36. **Found:** 1464.36 [M+Na]⁺.

Tetrahydroxy-footed tetraphosphonate cavitand (Tiiii[OH, CH₃, Ph])

To a solution of **V** (1.77 g, 1.22 mmol) in CHCl₃(15 mL) and methanol (32mL) an aqueous 36% HCl solution was added. The resulting suspension was heated at 50°C overnight and the resulting residue was suspended in water. After filtration, pure compound **VI** was obtained as yellow light solid (1.26 g, 0.99 mmol, 81% yield). **¹H NMR (Acetone-d₆, 300 MHz):** δ (ppm) 8.29 (s, 2H, ArH_{DOWN}); 8.20 (m, 8H, P(O)ArH_{ORTO}); 7.73 (m, 4H+8H, P(O)ArH_{PARA} + P(O)ArH_{META}); 4.81 (t, 4H, ArCH₃, ³J = 7.6 Hz); 3.69 (t, 8H, CH₂CH₂CH₂OH, ³J = 5.3 Hz); 2.91 (m, 8H, CH₂CH₂CH₂O); 2.16 (s, 12H, ArCH₃); 1.60 (m, 8H, CH₂CH₂CH₂OH); **³¹P{¹H} NMR (Acetone-d₆, 161 MHz):** δ (ppm) 9.32 (s, P(O)); **ESI-MS:** *m/z* calcd for C₇₀H₇₂O₁₄P₄: (1264.36) [M+Na]⁺: 1287.36. **Found:** 1287.49 [M+Na]⁺.

Lipoic ester-footed tetraphosphonate cavitand (Tiiii[disulfide, CH₃, Ph])

To a solution of **Tiiii[OH, CH₃, Ph]** (395 mg., 0.312 mmol) in CH₂Cl₂ (2 mL), DCC (546 mg, 2.65 mmol), DMAP (95 mg, 0.78 mmol), and lipoic acid (514mg, 2.49 mmol) were added. The resulting suspension was heated at 50°C overnight. The solvent was removed in vacuo and a 3 : 1 dichloromethane / ether solution was added. The white solid was filtrated and washed with 2 : 1 dichloromethane / ether solution. The filtrate was collected and the solvent was evaporated in vacuo. The resulting solid was washed with ether (2 x 20 mL). The crude was purified by column chromatography (0.1-10% MeOH / CH₂Cl₂) (127 mg, 0.062 mmol, 20% yield). **¹H NMR (CDCl₃, 300 MHz):** δ (ppm) 8.08 (m, 8H, P(O)ArH_{ORTO}); 7.73 (m, 4H+8H+4H, P(O)ArH_{PARA} + P(O)ArH_{META} +

ArH_{DOWN}); 4.81 (t, 4H, ArCH, $^3J = 7.6$ Hz); 4.25 (t, 8H, CH₂CH₂CH₂O, $^3J = 6.2$ Hz); 3.52 (m, 4H, CH₂(S)CH₂CH(S)), 3.13 (m, 8H, CH₂(S)CH₂CH(S)), 2.42 (m, 8H, CH₂(S)CH₂CH(S)); 2.40 (m, 8H, CH₂CH₂CH₂O); 2.11 (s, 12H, ArCH₃); 1.94-1.57 (m, 32H, CH₂CH₂CH₂O + O(CO)CH₂CH₂CH₂CH₂+O(CO)CH₂CH₂CH₂CH₂CH₂ + O(CO)CH₂CH₂CH₂CH₂), 1.40 (m, 8, O(CO)CH₂CH₂CH₂CH₂); $^{31}\text{P}\{^1\text{H}\}$ NMR (CDCl₃, 161 MHz): δ (ppm) 7.31 (s, P(O)). **HR ESI-MS**: calculated. for the complex **Tiii[disulfide, CH₃, Ph] \cdot N-methylbutyl ammonium iodide** C₁₀₅H₁₃₀N₁O₂₀P₄S₈ [M+C₅H₁₄N]⁺:2104.58968. **Found**: 2104.60183.

Preparation of AuNPs

AuNPs were synthesised by a two-phase method: nanoparticles were prepared by dissolving 0.400 g (1.02 mmol) of hydrogen tetrachloroaurate(III) trihydrate in 30 mL of deionized water. The solution was then shaken in a separatory funnel with 80 mL of toluene solution containing 2.00 g (3.56 mmol) of tetra-n-octylammonium bromide (TOAB). The toluene phase was then recovered and combined with 0.018 mL (0.015 g, 0.07 mmol) of dodecyl mercaptane. A freshly prepared aqueous solution of sodium borohydride (25 mL, 0.386 g) was slowly added under vigorous stirring. After further stirring for 3 h, the organic phase was separated, concentrated to 10 mL and mixed with 70 mL of ethanol. The mixture was cooled overnight at -20°C and the dark precipitate was then recovered by filtration. The crude product was then purified by soxhlet extraction with acetone as cleansing solvent to remove all the unbound free thiol and residual TOAB impurities.

Elemental analysis: found (%) C = 24.7; H = 4.2; N = 0.0.

Preparation of Tiii-AuNPs

Dodecanthiol stabilized gold nanoparticles (20 mg) were mixed in dry chloroform with tetraphosphonate cavitand (13.52 mg 0.0067 mmol) at room temperature, for 5 days. The solvent was evaporated under N₂ flux and the resulting solid was suspended in a toluene / ethanol mixture (2:1). The suspension was then ultracentrifugated at 15000 rpm (2 runs of 15 minutes each). The supernatant was decanted off, the solid was collected and dried under vacuum. The washing procedure was repeated twice.

Fluorimetric Titration

3 mL of a 1x10⁻⁶ M solution of fluorescent pyrene guest derivative **2** in dichloromethane were prepared by repeated dilution of a concentrated mother solution (1x10⁻³ M) and a starting point spectra (blue line of Figure 1 in the text) was recorded. This solution was then titrated

adding 10 μl aliquots of a dichloromethane solution of **Tiii-AuNPs** prepared dissolving 1.5 mg of **Tiii-AuNPs** in 1 mL of dichloromethane. After every addition the solution was left without any agitation for 5 minutes after each addition in order to achieve the equilibrium, then an emission spectra was recorded (λ exc = 345 nm). The aliquots were added until no more changes in the spectrum were observed, i.e. until the achievement of the equivalent point. This required the addition of 130 μl of **Tiii-AuNPs** solution corresponding to the addition of 0.2 mg of **Tiii-AuNPs**. The experiment was repeated three times. The **Tiii-AuNPs** aliquots added ranged between 130 and 140 μl .

DLS measurements

Nanoparticles hydrodynamic diameter distributions were obtained through Dynamic Light Scattering measurements employing a Malvern Nano ZS instrument with a 633 nm laser diode. Samples were housed in semi-micro (1400 μL volume) quartz cells of 1cm optical path length, using chloroform as solvent (CHROMASOLV[®] Plus, for HPLC, $\geq 99.9\%$, amylene stabilized). All DLS measurements were carried on 400 μL solutions. NPs suspensions were prepared through sonication in chloroform at room temperature (10 min). Solvent and suspensions used were thoroughly filtered (PTFE membrane syringe filter, 0.20 μm) before any DLS measurement.

The width of DLS hydrodynamic diameter distribution is indicated by PdI (Polydispersion Index). In case of a mono-modal distribution (gaussian) calculated by means of cumulant analysis, $\text{PdI} = (\sigma/Z_{\text{avg}})^2$, where σ is the width of the distribution and Z_{avg} is average diameter of the particles population respectively.

The hydrodynamic diameter values determined during the titrations with ditopic guest **1** ($[\text{Tiii}] = 5 \times 10^{-5} \text{ M}$) are mediated upon three different measurements, while the hydrodynamic diameter of the assembly-disassembly experiments with guest **1** and **3** (d_{H} Volume Mean) are the mean values (\pm standard deviation) of ten measurements of the same suspension.

2.7 References and Notes

- 1 D.Astruc, *Organometallic Chemistry and Catalysis*; Springer **2007**.
- 2 *Cluster and Colloids: From Theory to Applications*, Ed. Gunther Schmid, Wiley VCH, **2007**.
- 3 Daniel M.C.; Astruc D. *Chem. Rev.* **2004**, *104*, 293 – 346.
- 4 Goesmann, H.; Feldmann, C. *Angew. Chem. Int. Ed.* **2010**, *49*, 2 - 36.
- 5 Dahl, J.A.; Maddux, B.L.S.; Hutchinson, J.E. *Chem. Rev.* **2007**, *107*, 2228 - 2269.
- 6 Brust, M.; Walker, M.; Bethell, D.; Schiffrin, D.J.; Whyman, R.J. *J. Chem. Soc.; Chem. Commun.* **1994**, 801- 802.
- 7 Caragheorghopol, A.; Chechik, V. *Phys. Chem. Chem. Phys.* **2008**, *10*, 5029 – 5041.
- 8 Shenhar, R.; Rotello, V.M. *Acc. Chem. Res.* **2003**, *36*, 549 - 561.
- 9 Martinez-Manez, R.; Sancenon, F.; Hoffmann, K.; Rurack, K.; Descalzo, A.B., *Angew. Chem. Int. Ed.* **2006**, *45*, 5924-5948.
- 10 Beer, P.D.; Cormode, D.P.; Davis, J.J. *Chem. Commun.* **2004**, 414 - 415.
- 11 a) Arduini, A. Demuru, D.; Pochini, A.; Secchi, A. *Chem. Commun.* **2005**, 645 - 646; b) Tshikudo, T.R.; Demuru, D.; Wang, Z.; Brust, M.; Secchi, A.; Arduini, A.; Pochini, A. *Angew. Chem. Int. Ed.* **2005**, *44*, 2913-2916.
- 12 Gupta, S.; Zhang, Q.; Emrick, T.; Balazs, A.C.; Russel, T.P. *Nat. Mat.* **2006**, *5*, 229 - 233.
- 13 Zhao ,Y., Thorkelsson, K., Mastroianni,A. J.; Schilling, Y.; Luther,J.M.; Rancatore, B. J.; Matsunaga,K.; Jinnai, H.; Wu, Y.; Poulsen, D.; Frechet, J.M.; Alavisatos A.P.; Xu,T. *Nat. Mater.* **2009**, *8*, 979 - 985.
- 14 Ofir, Y.; Samanta, B.; Rotello, V.M. *Chem. Soc. Rev.* **2008**, *37*, 1814 - 1825.
- 15 Boal, A.K.; Ilhan, F.; Derouchey, J.E.; Thurn-Albrecht, T.; Russell, T.P.; Rotello, V.M. *Nature* **2000**, *404*, 746 - 748.
- 16 B. L. Frankamp, O. Uzun, F. Ilhan, A. K. Boal and V. M. Rotello, *J. Am. Chem. Soc.* **2002**, *124*, 892 – 893.
- 17 Mulder, A.; Huskens, J.; Reinhoudt, D.N. *Org. Biomol. Chem.* **2004**, *2*, 3409 - 3424.
- 18 Frankamp, B.L.; Boal, A.K., Rotello, V.M. *J. Am. Chem. Soc.* **2002**, *124*, 15146 - 15147.

- 19 (a) A.C. Balazs, T. Emrick and T. Russel *Science* **2006**, *314*, 1107 - 1110; (b) Y. Zhao, K. Thorkelsson, A. J. Mastroianni, T. Schilling, J. M. Luther, B. J. Rancatore, K. Matsunaga, H. Jinnai, Y. Wu, D. Poulsen, J. M. Frechet, A. P. Alavisatos and T. Xu *Nat. Mater.* **2009**, *8*, 979 - 985; (c) R. Oren, Z. Liang, J. S. Bernard, S.C. Warren, U. Wiesner and W.T.S. Huck *J. Am. Chem. Soc.* **2009**, *131*, 1670 - 1671; (d) C. Durand-Gasselin, M. Capelot, N. Sanson and N. Lequeux *Langmuir* **2010**, *26*, 12321 - 12329.
- 20 (a) J. Liu, J. Alvarez, W. Ong and A.E. Kaifer *Nano Lett.* **2001**, *1*, 57 - 60; (b) Z. Liu and M. Jiang, *J. Mater. Chem.* **2007**, *17*, 4249 - 4254.
- 21 F. Ciesa, A. Plech, C. Mattioli, L. Pescatori, A. Arduini, F. Rossi and A Secchi *J. Phys. Chem. C*, **2010**, *114*, 13601 - 13607.
- 22 O. Crespo-Biel, B. Dordi, D.N. Reinhoudt and J. Huskens *J. Am. Chem. Soc.* **2005**, *127*, 7594 - 7600.
- 23 For the nomenclature adopted for phosphonate cavitand see: R. Pinalli, M. Suman and E. Dalcanale *Eur. J. Org. Chem.* **2004**, 451 - 462.
- 24 E. Biavardi, M. Favazza, A. Motta, I. L. Fragalà, C. Massera, L. Prodi, M. Montalti, M. Melegari, G.C. Condorelli and E. Dalcanale, *J. Am. Chem. Soc.* **2009**, *131*, 7447 - 7455.
- 25 D. Menozzi, E. Biavardi, C. Massera, F.-P. Schmidtchen, A. Cornia and E. Dalcanale *Supramol. Chem.* **2010**, *22*, 768 - 775.
- 26 (a) R.M. Yebeutchou, F. Tancini, N. Demitri, S. Geremia, R. Mendichi and E. Dalcanale *Angew. Chem. Int. Ed.* **2008**, *47*, 4504 - 4508; (b) E. Biavardi, G. Battistini, M. Montalti, R.M. Yebeutchou, L. Prodi and E. Dalcanale *Chem. Commun.* **2008**, 1638 - 1640.
- 27 (a) A. Wei *Chem. Commun.*, **2006**, 1581-1591; (b) M. S. Vickers, J. Cookson, P. D. Beer, P. T. Bishop and B. Thiebaunt *J. Mater. Chem.* **2006**, *16*, 209 - 215.
- 28 L. Pirondini, D. Bonifazi, E. Menozzi, E. Wegelius, K. Rissanen, C. Massera and E. Dalcanale *Eur. J. Chem. Org.*, **2001**, 2311 - 2320.
- 29 B. Neises and W. Steglich, *Angew. Chem. Int. Ed.*, 1978, **17**, 522 -524.
- 30 C. A. Waters, A.J. Mills, K.A. Johnson and D. J. Schiffrin *Chem. Commun.* **2003**, 540 - 541.

- 31 M.J. Hostetler, J.E. Wingate, C.-J. Zhong, J.E. Harris, R.W. Vachet, M.R. Clark, J.D. Londono, S.J. Green, J.J. Stokes, G.D. Wignall, G.L. Glish, M.D. Porter, N.D. Evans, R.W. Murray, *Langmuir* **1998**, *14*, 17 - 30.
- 32 G. Battistini, P.G. Cozzi, J.-P. Jalkanen, M. Montalti, L. Prodi, N. Zaccheroni and F. Zerbetto *ACS Nano* **2008**, *2*, 77 - 84.
- 33 F. Tancini, R. M. Yebeutchou, L. Pirondini, R. De Zorzi, S. Geremia, O. A. Scherman and E. Dalcanale *Chem.-Eur. J.* **2010**, *16*, 14313 - 14321.
- 34 For similar case see: O. Crespo-Biel, A. Jukovic, M. Karlsson, D.N. Reinhoudt and J. Huskens *Isr. J. Chem.* **2005**, *45*, 353 - 362.

Polymer-nanoparticles network: assembly kinetics and solvent dependence

3

3.1 Introduction

Gold nanoparticles (AuNPs) are innovative materials for optical, electronic and sensing applications, due to their unique physical properties.¹

Building and patterning of the AuNPs into two- and three dimension organized structures by manipulation of individual units is of interest to realize nanodevices for specific applications. Although chemical principles can be exploited for the fabrication of nano-objects with atomic scale precision, the assembly of nanoscale components into hierarchically ordered multiscale architectures remains a considerable challenge.² Both “bottom-up” (self-assembly) and “top-down” technologies (e.g. lithographic techniques) have been proposed to assemble devices of nano-dimensions.³ However, an ideal nanoparticle assembly method should (1) permit construction of various topologically complex superstructures; (2) allow for manipulation of the structural features of the network, including nanoparticle size and interparticle spacing, and (3) allow for assembly of nanoparticles of various compositions.⁴ Methods involving polymers,⁵ dendrimers,⁶ DNA⁷ and solvent-induced phase separation⁸ have been successfully demonstrated. Variation in the synthetic components and synthetic conditions deeply impacts particle sizes and interparticle spacing in the context of superstructures realization.

In the previous chapter, we reported the self-assembly of hybrid network formed via guest controlled aggregation of Tiiii-AuNPs using *N*-methylpyridinium terminated poly(ethylene glycol) PEG **1**.

Herein, we report the kinetics and solvent-dependent changes of guest controlled self-assembled network previously prepared. We specifically examine how both the temperature and the solvents can affect the network growth, which is globally under thermodynamic control, but sensitive to kinetic aspects, providing guidelines which can be extended to other host-guest driven self-assembled networks.

3.2 Results and Discussion

3.1 Assembly Dynamics.

The formation of the network is induced by mixing the two system components: tetraphosphonate cavitand decorated nanoparticles and *N*-methylpyridinium-terminated PEG (Figure 3.1).

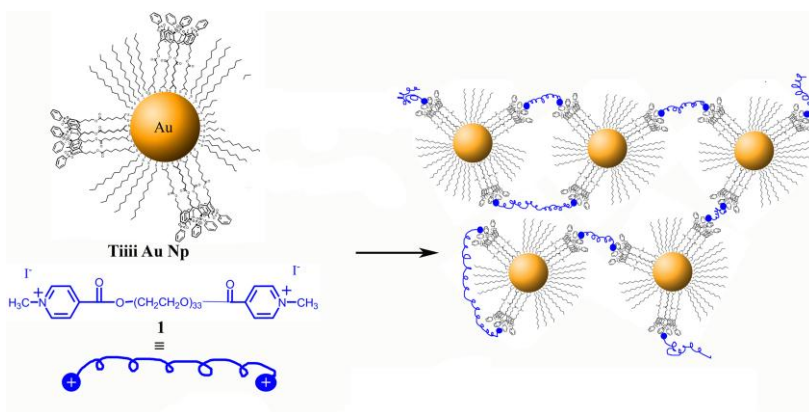


Figure 3.1 Self-assembled network driven by molecular recognition

Modified gold nanoparticles were dissolved in chloroform (1 mL) and put in a glass cuvette in the spectrometer at a given temperature, then few μL of functionalized PEG guest solution were added. Both concentrations and quantities were selected in order to obtain an excess of guest (roughly 10:1) without a significant dilution of the starting solution. The assembly process was monitored by a continuous acquisition of the DLS correlation curves, as reported in Figure 3.2 for measurements performed at 16 °C.

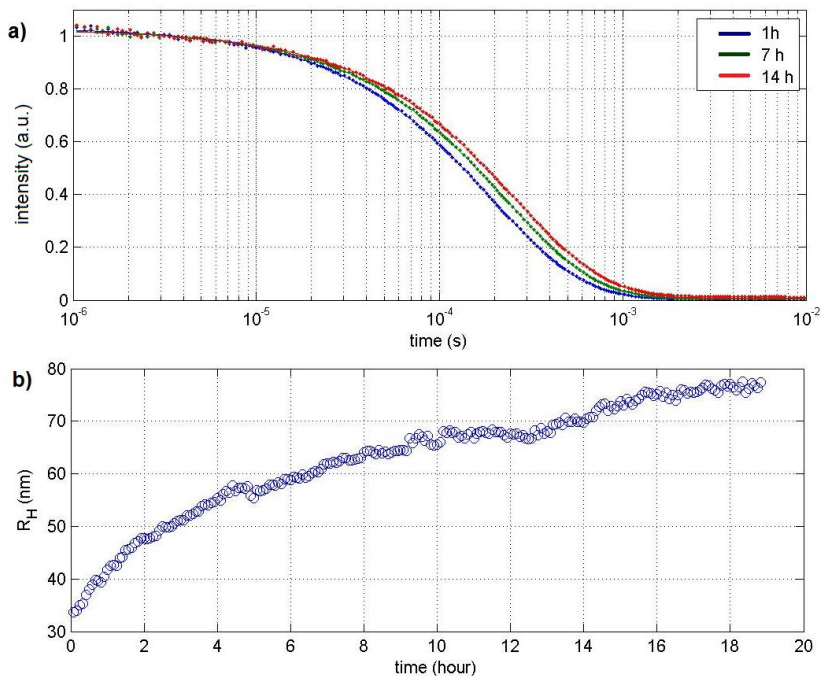


Figure 3.2 a) Experimental DLS autocorrelation curves with corresponding interpolation function (line) acquired at 16°C measured 1 (blue trace), 7 (green trace) and 14 (red trace) hours after guest addition; b) Network size as function of time during the assembling.

Figure 3.2a shows the DLS correlation curves at different times after guest addition while in Figure 3.2b is plotted the evolution of networks size as a function of time, as determined by the analysis of the correlation curves. The normalized correlation curves are accurately fitted (as shown in Figure 3.2a) by a stretched exponential function or Kohlrausch-Williams-Watts (KWW) function:⁹

$$f(t) = \exp\left(-\left(\frac{t}{\tau}\right)^\beta\right)$$

typical for non polydisperse samples, where t is the time, τ the characteristic correlation decay and the β exponent ($0 < \beta < 1$) reflects the heterogeneity of the system ($\beta = 1$ for monodisperse sample). The mean network size r is related with the decay time τ through the relation

$$r = \frac{kT}{6\pi\eta} \tau q^2$$

where T is the temperature, K the Boltzmann constant, η the solvent viscosity q the scattering vector.

We found that, during the network assembly process, the correlation curves maintain such functional form with the β parameter at a constant value ($\beta = 0.88$). The absence of a multiple exponentials form of the DLS data and the time invariance of the heterogeneity parameter β , let us conclude that network grows with a monodisperse size distribution or without nucleation process, starting at different times or with different growth rates. The mean size r of the network as function of time, determined from the correlation decay times τ (fixed the heterogeneity parameter β), presents an exponential behavior, as shown in Figure 3.2b, characterized by a final asymptotic value, in the range of 80 nm. However such trend is not accurately interpolated by an exponential functional, therefore we define, in the present work, as the characteristic network growth time, the time required to reach the half of the final size.

The characteristic network growth times measured in the temperature range 16-55°C, shown in Figure 3.3, display an Arrhenius-like behavior.

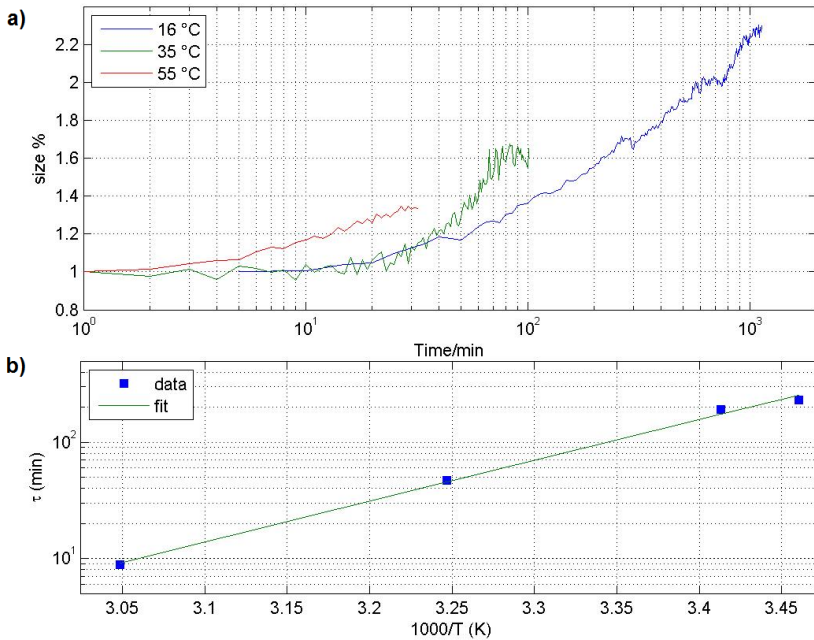


Figure 3.3 a) Relative network growth as a function of time at different temperature (16°C blue trace; 35°C green trace; 55°C red trace); b) Characteristic growth times as function of temperature.

The experimental data indicate that the temperature influences not only the dynamics of the process but also its yield: higher temperatures accelerate the network formation and decrease their final asymptotic size, as can be observed from the data plotted in Figure 3.3a. Such results can be explained supposing that thermally activated processes with higher activation energy induces a disassembly of the network, therefore at higher temperatures the equilibrium of assembly↔disassembly processes results in a smaller size of the formed network. The reported results appear to be contrary to a purely thermodynamically driven assembly mechanism, which would predict an increase of branching points, which eventually lead to cross-linked or densely compacted nanoparticles aggregation. Thus the temperature-dependent behavior suggests the presence of a secondary competing mechanism, possibly involving disassembly processes.

In order to check such hypothesis we studied also the temperature effect in the disassembly process. The network disassembly has been obtained by addition of a competitive guest in solution, *N*-methylbutyl ammonium iodide **2**. The guest exchange is driven by the formation of stronger complex between the tetraphosphonate cavitand and quaternary ammonium salt,¹⁰ unbinding the gold nanoparticle from the network (Figure 3.4).

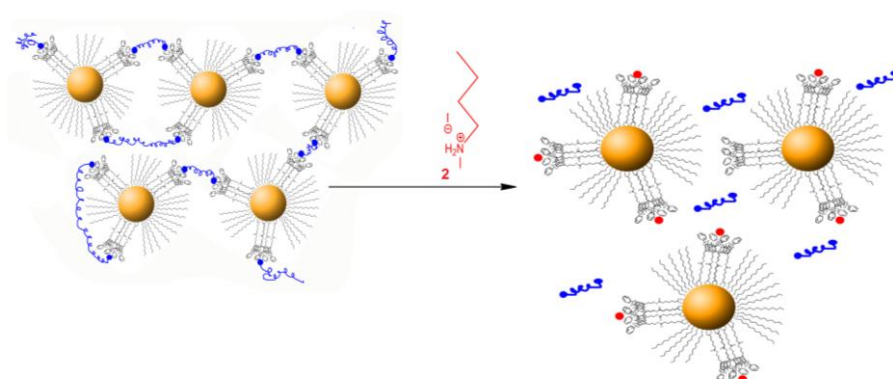


Figure 3.4 Network disassembly induced by guest addition

The disassembly process induced by **2** is effective already at room temperature and it is almost complete in a short period of time (55 minutes) (Figure 3.5). Importantly, the final hydrodynamic radius found (≈ 50 nm) did not correspond to initial cavitand-functionalized AuNPs dimension previously observed (of about 8 nm; for further details see Chapter 2), for intrinsic limitation of the instrument, whose lower limit of detection is about 50 Å.

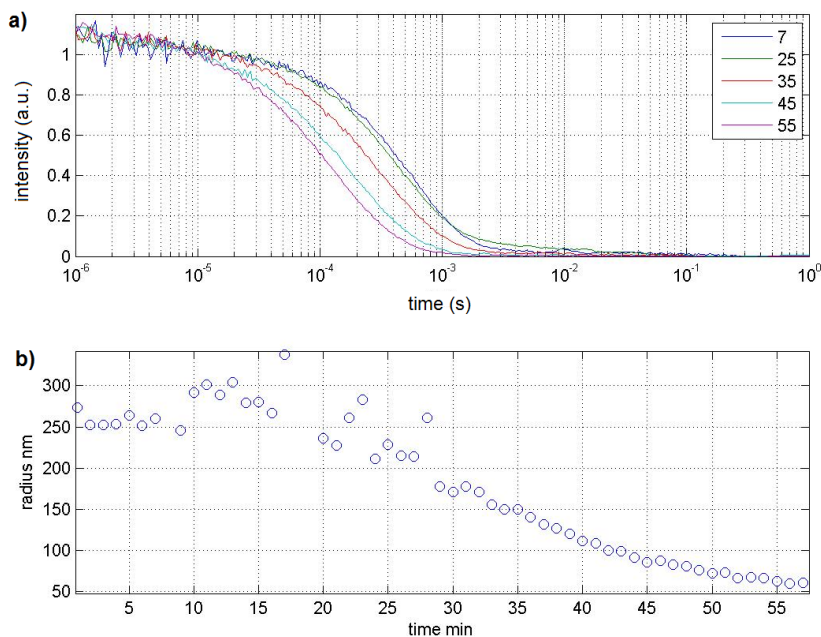


Figure 3.5 a) Experimental DLS autocorrelation curves with corresponding interpolation function acquired at room temperature, after short period of time; b) Network size as function of time during the disassembly induced by guest **2**.

The evolution of the characteristic size of networks during such process is reported in Figure 3.6, at 55 °C (blue trace).

The results confirm the enhancement effect of temperature which accelerates both assembly and disassembly processes. Contrary to the assembly process, the disassembly is a first order process: the trend of networks size as function of time is now accurately fitted by a simple exponential function.

We, thus, inferred that the temperature dependence of network assembly is a consequence of host-guest complex formation. While the molecular recognition event is both enthalpy and entropy driven,¹¹ the

network assembly is entropy opposed,¹² therefore at lower temperatures the enthalpic contribution is dominant, leading to larger objects.

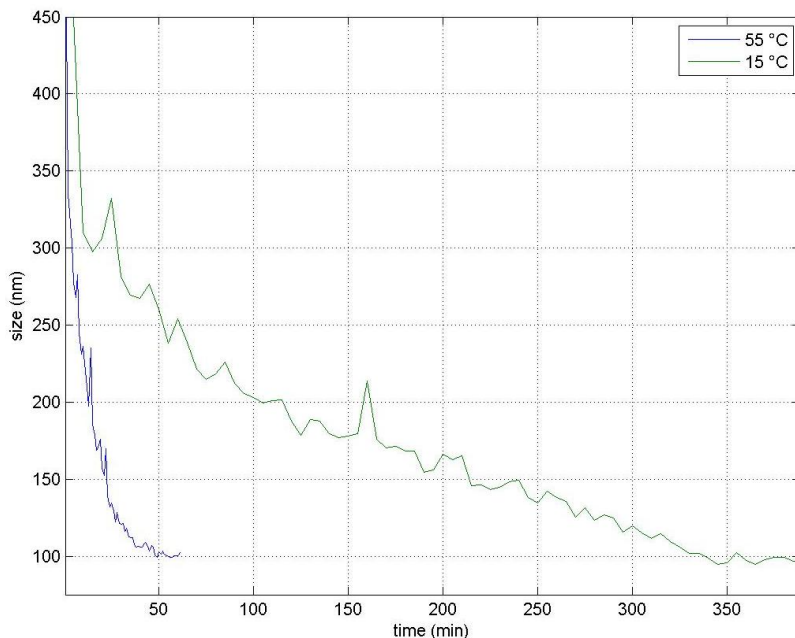


Figure 3.6 Network size as a function of time after competitive guest addition at different temperatures 55°C (blue trace) and 15°C (green trace).

Finally we monitored the assembly process also with optical absorption spectroscopy, in the visible region, in order to obtain a simpler and faster tool to measure the network formation.

Absorption spectra of network solution were acquired during the formation process and data related with DLS measurements carried out at the same experimental conditions. From the analysis of the absorption spectra acquired at different times (Figure 3.7a), parallel to the network growth, an increase of the background absorption is observed in the infrared region with concomitant shift towards longer wavelength of the absorption peak, due to the gold plasmon resonance. This second feature is in accordance with previous observation. The aggregation process leads to a moderate red shift of the Plasmon Band Resonance (PBR) of the AuNPs. We also found an experimental relation between the network size and their optical features, in particular between size and NIR absorption as reported in Figure 3.7b.

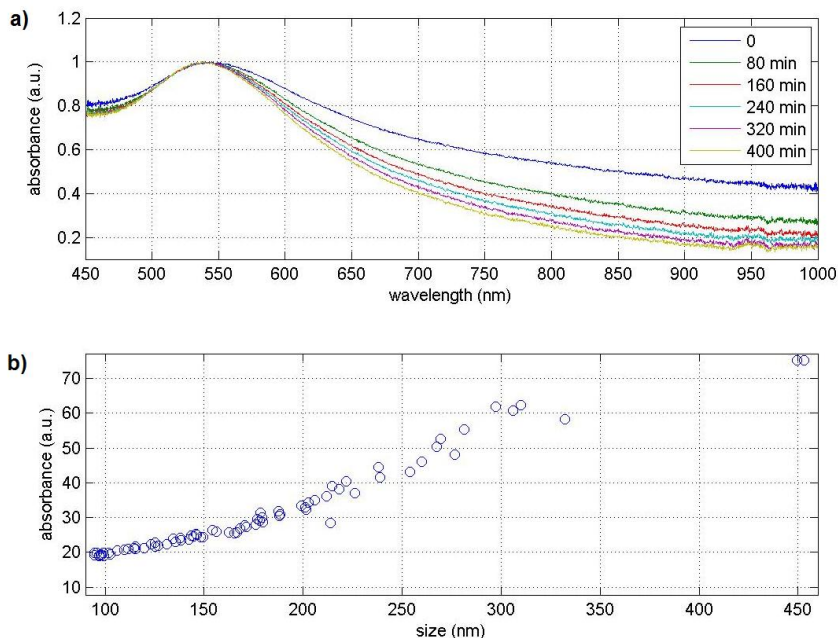


Figure 3.7 a) Absorption spectra of network growth at different time; b) Correlation between network size and NIR absorption.

3.2.2 Solvent Effect on Network Formation.

We studied the solvent influence on network formation as a function of the temperature, selecting three different solvents. We characterized first the network dissolved in chloroform, where both components have a good solubility and then we selected toluene and ethanol which have different affinity towards the AuNPs and the pegylated guest. In chloroform there is no temperature effects on the networks size. The DLS decay times measured as a function of temperature reflects the trend of the viscosity of the pure solvent, therefore the calculated size results constant (Figure 3.8).

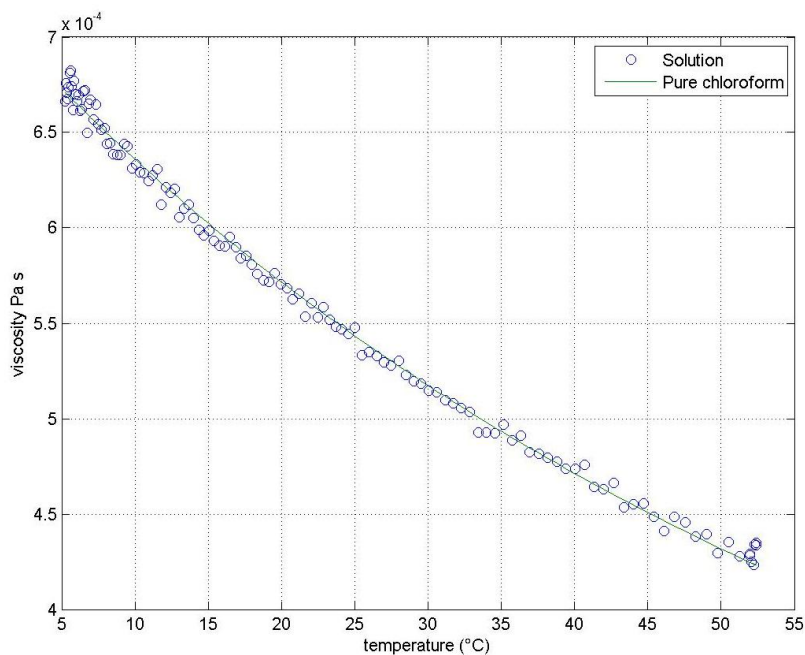


Figure 3.8 Solution viscosity of the network in chloroform as function of temperature.

The same experiment in toluene, shown in Figure 3.9, evidences a deviation of the DLS decay time from the pure solvent viscosity which is consistent with an increase in network size at lower temperatures.

Here we remark however, that with DLS technique both solute size and solution viscosity are calculated from the single measured parameter τ , in principle the reported effect could be also consistent with a deviation of the solution viscosity respect that of the pure solvent.

Probably, in the low temperature regime the nanoparticles were brought very close together accounting for an apparent increase of the viscosity. Also, the solubility of PEG in toluene might positively influence the network dimension. In the high temperature regime, the thermodynamic control is retained: the disassembly process is favoured leading to a dimensional decrease.

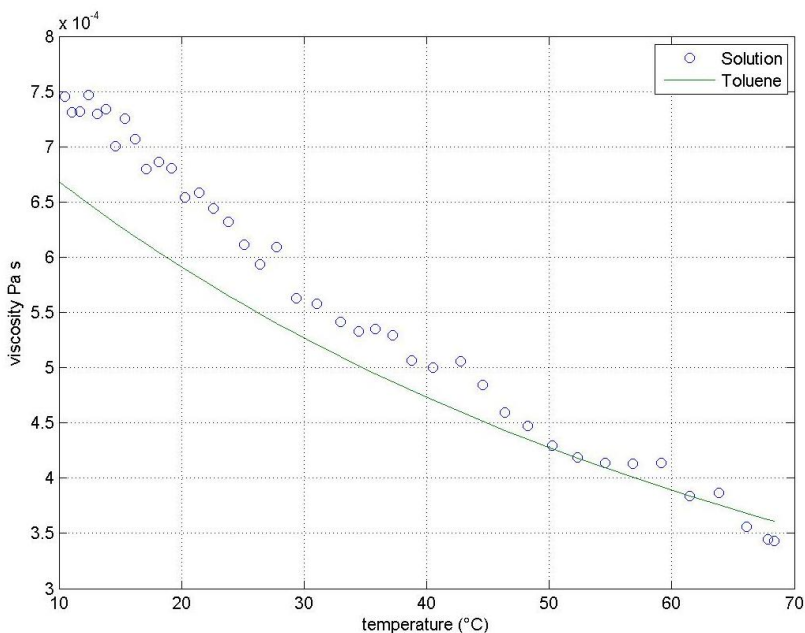


Figure 3.9 Solution viscosity of the network in toluene as function of temperature.

Finally the monitoring of the ethanol solution displayed an opposite sign behavior respect that observed in toluene (Figure 3.10). The DLS decay times decrease at lower temperature respect to the solvent viscosity, more precisely a transition takes place at a temperature of about 20 °C. Such transition corresponds to a shrinkage of the network of about 20%. These effects can be interpreted in two different ways: (i) a shrinking of the polyethylene oxide random coil observed in ethanol solution¹³ at low temperature; in our case the size reduction of the polymeric chains linking the gold nanoparticles reduces the entire network structure; (ii) the competitive effect of the solvent on the complexation strength. In fact, moving from chlorinated solvents to alcohols the association constant of the host-guest complex drops of two order of magnitude,^{11,14} moreover, ethanol is a suitable guest for tetraphosphonate cavity,¹⁴ competing with the methylpyridinium moieties, leading to a whole decrease of the number of cross-linking interactions. None of the two hypotheses explain the temperature threshold at 20°C. Experiments are in progress to determine the random coil dimensions of **1** in the three solvents.

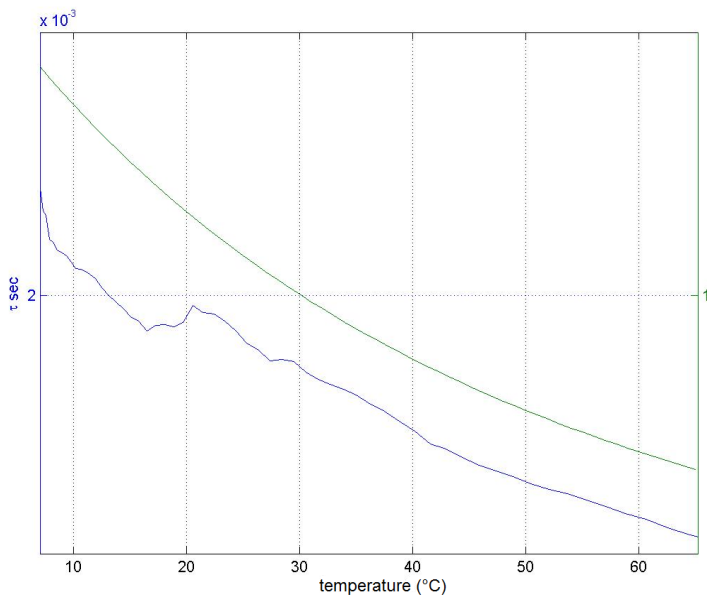


Figure 3.10 Solution viscosity of network in ethanol as function of temperature (pure ethanol green trace; network in solution blue trace).

3.3 Conclusions

In summary, we have studied the assembling dynamics of a supermolecular network composed by gold nanoparticles linked with a polymeric chain. In particular, we focused on the effects of two main parameters, namely temperature and solvent.

The experiments evidenced that the networks formation is highly temperature dependent, in fact at 16 °C larger objects were detected, whereas smaller ones are observed at higher temperature. This behavior is related to the disassembly process, which is predominant at higher temperatures; indeed the guest induced disassembly is faster at 55 °C. Therefore, since the network formation is under thermodynamic control, at lower temperature the enthalpic effect is predominant, leading to the larger objects observed.

Moreover, we studied the properties of the system in different solvents as a function of temperature. In toluene, at lower temperatures, we observed an increase network dimensions, which lead to a high deviation from the pure solvent behavior, which is restored at higher temperature. In ethanol, instead, substantial shrinkage of the networks is observed. Since alcohols are suitable guests for tetraphosphonate cavitands, the competitive effect exerted by the solvent could lead to the smaller objects observed, with concomitant deviation from the pure solvent behavior. Alternatively, the solvent affects the PEG random coil average dimension. Chloroform turned out to be the best solvent for the network formation, since it did not lead to deviations from the pure solvent behavior during the assembly/disassembly process.

The information inferred from these studies can be useful for the prediction of the temperatures and solvents effects for similar systems, based on guest induced aggregation of gold nanoparticles.

3.4 Acknowledgements

This work has been conducted in collaboration with Paolo Camorani of the Physis Department of University of Parma.

3.5 Experimental Section

The dynamic light scattering DLS measurements were carried out using a Malvern PCS 100 spectrometer, equipped with an Ar⁺ laser (Coherent Innova 70 C) operating at the wavelength $\lambda=647$ nm which is well outside the gold nanoparticles absorption band (peak at $\lambda = 522$ nm). The sample cell, a glass round cuvette of 10 mm diameter, is immersed in a index matching bath, where the temperature is controlled through an external thermal bath with an accuracy of 0.1 °C. The spectrometer includes a photomultiplier tube, operating in photon counting mode, mounted on a rotating arm provided by a goniometer spanning in an angles range of 10-150°. A computer equipped with an acquisition board (NI PCI-6602E) has been employed for the acquisition of the photon pulses and for computation of the signal autocorrelation function on a logarithmic scale spanning on 6 decades of time (10⁻⁵-10 sec). The photons arrival times have been continuously acquired and stored during the experiments with 100 ns resolution. The DLS autocorrelation functions have been calculated from the data acquired at different time intervals to characterize the processes kinetics.

3.6 References and Notes.

1. *Cluster and Colloids: From Theory to Applications*, Ed. Gunther Schmid, Wiley VCH, **2007**.
2. Li, M.; Johnson, S.; Guo, H.; Dujardin, E.; Mann, S. *Adv. Funct. Mat.*, **2011**, *21*, 851 – 859.
3. Ofir, Y.; Samanta, B.; Rotello, V. M. *Chem. Soc. Rev.*, **2008**, *37*, 1814-1825.
4. Chen, C.-L.; Rosi, N.L. *J. Am. Chem. Soc.*, **2010**, *132*, 6902 – 6903.
5. Boal, A.K.; Ilhan, F.; DeRouchey, J.E.; Thurn-Albrecht, T.; Russell T.P.; Rotello V.M. *Nature*, **2000**, *404*, 746-748.
6. Crespo-Biel, O.; Dordi, B.; Reinhoudt, D.N.; Huskens, J. *J. Am. Chem. Soc.*, **2005**, *127*, 7594-7600.
7. a) Aldaye, F.A.; Palmer, A.L.; Sleiman, H.F. *Science* **2008**, *321*, 1795 – 1799; b) Mcfarlane, R.J.; Lee, B.; Jones, M.R.; Schatz, G.C.; Mirkin, C.A. *Science*, **2011**, *334*, 204 - 208.
8. Tam, J.M., Murthy, A.K.; Ingram, D.R., Nguyen, R.; Sokolov, K.V.; Johnston, K.P. *Langmuir*, **2010**, *26*, 8988 - 8999.
9. a) Li, J.; Li, W.; Huo, H.; Luo, S.; Wu, C. *Macromolecules*, **2008**, *41*, 901 – 911; b) Parashchuk, O. D.; Laptinskaya, T.V.; Ananieva, M.S.; Parashchuk D.Y. *Soft Matter*, **2011**, *7*, 5585 – 5594.
10. a) Biavardi, E.; Favazza, M.; Motta, A.; Fragalà, I.L., Massera, C.; Prodi, L.; Montalti, M.; Melegari, M.; Condorelli, G.G.; Dalcanale E. *J. Am. Chem. Soc.* **2009**, *131*, 7447 – 7455; b) Biavardi, E.; Battistini G.; Montalti, M.; Yebeutchou, R.M.; Prodi, L.; Dalcanale, E. *Chem. Commun.* **2008**, 1638 1640.
11. Tancini, F.; Yebeutchou, R.M.; Pirondini, L.; De Zorzi, R.; Geremia, S.; Sherman, O.A.; Dalcanale E. *Chem. Eur. J.*, **2010**, *16*, 14313 – 14321.
12. Whitesides, G.M.; Mathias, J.P.; Seto, C.T. *Science*, **1991**, *254*, 1312 – 1319.
13. a) Bedrov, D.; Smith, G.D. *J. Chem. Phys.*, **2003**, *118*, 6656 – 6663; b) Oesterhelt, F.; Rief, M.; Gaub, H.E. *New J. Phys.*, **1999**, *1*, 6.1; c) Kreuzer, H.J.; Wang R.L.C.; Grunze, M. *New J. Phys.*, **1999**, *1*, 21.1.
14. Menozzi, D.; Biavardi, E.; Massera, C., Schmidtchen, F.-P.; Cornia, A.; Dalcanale, E. *Supramol. Chem.*, **2010**, *11*, 768 – 775.

Cavitand-functionalized SWCNTs for *N*-methylammonium salts sensing in water

4

4.1 State of the Art.

Carbon nanotubes (CNTs) isolated for the first time in 1991 by Ijima,¹ and they are hollow cylinders formed by rolling a graphite sheet. Depending on the orientation of the tube axis relative to the carbon network, different types of CNTs, described by the indices of their chiral vector, n and m , can be obtained.² The CNTs that are formed by connection of the head and tail of the chiral vector are referred to by their respective indices. Armchair CNTs ($n=m$) usually show metallic conductivity, while zigzag ($m=0$) or chiral ($n \neq m$) CNTs are semiconducting (Figure 4.1).

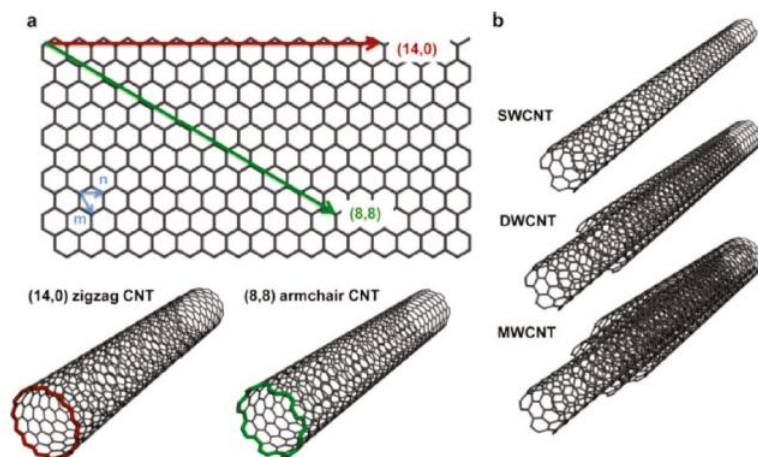


Figure 4.1 Structural variety of CNTs a) Orientation of the carbon network in armchair (n,n); and zig-zag ($n,0$) CNTs. b) Single, double, multi walled CNTs.

Additionally, carbon nanotubes can vary by the number of carbon layers in their sidewalls. Single walled CNTs (SWCNTs), double walled (DWCNTs) and multi walled (MWCNTs) are currently synthesized and commercially available.

Over the years, CNTs have attracted a great deal of attention due to their unique and spectacular properties, which are structure related. In fact CNTs possess outstanding electrical, thermal and mechanical properties. For example a current density as high as 10^9 A/cm², thermal conductivity of about 3000 W/MK, and Young modulus of 1.8 TPa are observed in pristine nanotube.²

However, a huge hurdle in the widespread use of CNTs lie in their insolubility in common organic solvents and water. They can be dispersed in some solvents by sonication, but precipitation is observed when the process is interrupted, furthermore, long sonication time could lead to alteration of electrical properties.³

The key to overcome these problems is chemical modification. Functionalization of the side wall of CNTs can improve solubility and, at the same time, add a further active functions which facilitate the integration in inorganic, organic and biological systems.⁴

The main approaches for the modification of the carbon structures can be grouped in three categories:

- Noncovalent adsorption or wrapping of various functional molecules;
- Covalent attachment of chemical groups through reaction onto the π -conjugated skeleton of CNT;
- Endohedral filling of their inner empty cavity

Noncovalent functionalization of CNTs is particularly attractive because it offers the possibility of decorating CNTs without affecting their electronic properties. The noncovalent interaction is based on van der Waals forces or π - π stacking.

The covalent approach has the remarkable potential to provide higher degree of tunability of CNTs properties, compared with noncovalent methods. Nevertheless, very reactive addends are needed, because the strictly electronic requirements.⁵ Current efforts for CNTs functionalization have focused on halogenation, hydrogenation, alkylation, polar and pericyclic reactions.^{4,6} Among all, cycloadditions are very attractive having additional functional groups tolerance leading to higher degree of tunability (Figure 4.2).⁷

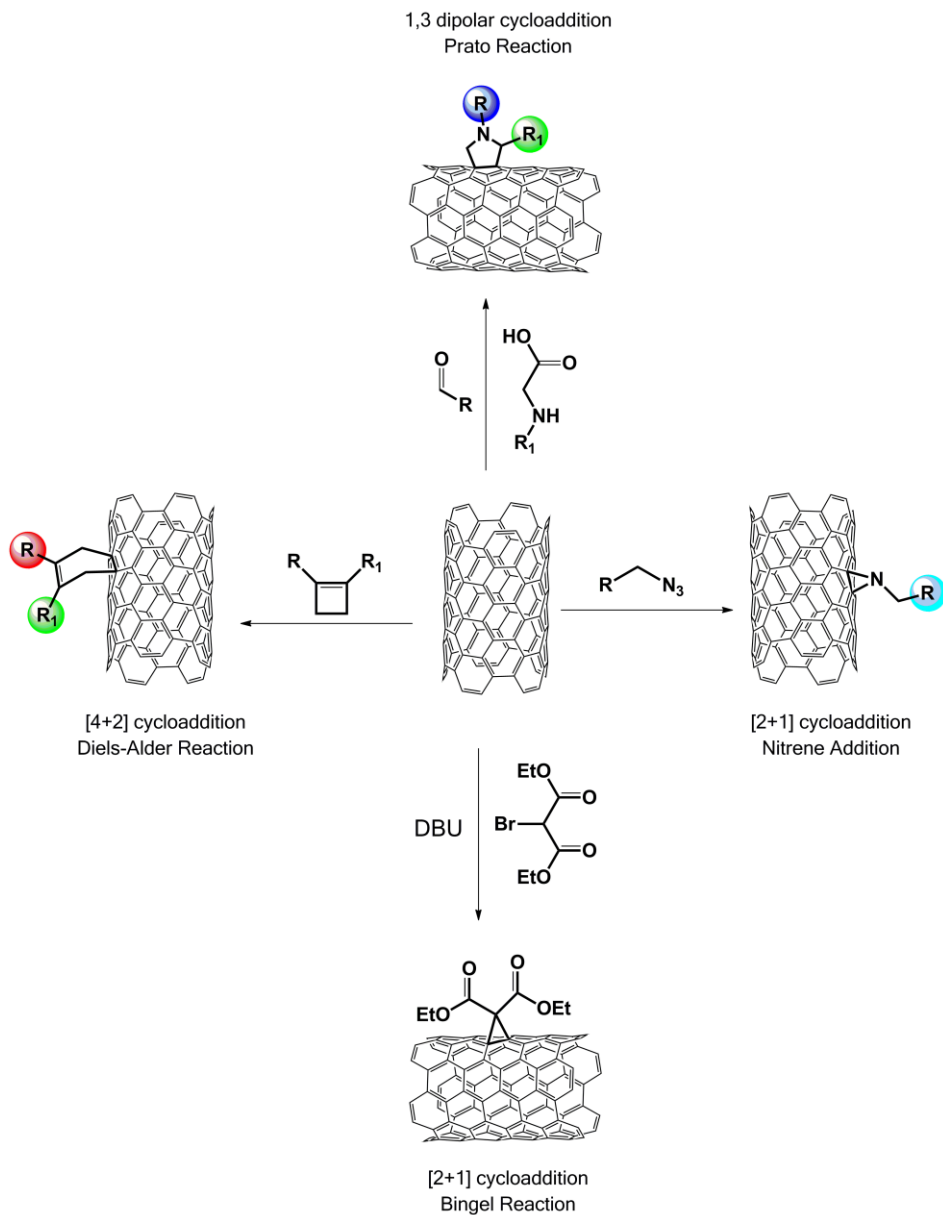


Figure 4.2 Cycloaddition reactions possible on CNTs.

In the 2002, Prato *et al.*⁸ reported on the successful modification of graphitic material using a 1,3 dipolar cycloaddition with an azomethine

ylides (Figure 4.2). The ylide is thermally generated *in situ* by condensation of an α -amino acid and an aldehyde, leading pyrrolidine fused ring. However, due to long reaction times, there are still some limitations. To overcome such constraints a microwave assisted cycloaddition is employed. Nevertheless, other functionalization, based on polar approach, have been reported.⁹ Diels-Alder reactions have been exploited to a lesser extent due to low reactivity of CNTs as diene; [2+1] cycloadditions, instead, are fairly studied, since the ease of reaction protocols.⁷

In the so called Bingel reaction, a cyclopropane ring is formed by addition of diethyl bromomalonate, under basic conditions (Figure 4.2). Conversely, an aziridine ring is observed in presence of nitrene intermediate, derived from an azide reagent. This second synthetic route present several advantages: i) the synthesis of the azide can be scaled under relatively mild conditions; ii) the functionalization process does not cause a severe damage of CNTs; iii) various functional group can be introduced onto CNT and iv) the reaction can be carried out either under UV irradiation or under thermal conditions.¹⁰

Once the surface of SWCNTs is modified it is possible to introduce additional functional groups by post-cycloaddition, using, for example click chemistry approach, which is tolerant even to biological frameworks.⁷

CNTs, either pristine or functionalized, have merged as innovative material due to their unique properties. It has been suggested their use in different field of applications, ranging from electronics (as electrode or capacitor) to catalysis (in fuel cells or as a support in heterogeneous catalysis).¹¹ Because the electronic properties, quasi monodimensional aspect and large surface-to-volume ratio, CNTs are very useful when developing extremely small sensors that are sensitive to the chemical and mechanical or physical environment.¹² In 2000, Kong *et al.*¹³ reported on the detection of NO₂ and NH₃ by exposure of pristine CNTs. Over the years an impressive number of examples appeared.¹⁴ However, the necessity of improving selectivity and fast response ask for innovative solutions.

Polymers, metal nanoparticles and DNA have been reported as functional materials for enhancing the selectivity of such systems.¹⁵ To boost both selectivity and sensitivity molecular recognition seems a powerful strategy.¹⁴

For example, Zhao *et al.* used pyrenecyclodextrins units to fabricate pyrene cyclodextrin-decorated SWCNTs via π - π stacking interactions.¹⁶ They were able to selective detect different kind of guest molecules, according to the association constant between the guest and the cyclodextrin (CD). The higher the association constant, the stronger is the signal shift (Figure 4.3).

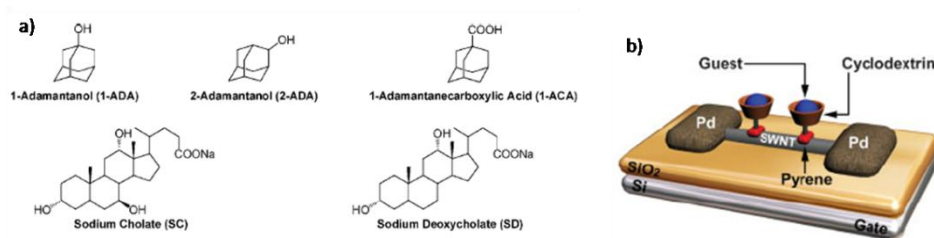


Figure 4.3 a) chemical structures of guest molecules and b) sensing device system.

Recently, Swager *et al.* reported on the selective detection of *p*-xylene, among a mixture of xylene isomers.¹⁷ The key feature is the introduction of a calixarene scaffold on a polythiophene polymer. The molecular recognition is shape driven, indeed, branched isomers cannot interact strongly with the cavity (Figure 4.4). Interestingly, the system is insensitive to humidity, this is due to the polymer layer that insulates SWCNTs from environmental influences.

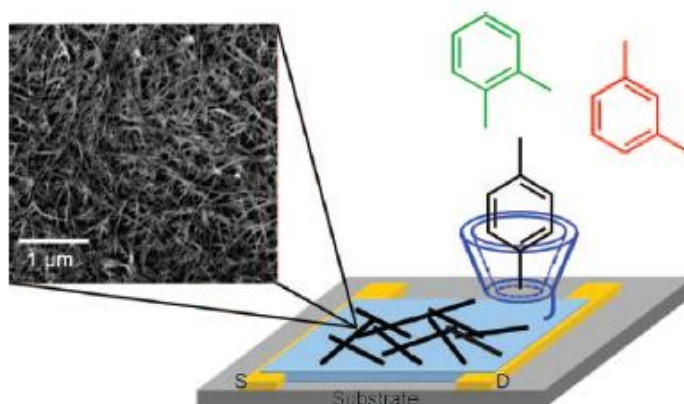


Figure 4.4 Schematic representation of the selective recognition of *p*-xylene.

Nowadays, controlling environmental pollution is of great interest, so building sensors for the detection of vapor phase pollutants are fashionable.¹²

In this regard, the Swager group reported on the fabrication of a sensor array based on multiwalled carbon nanotubes.¹⁸ They were able to switch the properties of the sensor device varying the functional groups on the side wall of the CNTs (Figure 4.5). For the modification they employed both direct covalent chemistry and post-functionalization strategies.

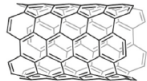
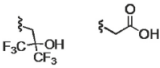
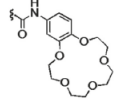
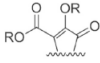
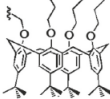

<p>MWCNT</p> 	<p>H-bond Acidity</p>  <p>Targeted Analytes: H-bond Acceptors such as Ethers, Ketones</p>	<p>H-bond Basicity</p>  <p>Targeted Analytes: H-bond Donors such as Acids, Alcohols</p>
<p>Polarity</p>  <p>R = allyl or propargyl</p> <p>Targeted Analytes: Vapors with High Polarity Such as Ketones, Ethers</p>	<p>Polarizability</p>  <p>Targeted Analytes: Aromatic and Chlorinated Hydrocarbons</p>	<p>Nonpolar Adsorption</p>  <p>Targeted Analytes: Aliphatic Hydrocarbons</p>

Figure 4.5 Selected recognition groups for differential interactions with target analytes.

By means of this library, they were able to selective detect twenty different volatile organic compounds (VOCs), with excellent device-to-device reproducibility. As expected, the chosen functionality, induced different conductance changes in the individual sensors for each of the VOCs, thereby creating a unique multidimensional response pattern. Alternatively, the detection of persistent organic pollutants (POPs) in liquid phase has been reported.¹⁹ CD decorated-SWCNTs were dipped in an aqueous solution of different POPs. Conductance decrease, of the sensor array, is observed upon guest inclusion.

Very attractive is the use of CNTs as sensor platform in biosensing for DNA, antigen-antibody, cells and several biomolecules.²⁰ The key step in CNTs-based biosensing is the immobilization of biomolecules on the surface of CNTs as recognition element. Also in this case supramolecular chemistry plays an important role. For example glucose oxidase was immobilized on CNTs sidewall by host-guest chemistry for glucose detection (Figure 4.6).²¹

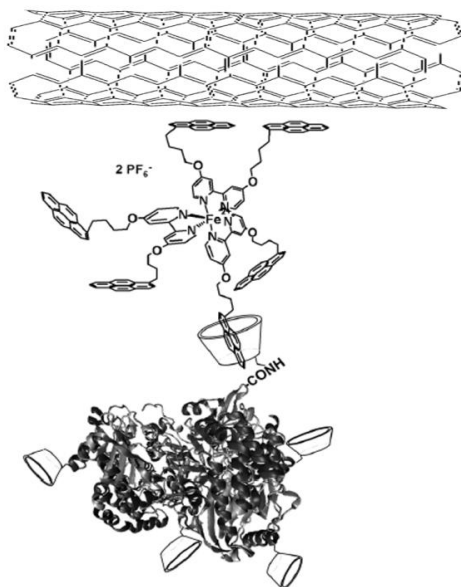


Figure 4.6 *Glucose biosensor by supramolecular assembly.*

A tris bipyridinyl iron complex is decorated on the periphery with six pyrene units. The metal complex was then attached to CNT sidewall by π -stacking interactions. Glucose oxidase (GOx) is modified by β -cyclodextrin (β -CD) due to the fact that pyrene molecules can be included in. The glucose sensor is self-assembled in water, with very high performance in glucose detection, by oxidation of glucose with concomitant reduction of oxygen in H_2O_2 .

In this thesis we will explore the covalent functionalization of SWCNTs with a tetraphosphonate cavitand by means of [2+1] cycloaddition reaction. We will fabricate a cavitand-decorated SWCNTs device in order to detect methyl ammonium salts in water.

4.2 Introduction.[§]

Carbon nanotubes (CNTs) are a desirable platform for sensor engineering, because of their electrical properties and quasi one-dimensional structure.²² Although very sensitive, pristine CNTs lack in selectivity.^{12a,14} Polymers,²³ metal nanoparticles²⁴ and biomolecules²⁵ have used to improve CNTs sensing properties. Embedding molecular recognition units is the ultimate strategy for imparting high selectivity and sensitivity into sensor systems.²⁶ So far, the host-guest approach has been shown to be a powerful tool for tailoring molecular recognition properties: introduction of cyclodextrins or calixarenes on the sidewall of CNTs lead to the selective recognition of either small molecules or volatile compounds.^{16,17,18,19,27}

Tetraphosphonate cavitands, another powerful class of molecular receptors, offer remarkable complexation capabilities toward charged N-methylammonium species.²⁸ The complex between tetraphosphonate cavitand and N-methylbutylammonium chloride exhibits a high K_a value, about $4 \cdot 10^5 \text{ M}^{-1}$ in methanol,²⁹ making tetraphosphonate cavitands an interesting candidate for specific sensing of methylammonium species.

Herein we explore the molecular recognition properties offered by the tetraphosphonate cavitand **Tiiii[N₃, CH₃, Ph]**³⁰ **1** (Chart 1) installed on single-walled CNTs (**SWCNTs**), toward small ammonium ions in the liquid phase. While non-covalent attachment of the receptors to the CNTs has been shown to provide good sensing results in other systems, we chose a covalent attachment strategy for a better long-term stability of the material under liquid sensing conditions.

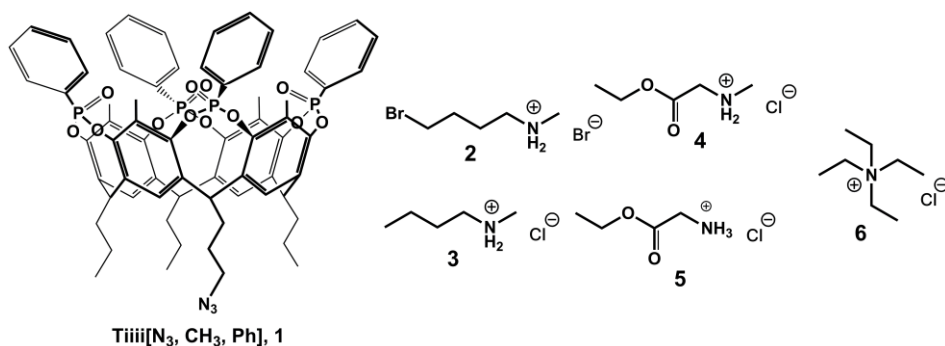
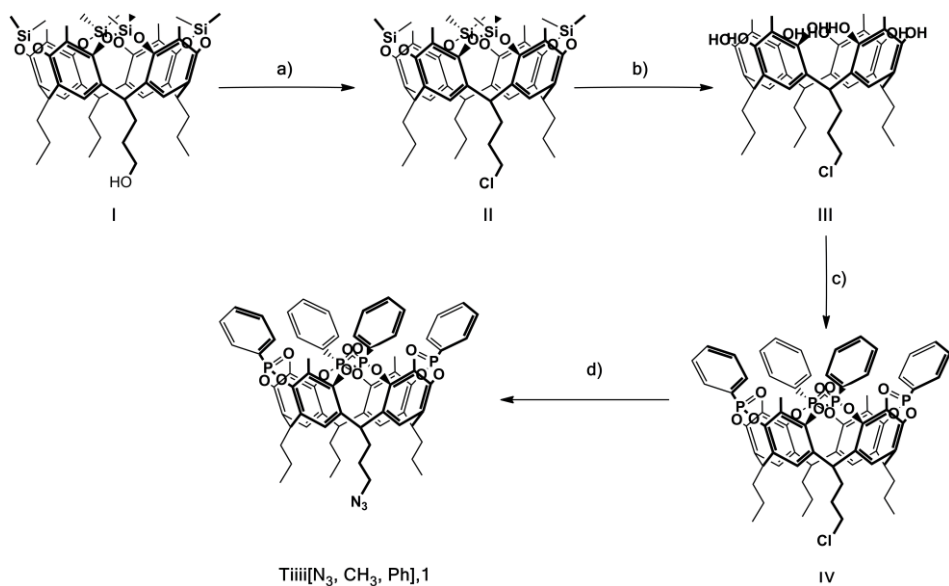


Chart 4.1 Molecules used in this chapter.

[§] A communication summarizing the content of this chapter is submitted.

4.3 Results and Discussions.

The introduction of an azide group at the lower rim of this cavitand allows the covalent functionalization of **SWCNTs** by a thermal [2+1] cycloaddition reaction,^{4,10} with very limited structural damage to the CNTs compared to other methods such as oxidation with nitric acid.^{11a} The designed tetraphosphonate cavitand **Tiiii**[N₃, CH₃, Ph], **1**, from now onward referred as **Tiiii**, was prepared in four steps and 16% overall yield, starting from the monohydroxy footed silyl cavitand.^{28a,31} The key steps of the synthesis were the stereospecific introduction of four inward-pointing phosphonate bridges at the upper rim of the resorcinarene skeleton and the installation of an azide moiety (Scheme 4.1)



Scheme 4.1 Synthesis of **Tiiii**[N₃, CH₃, Ph], **1**: a) SOCl₂, toluene, DMF, 50°C, 3h, 93%; b) TBAF, THF, r.t., 30 min., quantitative; c) 1- PhPCl₂, py, 75°C, 3h; 2- H₂O₂, r.t. 1h, 56% over two steps; d) NaN₃; DMF, 50°C, 16h, 86%.

The covalent functionalization of **SWCNTs** was achieved by a thermal aziridination, in o-DCB at 160°C for 2 days (Figure 4.7).

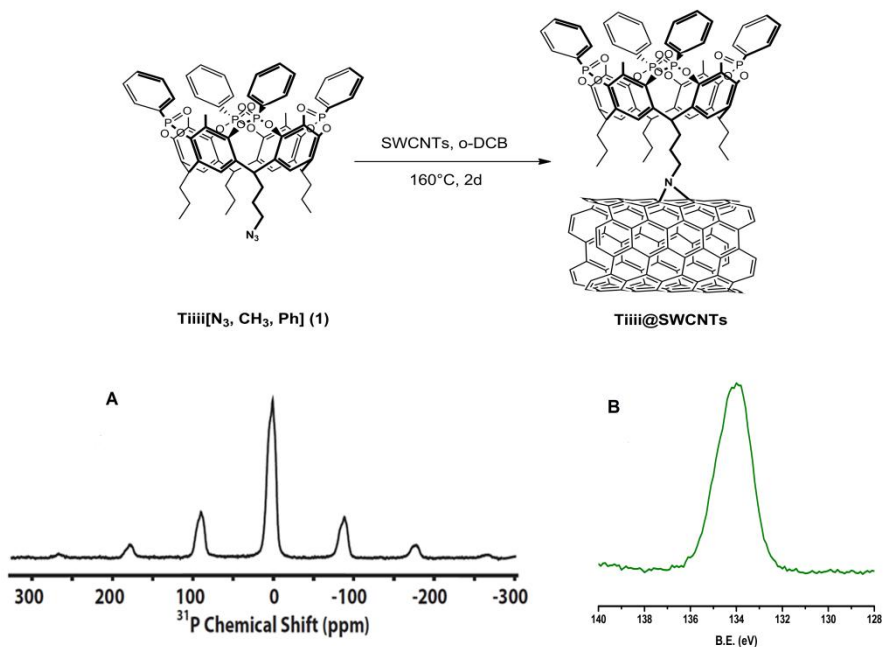


Figure 4.7 SWCNTs functionalization with **TiIII[N₃, CH₃, Ph] (1)**; a) ³¹P MAS-NMR spectra of **TiIII@SWCNTs**; b) XPS analysis: P 2p region.

The covalently functionalized **TiIII@SWCNTs** were characterized by attenuated total reflectance fourier transform infrared spectroscopy (ATR FTIR), X-ray photoelectron spectroscopy (XPS) and ³¹P magic-angle spinning nuclear magnetic resonance (MAS NMR). The infrared spectra (between 1000 and 1500 cm⁻¹) of **TiIII@SWCNTs** showed a broad band arising from the stretching of the PO bonds, P-phenyl group and the aromatic skeleton, which overlap with one another. By comparison with **TiIII** ATR FTIR spectra the azide peak is no longer visible, indicating the aziridination of the **SWCNTs** (Figure 4.8).

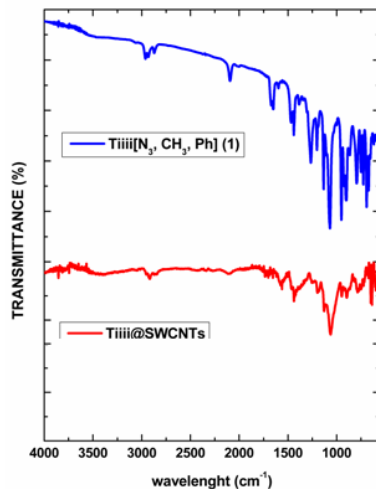


Figure 4.8 ATR-FTIR spectra of **TiIII[N₃, CH₃, Ph] (1)** (blue line) and **TiIII@SWCNTs** (red line).

XPS confirmed the presence of the cavitand as evident by the P 2p and N 1s peaks at a density of one cavitand for every 50 CNT carbon atoms (based on the P 2p vs. C 1s signal- Figure 4.7 b). MAS NMR was utilized to further analyze the functionalized CNTs. The use of this technique is increasing for the characterization of modified CNTs based on the ¹³C nucleus.³² However, obtaining high-resolution ¹³C NMR spectra of CNTs remains a challenge due to the low isotopic abundance (1.1%, ¹³C) and great variability of carbon sites with different chemical shifts commonly seen in CNT sample.^{32c} In contrast to this, a very clear MAS NMR spectrum of **TiIII@SWCNTs** was obtained by probing ³¹P of the cavitand benefiting from high natural abundance (100%) and high gyromagnetic ratio leading to greater sensitivity (Figure 4.7 a).

In order to evaluate the molecular recognition capabilities of **TiIII@SWCNTs**, we treated a dichloromethane suspension of the functionalized **SWCNTs** with XPS diagnostic guest 4-bromo-*N*-methylbutylammonium bromide, **2** (Figure 4.9 red trace).³³ After washing to remove any unbound **2**, the CNTs were analyzed by XPS. The presence of the Br 3d XPS signals indicated successful binding of **2** to **TiIII@SWCNTs**. Finally, the sample was subjected to an intense washing with 1,8-diazabicyclo[5.4.0]undec-7ene (DBU). In previous experiments, it has been shown that DBU can deprotonate the guest, breaking the cavitand-guest complex. Protonated DBU cannot interact

with the cavity, by steric hindrance, leaving free host.³⁴ Indeed treatment with DBU leads to deprotonation of the guest **2** and decomplexation as evident by the disappearance of the Br 3d signal in the XPS spectrum (Figure 4.9 green trace). Pristine **SWCNTs** were used in a control experiment and no Br signals were detected, ruling out non-specific interactions of the guest with the CNTs.

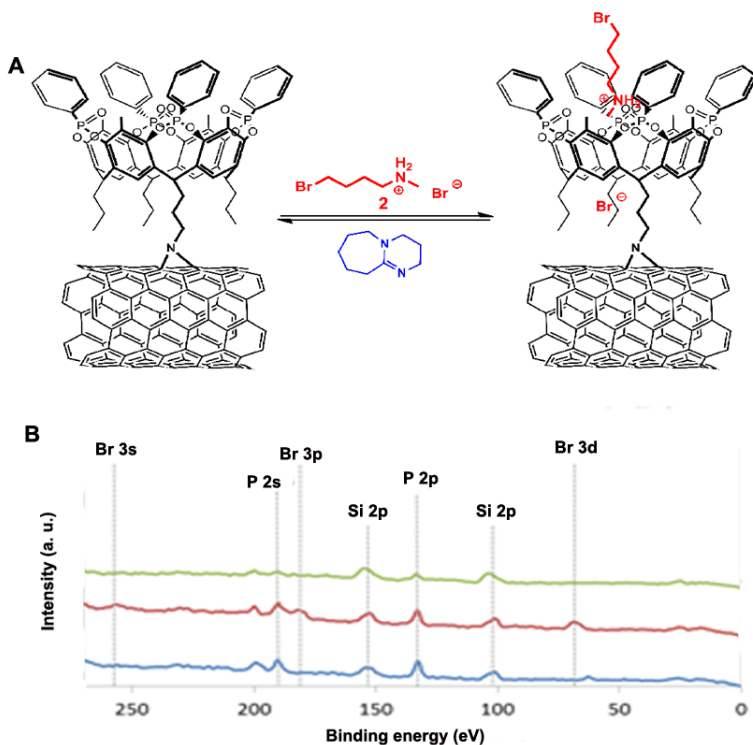


Figure 4.9 XPS binding study with **TiIII@SWCNTs**. A) Reversible binding of **2** B) XPS analysis of **TiIII@SWCNTs** before exposure to **2** (blue), after exposure to **2** (red) and after subsequent washing with DBU (green). Si signals are due to the utilized Si substrate.

To further confirm that the guest binds directly to the cavitand on the CNTs, **TiIII@SWCNTs** were treated with a solution of N-methylbutylammonium chloride, **3** and subsequently analyzed by ³¹P MAS NMR. The ³¹P environment undergoes a structural change when an interaction exists between **TiIII@SWCNTs** and the guest. This is seen using in the NMR spectrum (Figure 4.10 b green trace) as a sharp

resonance appearing above the broader resonance. This can be associated with a different chemical environment of the host-guest complex. This is in accordance with solution NMR of the cavitand guest complex that is not attached to CNTs backbone.^{28b}

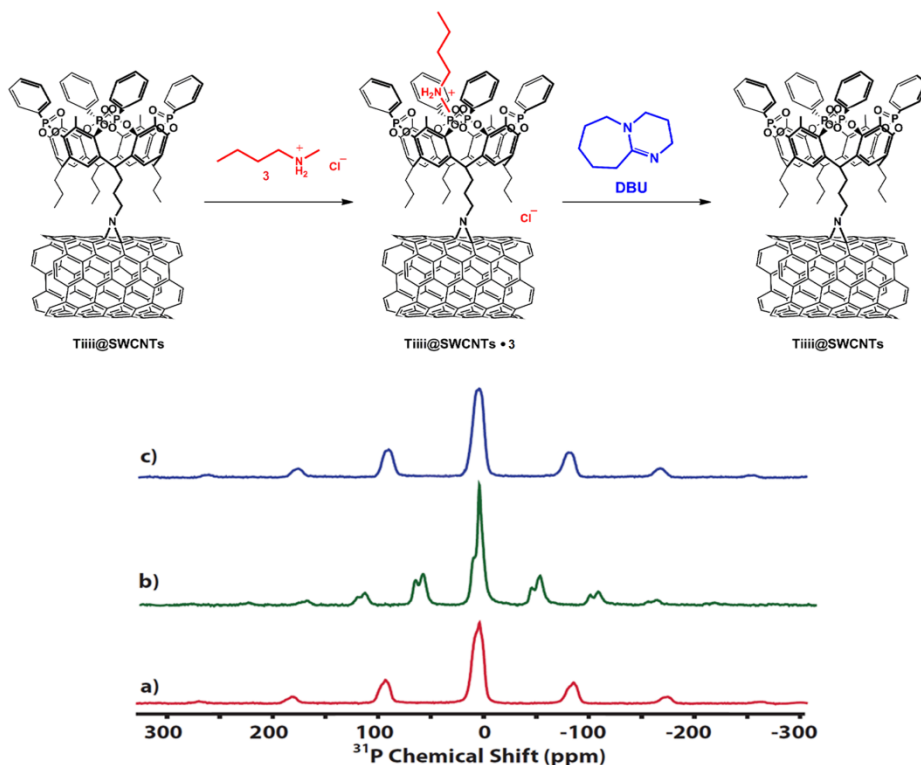


Figure 4.10 Guest-Host binding studies using ³¹P MAS NMR showing reversibility of the host molecule: a) **TiIII@SWCNTs** (black trace); b) after guest molecule incorporation (green trace) and c) after base treatment (blue trace).

Again the sample was treated with DBU. MAS NMR of the product after this washing step returned to the initial parameters of **TiIII@SWCNTs** spectrum confirming the successful removal of the guest (Figure 4.10c, blue trace). Noteworthy, the formation of the host-guest complex can be triggered by the choice of acidic or basic conditions.

These results prompted us to investigate the functionalized SWCNTs in a chemoresistive device for the detection of sarcosine, the N-methylated derivative of glycine. Sarcosine is structurally related to the previously studied guests and has been proposed as a biomarker for the

progression of prostate cancer,³⁵ although the debate is still open.³⁶ In aqueous environment, **Tiiii** binds sarcosine over glycine with complete selectivity.³⁷ The source of this exquisite selectivity is the presence of water insensitive CH₃- π interactions between the N-methyl residue of sarcosine and the **Tiiii** cavity, which triggers the formation of two H-bonds and the setting of cation-dipole interactions between the cavitand and sarcosine.

To prepare the sensor, an aliquot of the reaction solution of **Tiiii@SWCNTs** was directly deposited onto a glass slide decorated with two Au electrodes. After washing the device to remove any excess of reagent and subsequent drying, the device was put into an enclosure which was connected to a syringe pump. Using the setup, the device was alternately exposed to Milli-Q water to a solution of an analyte while the current through the CNT network (at $U = 50$ mV) was measured.

Initial measurements with sarcosine showed an increase in current when a device with **Tiiii@SWCNTs** was exposed to the analyte at pH 7. The magnitude of the change in current was however strongly dependent on the pH of the solution and at pH 5 no change in current was observed upon exposure of the device to sarcosine.

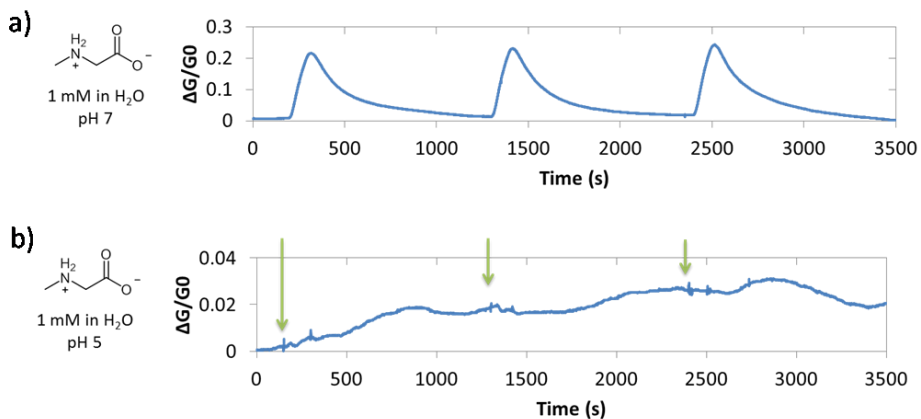


Figure 4.11 Sensing of sarcosine with **Tiiii@SWCNTs** at a) pH 7; b) at pH 5 (arrows indicate exposure to analyte).

We attributed this strong pH dependence to the increased ionic strength of the medium which masks the analyte response. In order to eliminate this potential source of error, we investigated the hydrochloride salt of

sarcosine ethyl ester (**4**). As controls, glycine ethyl ester hydrochloride (**5**) tetraethylammonium chloride (**6**) that is too bulky for binding, were chosen.

Exposing the device to **4** resulted in an increase in current similarly exposing it to sarcosine while exposure to **5** or **6** led to a current decrease (Figure 4.13 B; and experimental part for further details). In many chemoresistive sensing systems a current change in the same direction is observed for the desired analytes and controls, albeit usually stronger for the target molecule. Instead, a current switch in the opposite directions for the target analyte and interferences is unprecedented, especially for compounds as closely related as **4** and **5**. Observing a change with a different sign can provide a powerful level of selectivity as it can potentially distinguish between analytes regardless of their concentration. Controls with pristine **SWCNTs** showed a decrease in current for all investigated analytes (Figure 4.13 A and B). In order to minimize the effect of a changing ionic strength of the solution on the sensing response, a device with **Tiii@SWCNTs** was alternately exposed to a 1 mM solution of **4** and **5** (instead of an analyte solution and water). An increasing current was observed in this case as well when switching to **4** (Figure 4.12).

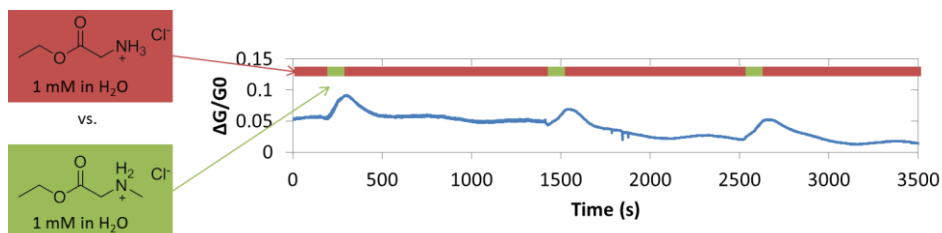


Figure 4.12 Alternating exposure of **Tiii@SWCNTs** to **4** and **5** at pH 5. Red bars indicate times during which the device was exposed to **5**, while green bars indicate exposure to **4**.

Finally, the detection limit for **4** was determined to be 0.02 mM (Figure 4.13 C). It should be noted that the devices exhibited very good stability and no significant change in sensitivity was observed over several months of regular operation.

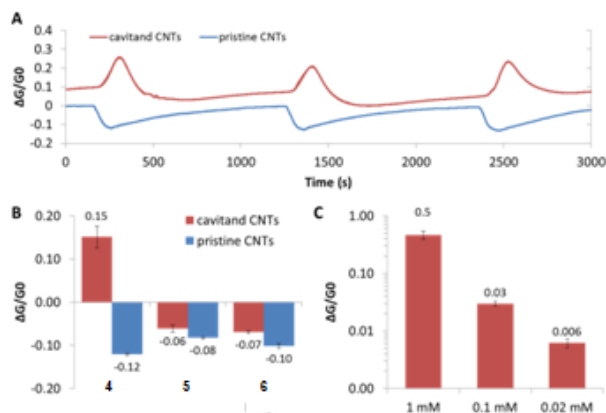


Figure 4.13 Liquid flow sensing experiments with **TiIII@SWCNT**-based devices. A) **TiIII@SWCNT** and pristine SWCNTs show opposite responses upon exposure to a 1 mM solution of **sarcosine ethyl ester hydrochloride, 4**. B) Comparison of the current change upon exposure of **TiIII@SWCNT** and pristine SWCNTs devices to **4** (**sarcosine ethylester hydrochloride**), **5** (**glycine ethylester hydrochloride**) and **6** (**tetraethylammonium chloride**). C) Response of **TiIII@SWCNT** devices to different concentrations of **4**.

4.4 Conclusions.

In summary, we have illustrated the use of covalent functionalized SWCNTs as a selective sensor in water. By introducing a tetraphosphonate cavitand as a specific molecular receptor, it was possible to selectively recognize the N-methylammonium species. The covalent functionalization provided a high stability of a **Tiiii@SWCNTs**-based device and allowed its use in liquid sensing. In a proof of concept experiment we demonstrated the selective detection of sarcosine ethyl ester hydrochloride **4**, up to 0.02 mM concentration. Interestingly, the sign of the current change upon exposure to the analyte is opposite of the controls allowing selective detection of the analytes, regardless their concentration. Studies concerning the sensing mechanism are ongoing in our laboratories.

4.5 Acknowledgment.

Special thanks to Prof. T.M. Swager, J. Schnorr and Dr. Vladimir Michaelis from the Department of Chemistry of Massachusetts Institute of Technology.

4.6 Experimental Section.

Monochloro silylcavitand (II).

To a solution of monohydroxy footed silylcavitand (0.76 g, 0.80 mmol) in dry toluene (15 mL), 5 drops of DMF were added. The suspension was cooled to 0°C and thionyl chloride was slowly added (2.40 mmol, 175 μ l). The resulting suspension was stirred for 2h at 50°C. The solvent was evaporated; the residue was dissolved in chloroform and washed with water and dried over MgSO₄. The removal of the solvent gave **II** as a brownish solid (0.72g, 0.74 mmol, 93%). **¹H-NMR (CDCl₃, 400 MHz):** δ = 7.21 (bs, 4H, ArH); 4.65 (t, 4H, ³J= 7.9 Hz, ArCH); 3.64 (t, 2H, ³J= 6.4 Hz, CH₂CH₂Cl); 2.39 (m, 2H, CH₂CH₂CH₂Cl); 2.21 (m, 6H, CH₂CH₂CH₃); 1.95 (s, 12H, ArCH₃); 1.82 (m, 2H, CH₂CH₂Cl); 1.35 (m, 6H, CH₂CH₂CH₃); 1.09 (t, 9H, ³J=7.3 Hz, CH₂CH₂CH₃); 0.55 (s, 12H, SiCH_{3,out}); -0.63 (s, 12H, SiCH_{3,in}). **ESI-MS:** *m/z* calcd. for C₅₂H₇₁ClO₈Si₄ (970.4), [M+Na]⁺: 993.4. Found: 993.5 [M+Na]⁺.

Monochloro resorcinarene (III).

To a solution of **II** (0.59 g., 0.60 mmol) in THF (15mL), acetic acid (6 mmol, 350 μ L) and 80% w,w TBAF (6 mmol, 1.90 mL) were added at 0°C. The solution was stirred for 30 min at room temperature, then NH₄Cl_(aq) was added. The solution was diluted with ethyl acetate and the organic layer was separated, washed three times with NH₄Cl_{aq}, then NaCl_{aq} and dried over MgSO₄. The removal of the solvent afforded **III** as a brown solid (0.47 g, 0.60 mmol, quantitative yield). **¹H-NMR (Acetone-d₆, 300 MHz):** δ = 8.37 (m, 8H, ArOH); 7.51 (s, 2H, ArH); 7.50 (s, 2H, ArH); 4.49 (t, 4H, ³J=7.9 Hz, ArCH); 3.71 (t, 2H, ³J= 6.7 Hz, CH₂CH₂Cl); 2.53 (m, 2H, CHCH₂CH₂CH₂Cl); 2.35 (m, 6H, CHCH₂CH₂CH₃); 2.13 (s, 12H, ArCH₃); 1.83 (m, 2H, CH₂CH₂CH₃); 1.38 (m, 6H, CH₂CH₂CH₃); 1.02 (t, 9H, ³J=7.3 Hz, CH₂CH₂CH₃). **ESI-MS:** *m/z* calcd. for C₄₄H₅₅ClO₈ (746.4), [M+Na]⁺ 769.6. Found: 769.50. [M+Na]⁺.

Monochloro footed tetraphosphonate cavitand Tiiii[Cl,CH₃, Ph] (IV).

To a solution of **III** (0.47g, 0.63 mmol) in freshly distilled pyridine (12 mL), dichlorophenylphosphine (380 μ L, 2.84 mmol) was added slowly at room temperature. After 3 hours of stirring under N₂ at 75 °C, the solution was cooled down to room temperature and 4.5 mL of aqueous

35% H₂O₂ were added. The resulting mixture was stirred for 1 h at room temperature, then the solvent was removed in vacuo. Addition of water resulted in the precipitation of a white powder. The crude was purified by column chromatography (Eluant 9:1 DCM:EtOH) affording **IV** as a brownish solid (0.44 g, 0.35 mmol, 56 %). **¹H-NMR (CDCl₃, 400 MHz):** δ = 8.13 (m, 8H, P(O)Ar**H_O**); 7.68 (m, 4H, P(O)Ar**H_P**); 7.58 (m, 8H, P(O)Ar**H_M**); 7.40 (bs, 4H, Ar**H**); 4.84 (t, 4H, ³J= 7.8 Hz, Ar**CH**); 3.74 (t, 2H, ³J= 7.2 Hz, CH₂**CH₂Cl**); 2.63 (m, 2H, **CH₂CH₂CH₂Cl**); 2.43 (m, 6H, **CH₂CH₂CH₃**); 2.20 (s, 12H, Ar**CH₃**); 1.92 (m, 2H, CH₂**CH₂CH₂Cl**); 1.47 (m, 6H, CH₂**CH₂CH₃**); 1.09 (t, 9H, ³J= 7.3 Hz, CH₂CH₂**CH₃**). **³¹P{¹H} NMR (CDCl₃, 161.9 MHz):** δ = 7.70 (bs,P(O)). **ESI-MS:** *m/z* calcd. for **Tiii[Cl, CH₃, Ph]** C₆₈H₆₇ClO₁₂P₄ (1234.32); [M+Na]⁺ 1257.75. Found:1257.78 [M+Na]⁺.

Monoazide footed tetrphosphonate cavitand Tiii[N₃, CH₃, Ph] (1).

To a solution of **Tiii[Cl, CH₃, Ph] (IV)** (0,44 g, 0.35 mmol) in DMF (15 mL), sodium azide was added (68 mg, 1.1 mmol). The solution was stirred overnight at 55°C. Then the solvent was evaporated and the crude was suspended in water and filtered affording **1** as a brown solid (0,38 g., 0.31 mmol, 86%). **¹H-NMR (CDCl₃, 400 MHz):** δ = 8.14 (m, 8H, P(O)Ar**H_O**); 7.65 (m, 4H, P(O)Ar**H_P**); 7.57 (m, 8H, P(O)Ar**H_M**); 7.19 (s, 4H, Ar**H**); 4.87 (m, 4H, Ar**CH**); 3.48 (t, 2H, ³J= 6.2 Hz CH₂**CH₂N₃**); 2.38 (m, 20H, **CH₂CH₂CH₂N₃** + **CH₂CH₂CH₃** + Ar**CH₃**); 1.73 (m, 2H, CH₂**CH₂CH₂N₃**); 1.47 (m, 6H, CH₂**CH₂CH₃**); 1.09 (t, 9H, ³J= 7.2 Hz, CH₂CH₂**CH₃**). **³¹P{¹H} NMR (CDCl₃, 161.9 MHz):** δ = 6.13 (bs P(O)). **HR ESI-MS:** calculated for C₆₈H₆₇N₃O₁₂P₄ (1241.36752) [M+Na]⁺: 1264.35729. Found:1264.35674.

General procedure for SWCNTs functionalization

10 mg of SWCNTs were placed in a schlenk and purged with argon for 10 minutes. **Tiii[N₃, CH₃, Ph] (1)** (200 mg, 0.16 mmol) was introduced with the addition of 1 mL of o-DCB. The suspension was sonicated for 10 minutes, then heated at 160°C for two days under argon. After evaporation of the solvent, the crude was dispersed in dichloromethane and sonicated for 10 min. Filtered on 2 μm millipore filter and washed with hexane, dichloromethane, acetone.

XPS complexation studies

To a dichloromethane (1 mL) suspension of **Tiiii@SWCNTs** (5 mg, 0.9 μM of cavitand) a guest solution in dichloromethane was added (5 equivalent of 4.3 μM dichloromethane solution). After 12h the suspension was filtered and the solid washed with dichloromethane. The solid was collected, dried, redispersed in dichloromethane and dropcasted on silicon slide for XPS measurement. After the XPS measurement, the material was sonicated with DBU (9.2 equiv relative to initially used guest) in 5 mL DCM for 10 min and then stirred over night. Afterward, the **Tiiii@SWCNTs** were collected by filtration, washed with DCM, dried and drop-cast for an XPS measurement.

As a control experiment, pristine SWCNTs (5 mg) were treated with a similar guest solution for 12 h. The sample was washed and dried in a similar fashion and then analyzed by XPS.

Solid State-NMR complexation studies

Tiiii@SWCNTs (40 mg, 7.5 μM) was treated with 5 equivalent of N-methylbutyl ammonium chloride (4.29 mM solution in dichloromethane). After 12h the suspension was filtered and the solid washed with dichloromethane. The powder was collected, dried and submitted for MAS NMR experiments.

The **Tiiii@SWCNTs•2** complex was redispersed in dichloromethane and treated with a excess of DBU solution (4.29 mM solution in dichloromethane). After 12h the suspension was filtered and the solid washed with dichloromethane. The powder was collected, dried and submitted for MAS NMR experiments.

^{31}P MAS NMR: NMR experiments were conducted on a home-built 360 ($B_0 = 8.4\text{T}$) spectrometer (courtesy of Dr. David Ruben) with a 4 mm triple-channel chemagnetics MAS probe. Samples were ground using a mortar and pestle, and placed within ZrO_2 rotors (60 μl volume). Spectral acquisition included Bloch and Hahn-echo experiments, using between 128 and 4096 co-added transients, spinning frequency (ω_r) between 0 and 12 kHz and high power ^1H decoupling ($\nu_{\text{rf}} = 83\text{ kHz}$) when required. Recycle delays were optimized for each sample and were typically 35 seconds. All ^{31}P data were referenced using 85% H_3PO_4 (0.0 ppm).

General procedure for sensing device preparation

Glass slides (VWR Microscope Slides) were cleaned by ultrasonication in acetone for 10 min, and after drying they were treated with ozone for 3 minutes. Using an aluminum mask, layers of chromium (10 nm) and gold (75 nm) were deposited leaving a 1 mm gap using a metal evaporator purchased from Angstrom Engineering.

1 mg of SWCNTs were put in a schlenk flask and purged with argon for 10 minutes. Afterward, **Ti^{III}[N₃, CH₃, Ph] (1)** (13 mg, 0.0105 mmol) in 100 μ l of *o*-DCB was introduced. The suspension was sonicated for 10 minutes, then heated at 160°C for two days under argon. The crude was directly drop-cast between the Au electrodes on the glass slide. Subsequently, it was washed by immersing in DCM, methanol and hexanes until the respective washing solution stayed clear.

General procedure for sensing measurements

The devices were enclosed in a homemade Teflon liquid flow chamber for sensing measurement (see Figure 4.14). The gold electrodes of the device are contacted with connections to the outside of the chamber, and two ports on opposite sides of the chamber allow to direct a continuous flow of liquid through the chamber.

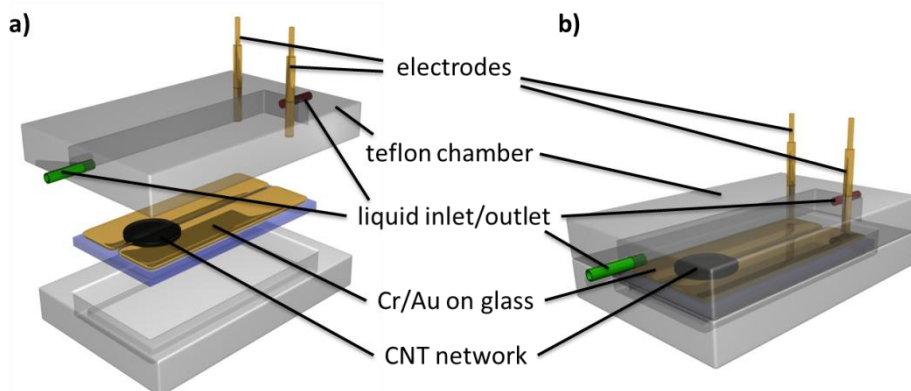


Figure 4.12 *Liquid flow chamber for sensing measurements.*

The inlet port of the flow chamber was connected to a tubing system with two 3-way valves that allowed directing a liquid from one of two syringes through the chamber (see Figure 4.13). By connecting both syringes to the same syringe pump, a constant flow rate of 0.5 mL/min was maintained for both syringes.

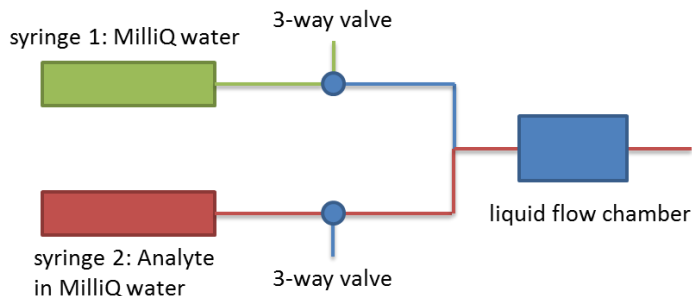
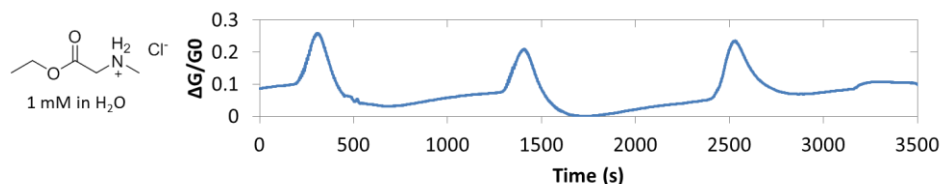


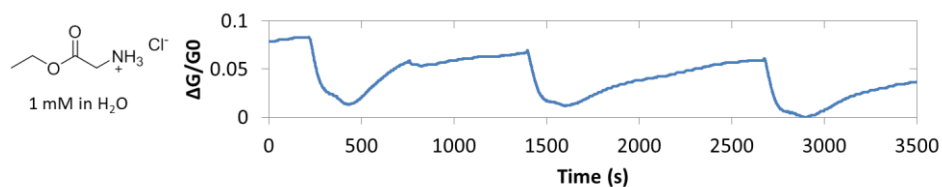
Figure 4.13 Setup for liquid flow sensing measurements. Using two 3-way valves, a liquid from one of two syringes could alternately be directed through the liquid flow chamber with the measurement device. Both syringes were connected to the same syringe pump ensuring the same flow rate for both liquids.

Electrochemical measurements were performed using an PalmSens handheld potentiostat connected to a laptop computer. A constant bias voltage of 0.05 V was applied across the device, while current vs. time was measured.

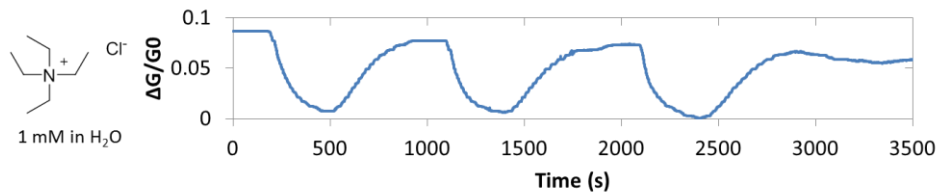
In a typical measurement, the device was first exposed to MilliQ water. Subsequently, a 1 mM analyte solution in water was directed through the device for 100 s, followed by MilliQ water for 1000 s. In each measurement, the device was exposed to analyte at least three times.



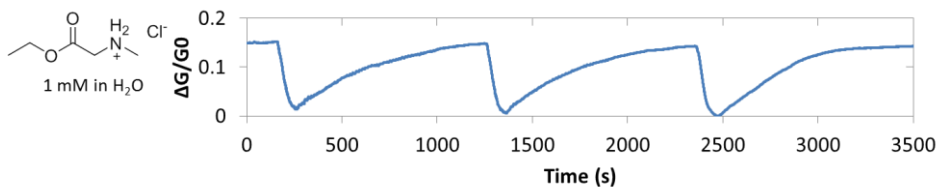
Sensing of **4** with **TiIII@SWCNTs** at pH 5.



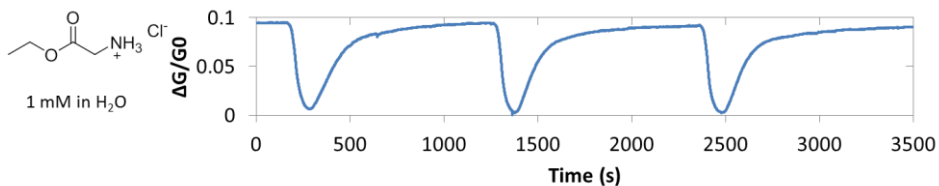
Sensing of **5** with **TiIII@SWCNTs** at pH 5.



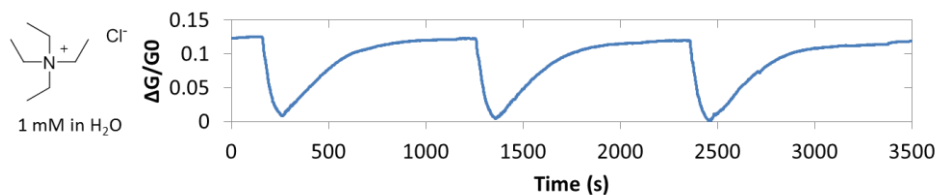
Sensing of **6** with **TiIII@SWCNTs** at pH 5.



Sensing of **4** with **pristine SWCNTs** at pH 5.



Sensing of **5** with **pristine SWCNTs** at pH 5.



Sensing of **6** with **pristine SWCNTs** at pH 5.

4.7 References and notes.

1. Ijima S. *Nature* **354**, 56 – 58.
2. *Carbon Nanotubes: Science and Applications*, Edt. M. Meyyappau, CRC Press, **2005**.
3. Lu, K.L.; Lago, R.M.; Chen, Y.K.; Green, M.L.H.; Harris, P.J.F.; Tsang, S.C. *Carbon* **1996**, *34*, 814 - 816.
4. Tasis, D.; Tagmatarchis, N.; Bianco, A.; Prato, M. *Chem. Rev.* **2006**, *106*, 1105 - 1136.
5. Banerjee, S.; Hemray-Benny, T.; Wong, S.S. *Adv. Mater.*, **2005** *17*, 17 - 29.
6. Peng, X.; Wong, S.S. *Adv. Mater.* **2009**, *21*, 625 - 642.
7. Kumar, I.; Rana, S.; Cho, J.W. *Chem. Eur. J.* **2011**, *17*, 11092 - 11101.
8. Georgakilas, V.; Kordatos, K.; Prato, M.; Guldi, D.M.; Holzinger, M.; Hirsch, A. *J. Am. Chem. Soc.* **2002**, *124*, 760 - 761.
9. Zhang, W.; Swager, T.M. *J. Am. Chem. Soc.* **2007**, *129*, 7714 - 7715.
10. Gao, C.; He, H.; Zhou, L.; Zheng, X.; Zhang, Y. *Chem. Mat.* **2009**, *21*, 360 – 370.
11. Schnorr, J.M.; Swager, T.M. *Chem. Mat.* **2011**, *3*, 646 - 657.
12. a) Potyrailo, R.A.; Surman, C.; Nagraj, N.; Burns, A. *Chem. Rev.* **2011**, *111*, 7315 - 7354; b) Snow, E.S.; Perkins, F.K.; Robinson, J.A. *Chem. Soc. Rev.* **2006**, *35*, 790 - 798; c) Kauffman, D.R.; Star, A. *Angew. Chem. Int. Ed.* **2008**, *47*, 6560 - 6570; d) Cao, Q.; Rogers, J.A. *Adv. Mater.* 2009, *21*, 29 - 53.
13. Kong, J.; Franklin, N.R.; Zhou, C.; Chapline, M.G.; Peng, S.; Cho, K.; Dai, H. *Science* **2000**, *687*, 622 - 625.
14. Liu, S.; Shen, Q.; Cao, Y.; Gan, L.; Wang, Z.; Steigerwald, M.L.; Guo X. *Coord. Chem. Rev.* **2010**, *254*, 1101 - 1116.
15. Lee, C.Y.; Sharma, R.; Radadia, A.D.; Masel R.I.; Strano, M.S. *Angew. Chem. Int. Ed.* 2008, *47*, 5018 - 5021.
16. a) Zhao, Y. L.; Hu, L.; Stoddard, J. F.; Gruner, G. *Adv. Mater.* **2008**, *20*, 1910 – 1915; b) Zhao, Y.L.; Stoddard, F.J. *Acc. Chem. Soc.* **2009**, 1161 - 1171.
17. Wang, F.; Yang, Y.; Swager, T. M. *Angew. Chem. Int. Ed.* **2008**, *47*, 8394 – 8396.
18. Wang, F.; Swager, T.M. *J. Am. Chem. Soc.* **2011**, *133*, 11181 - 11193.

19. Kong, L.; Wang, J.; Meng, F.; Chen, X.; Jin, Z.; Li, M.; Liu, J.; Huang, X.J. *J. Mater. Chem.* **2011**, *21*, 11109 – 11115.
20. Lei, J.; Ju, H. *Nanomedicine and Nanobiotechnology* **2010**, *2*, 496 – 509.
21. LeGoff, A.; Gorgy, K.; Holzinger, M.; Haddad, R.; Zimmerman, M.; Cosnier, S. *Chem. Eur. J.* **2011**, *17*, 10216 - 10221.
22. *Carbon Nanotubes and Related Structures: Synthesis, Characterization, Functionalization and Applications*, Edts. Guldi, D.M.; Martin, N., Wiley-VCH, **2010**.
23. a) Li, L.; Yang, Z.; Gao, H.; Zhang, H.; Ren, J.; Sun, X.; Chen, T.; Kia, H.G.; Peng, H. *Adv. Mat.* **2011**, *23*, 3730-3735; b) Kim, T.H.; Lee, B.Y.; Jaworski, J.; Yokoyama, K.; Chung, W.J.; Wang, E.; Hong, S.; Majumadar, A.; Lee, S.-W. *ACS Nano* **2011**, *5*, 2824 – 2830; c) Wei, B.; Zhang, L.; Chen, G. *New J. Chem.* **2010**, *34*, 453-457; d) Wang, F.; Gu, H.; Swager, T.M. *J. Am. Chem. Soc.* **2008**, *130*, 5392-5393.
24. a) Wei, G.; Xu, F.; Li, Z.; Jandt, K.D. *J. Phys. Chem. C* **2011**, *115*, 11453-11460; b) Fang, Y.; Guo, S.; Zhu, C.; Dong, S.; Wang, E. *Chem.-Asian J.* **2010**, *5*, 1838–1845; c) Lai, G.; Wu, J.; Ju, X.; Yan, F. *Adv. Funct. Mat.* **2011**, *21*, 2938–2943.
25. a) Tang, X.; Bansaruntip, S.; Nakayama, N.; Yenilmez, E.; Chang, Y.-I.; Wang, Q. *Nano Lett.* **2006**, *6*, 1632-1636; b) Wu, H.-C.; Chang, X.; Liu, L.; Zhao, F.; Zhao, Y. *J. Mater. Chem.* **2010**, *20*, 1036-1052.
26. a) Descalzo, A.B.; Martinez-Manez, R.; Sancenon, F.; Hoffmann, K., Rurack, K. *Angew. Chem. Int. Ed.* **2006**, *45*, 5924 - 5948; b) Pirondini, L.; Dalcanale, E. *Chem. Soc. Rev.* **2007**, *36*, 695 – 706.
27. Ogoshi, T.; Ikeya, M.; Yamagishi, T.; Nakamoto, Y.; Harada, A. *J. Phys. Chem. C* **2008**, *112*, 13079-13083.
28. a) Yebeutchou, R. M.; Tancini, F.; Demitri, N.; Geremia, S.; Mendichi, R.; Dalcanale, E. *Angew. Chem., Int. Ed.* **2008** *47*, 4504 - 4508; b) Yebeutchou, R.M., Dalcanale, E. *J. Am. Chem. Soc.* **2009**, *131*, 2452-2453.
29. Dionisio, M.; Oliviero, G.; Menozzi, D.; Federici, S.; Schmidtchen, F.P., Dalcanale, E.; Bergese, P. *J. Am. Chem. Soc.*, **2012**, *134*, *in press*.
30. For the nomenclature adopted for phopshonate cavitaand see: Pinalli, R.; Suman, M., Dalcanale, E. *Eur. J. Org. Chem.* **2004**, 451 - 462.

31. Hauke, F.; Myles, A.J.; Rebek J. Jr. *Chem. Commun.* **2005**, 4164 – 4166.
32. a) Singh P., Kumar J., Toma F. M., Raya J., Prato M., Fabre B., Verma S., Bianco A. *J. Am. Chem. Soc.* **2009**, *131*, 13555–13562; b) Singh, P.; Toma, F.M.; Kumar, J.; Venkatesh, V.; Raya, J.; Prato, M.; Verma, S.; Bianco A. *Chem Eur J.* **2011**, *17*, 6772–6780. c) Engtrakul C., Davis M. F., Mistry K., Larsen B. A., Dillon A. C., Heben M. J., Blackburn J. L. *J. Am. Chem. Soc.* **2010**, *132*, 9956 – 9957.
33. Biavardi E., Favazza M., Motta A., Fragalà I. L., Massera C., Prodi L., Montalti M., Melegari M., Condorelli G.G., Dalcanale E., *J. Am. Chem. Soc.* **2009**, *131*, 7447-7455.
34. Biavardi, E.; Battistini, G.; Montalti, M.; Yebeutchou, R.M.; Prodi, L.; Dalcanale, E. *Chem. Commun.* **2008**, 1638 – 1640.
35. Sreekumar A., Poisson L. M., Rajendiran T. M., Khan A.P., Cao Q., Yu J. , Laxman B., Mehra R., Lonigro R.J., Li Y., Nyati M.K., Ahsan A., Kalyana-Sundaram S., Han B., Cao X., Byun J., Omenn G.S., Ghosh D., Pennathur S., Alexander D.C., Berger A., Shuster J.R., Wei J.T. ,Varambally S., Beecher C., Chinnaiyan A.M., *Nature* **457**, 910 - 915.
36. Jentzmik, F.; Stephan, C.; Miller, K.; Schrader, M.; Ebersdobler, A.; Kristiansen, G.; Lein, M.; Jung, K. *Eur Urul* **2010**, *58*, 12-18.
37. Biavardi, E.; Todisco, C.; Maffei, F.; Motta, A.; Massera, C.; Condorelli, G.G.; Dalcanale, E. *Proc. Natl. Acad. Sci., U.S.A.* **2012**, *in press*.

Polymer blending as macroscopic expression of molecular recognition

5

5.1 State of the Art.

Supramolecular chemistry has been suggested as the ultimate strategy to fabricate new materials, with unique properties based on the reversible nature of the bonds between components.¹ One of the main fields of impact of supramolecular chemistry is polymer science.

Supramolecular polymers are defined as *polymeric arrays of monomeric units held together by reversible and highly directional secondary interactions, resulting in polymeric properties in dilute and concentrated solutions, as well as in the bulk.*²

Multiple hydrogen-bonding, metal coordination, hydrophobic interactions, π - π stacking and even host-guest interactions have been implemented for the polymerization process.² Both supramolecular homopolymers and A-B type copolymers can be obtained depending on the choice of the monomeric units: A-B heterotopic monomers form homopolymers, while homoditopic monomers lead to copolymers. (Figure 5.1).

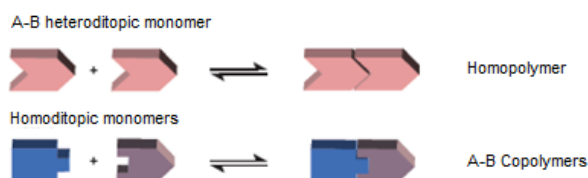


Figure 5.1 Self-complementary association (top); hetero-complementary association (down).

Any polymeric structure is thus possible, including linear homo- and copolymers, cross-linked networks and even branched structures. However, to obtain high molecular weight polymer, an high association constant is mandatory. Additionally, the molecular weight can be controlled by mean of introduction of monofunctional “chain stoppers”.² Development of supramolecular polymers is strictly related to their unique mechanical, electronic, biological and self-healing properties.³

As expected, the macroscopic properties depends, in turn, on the nature of the interactions between the molecular components. So, the constructed polymer chain can respond to external stimuli in a predictable way, just tailoring the connections between the monomers.⁴ Different secondary interactions has been exploited to build up such a systems, with multiple hydrogen-bonding motif as the best one to assure high molecular weight.² Indeed, the first example reported⁵ is based on the self-association of 2-ureido-4-pyrimidone, leading to four hydrogen bonding array (Figure 5.2).

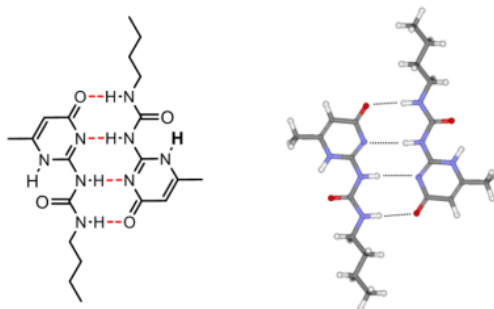


Figure 5.2 Homodimer of ureido-pyrimidone units.

Over the years, this approach was further improved to design supramolecular polymers based on orthogonal binding interactions. Schmuck reported on the synthesis of a small monomer which can polymerize by metal-ligand binding and ion pair formation (Figure 5.3).⁶

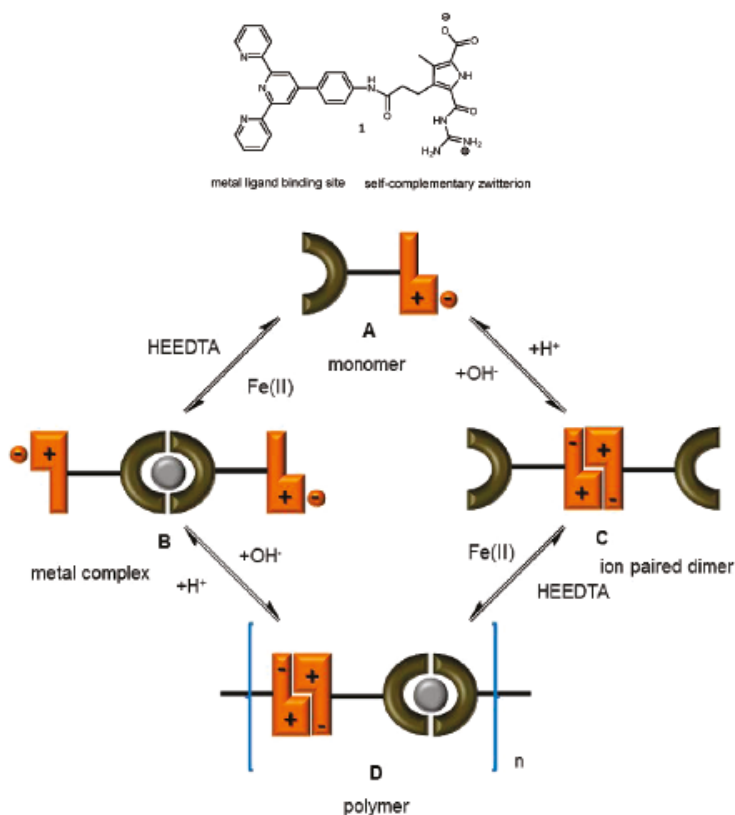


Figure 5.3 Self-assembly of a heteroditopic monomer, based on orthogonal binding interactions, namely metal-ligand coordination and ion pair formation.⁶

Nicely, the self-assembly can be switched on and off either by changing the pH or by adding and removing a metal ion. The polymerization is concentration dependent: at low concentration circular objects are observed, whereas increasing the concentration a linear polymer is formed. Moreover, the linear polymer has an apparent hydrodynamic radius of 25 nm, which means that an average seventy monomers are self-assembled.

The first example of noncovalent polymers, based on a directional pairwise hydrophobic motif using π - π interactions in aqueous medium, has been reported only recently (Figure 5.4).⁷

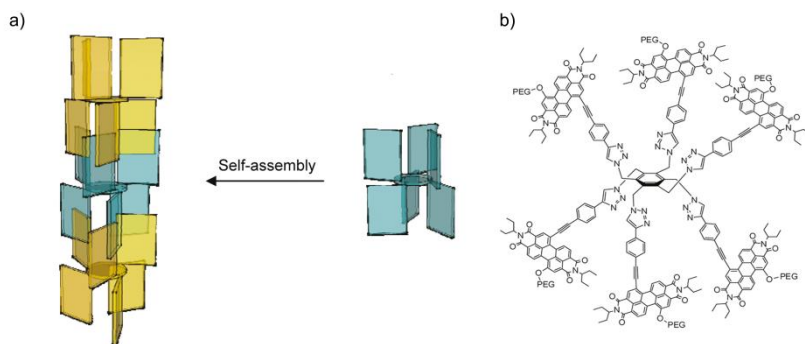


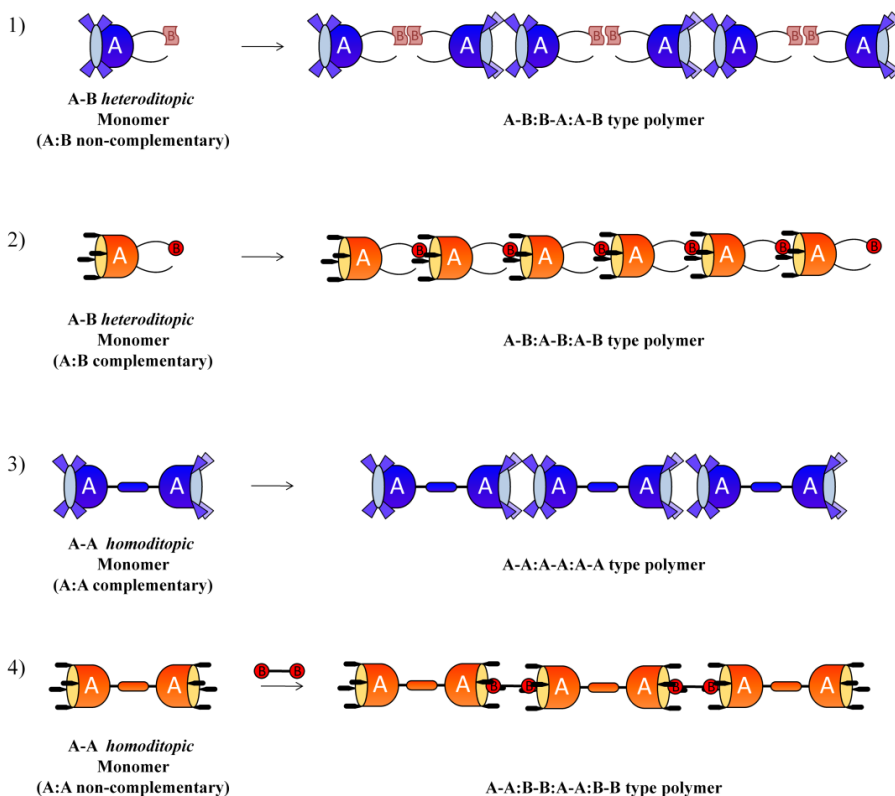
Figure 5.4 a) Self-assembly process of monomer in linear polymer by π - π interactions; b) highly aromatic monomer used in this studies.⁷

The self-assembly, in water, of highly aromatic monomer lead to a fiber having 240 nm in length. In this case the assembly/disassembly process is temperature dependent. Working at 279 K the monomers start to self-assemble, whereas at 373 K the polymer disaggregates.

The group of Dalcanale has exploited different orthogonal interaction modes for polymer assembly, all based on the use of cavitand monomers.⁸

Cavitand-based monomers are particularly appealing building-blocks for the realization of supramolecular polymers, thanks to their inherent versatility in terms of synthetic modularity and molecular recognition properties. In particular, the opportunity to functionalize the cavitand platform both at the upper and at the lower rim, allows to embed multiple self-assembly motifs on the same molecule, thus leading to complex supramolecular architectures, featuring orthogonal switching modes. On the basis of structural considerations, cavitand monomers can be classified into four main classes (Scheme 5.1). In the first class heteroditopic A-B monomers can be found, in which A:A and B:B interactions are respectively complementary. In this case a single monomer is present, but two interaction modes are active, leading to the formation of A-B:B-A:A-B type polymers. A second class includes heteroditopic A-B monomers, in which A:B interaction is complementary in nature. Also in this case a single monomer is involved, but just one interaction mode is active, and A-B:A-B:A-B type polymers are formed. The third class collects the homoditopic A-A

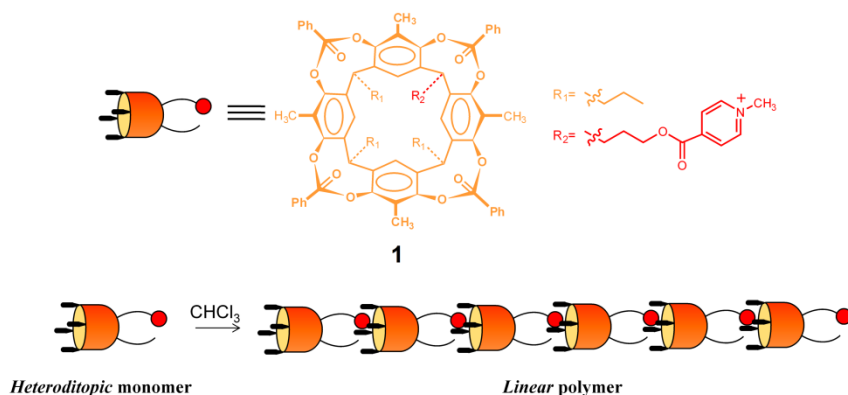
monomers, in which the A:A interaction is self-complementary. A single monomer and a single interaction are involved, leading to the formation of A-A:A-A:A-A type polymers. Finally, the fourth class includes the A-A monomers, in which the A:A interaction is not self-complementary. In this case two different homoditopic monomers are required, namely A-A and B-B, and the polymerization process proceeds thanks to the complementarity of the A:B interaction, leading to A-A:B-B:A-A:B-B copolymers.



Scheme 5.1 *Supramolecular polymerization motifs for cavitand monomers.*

In particular, phosphonate cavitands have been exploited in supramolecular polymers driven by host-guest interactions, since they fulfill the requirement for high association constants between the host and suitable guest. By exploiting the outstanding complexation properties of tetrakisphosphonate cavitands toward methylpyridinium guests, a new class of supramolecular polymers were self-assembled,

featuring not only a reversible nature, but also a remarkable plasticity, allowing structural switches from linear to star-branched architectures.⁹ In particular, cavitand **1** was prepared (Scheme 5.2), functionalized at the upper rim with four phosphonate bridges in their all inward-facing configuration, and at the lower rim with a single methylpyridinium unit. In this way both the host cavity and the guest moiety are placed in the same molecule on opposite sides, to exclude the possibility of self-association.



Scheme 5.2 A-B heteroditopic polymerization mode of cavitand **1**.

By isothermal titration calorimetry (ITC) the complexation properties of tetrakisphosphonate cavitand toward methylpyridinium guests were studied. It was found that, the complexation is driven not only by enthalpy but also by entropy. The effect of the solvent was demonstrated to be pivotal in the process. In particular an increase of two orders of magnitude was observed moving from methanol to methylene chloride. Additional information came from X-ray analysis. The homopolymer crystal structure presented linear polymeric chain which packs against four other antiparallel chains (Figure 5.5). The charges of the monomers bearing the guest functionality are counterbalanced by triflate anions located in between the lower rim alkyl chain, close to methylpyridinium cations.

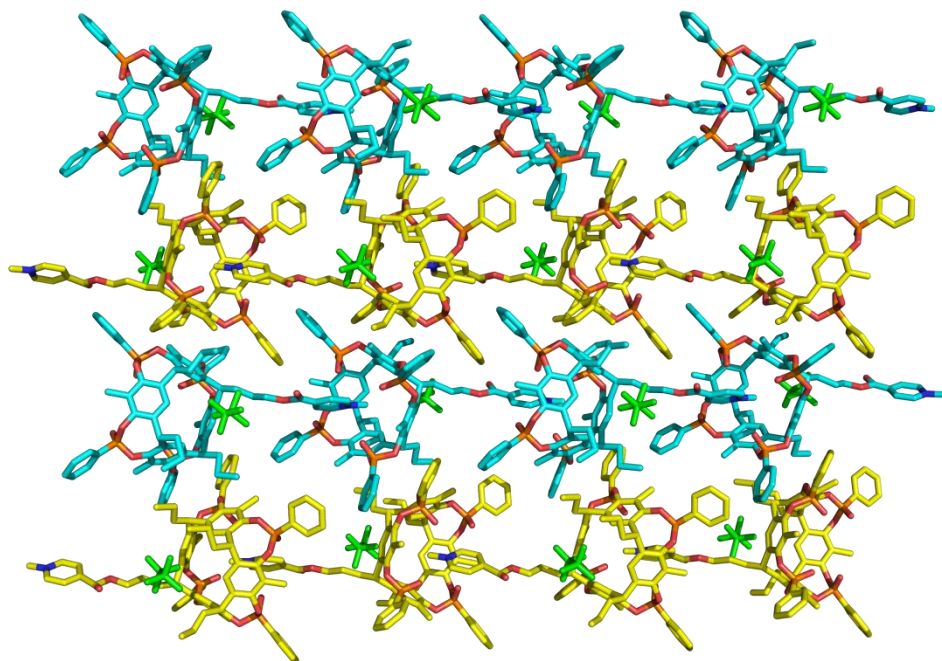


Figure 5.5 Views of the crystal packing of tetrathiosphosphate cavitand homopolymer.

Structurally similar but complexation inactive tetrathiosphosphate cavitand was used as a chain stopper, with concomitant control of the M_w . The presence of four P=S moieties, in place of four P=O bonds, completely prevents complexation by eliminating cation-dipole interactions between the cavitand and the charged nitrogen of the pyridinium unit.¹⁰ Its larger size does not preclude the insertion of methyl groups into the cavity, therefore the introduction of four P=S bridges has a little influence on CH- π interactions, which, however are not sufficient for complexation. While the stepwise addition of the stopper resulted in a linear decrease of M_w , the presence of 5,10,15,20-tetrakis(1-methyl-4-pyridinio)porphyrin tetra(p-toluene sulfonate) led to a substantial increase in M_w . Moreover, the porphyrin derivative acted as a template molecule, ordering the preformed, linear polymer chains into a star branched over-structure (Figure 5.6).

The polymer structure and MW determination were obtained via X-Ray analysis and viscosity measurements. In the case of rigid systems, exploiting for example the self-assembly between commercially available methyl viologen 2PF_6^- and ditopic host **2c**, X-Ray analysis provided direct evidence of the formation of linear supramolecular polymers (Figure 5.7).

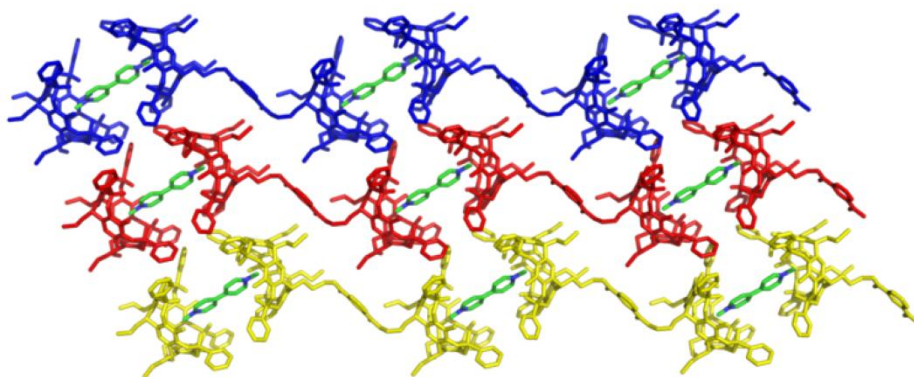


Figure 5.7 *Crystal structure of the **2c** methyl viologen A-A:B-B alternating copolymer.*

In the case of flexible systems, formed by self-assembly of ditopic host **2b**, featuring an adipic spacer connecting the cavitated units, and ditopic guest **3c**, bearing a polyethylenglycol linker, viscosimetry investigations accounted for the presence of a ring-chain equilibria, converging to the formation of linear polymeric species, in high concentration regimes.

Thanks to a suitable engineering of the host spacer, structural switches are possible. For example, the metal-directed conversion of linear polymeric chains into cross-linked supramolecular architectures was achieved via coordination of the pyridine units embedded in the spacer of ditopic host **2c**. In this case, neutral complex $(\text{CH}_3\text{CN})_2\text{PdCl}_2$ was selected as orthogonal curing agent, since it easily undergoes to ligand exchange of its trans acetonitrile ligands in the presence of pyridine, without competing for P=O binding.

The methodology for supramolecular polymer assembly is well established, although some issues associated to the widespread use of such architectures are still open: (i) achieve macroscopic expression of molecular recognition, (ii) trigger stimuli specific responses in polymeric materials and (iii) move self-assembly from the nano to the meso and macroscale.³

As for the first point, some approaches have been recently reported in the literature. Harada *et al.* described the formation of macroscopic objects by the association between acrylamide-based gels bearing host (cyclodextrin, CD) and polyacrylamide guests.¹² Only the complementary host-guest parts self-assemble in macroscopic networks, even visible to naked eye, with dye labeling (Figure 5.8).

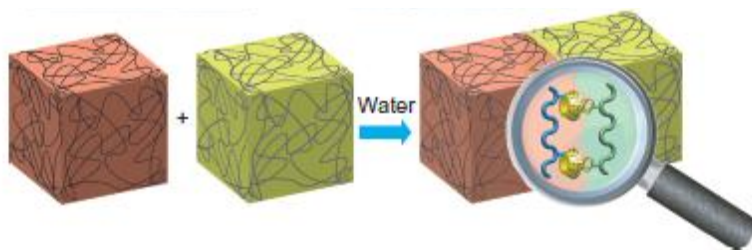


Figure 5.8 Schematic of the molecular recognition responsible for gels associations.

A different approach was employed by Zimmerman for polymer blending.¹³ In this case polystyrene and poly(butyl)methacrylate were functionalized with different complementary hydrogen-bonding arrays, respectively. The strong heterocomplex formation was responsible for the polymer blending. This was proved by several and complementary techniques, such as proton NMR, AFM and viscosity studies.

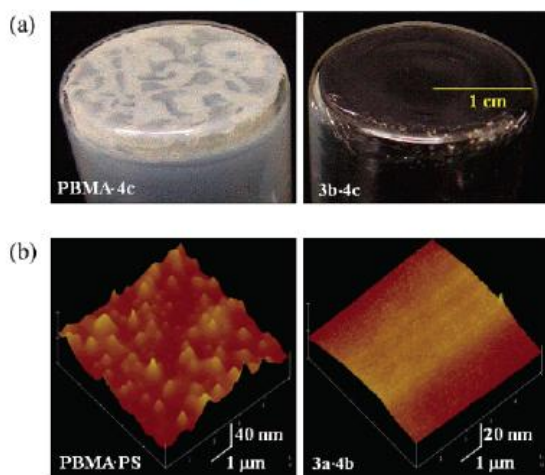


Figure 5.9 Photographs of the PS-PBMA before and after functionalization; b) AFM images of PS-PBMA before and after functionalization.

The selected system was demonstrated to be reversible under certain external stimuli, namely temperature and solvent polarity. Raising the temperature or switching from chloroform to dimethyl sulfoxide caused the breakage of multiple hydrogen-bonding motifs and concomitant macroscopic segregation of the two polymers. Changing the hydrogen-bonding units resulted in different triggering modes. Indeed, the introduction of redox-responsive units allows to switch the system by adding a chemical oxidant.¹⁴

Herein, we explore the use of host-guest chemistry to obtain the polymer blending as a macroscopic expression of molecular recognition. Specifically, we modified the structure of PS (polystyrene) with a tetraphosphonate cavitand host (PS-HOST) and PBMA (polybutylmethacrylate) with an N-methylpyridinium motif guest (PBMA-GUEST). In a detailed study we demonstrated the fundamental role played by the host-guest counterparts for achieving the polymer mixing and the ability to tune the properties of the polymer network as a macroscopic expression of molecular recognition.

5.2 Results and Discussion.

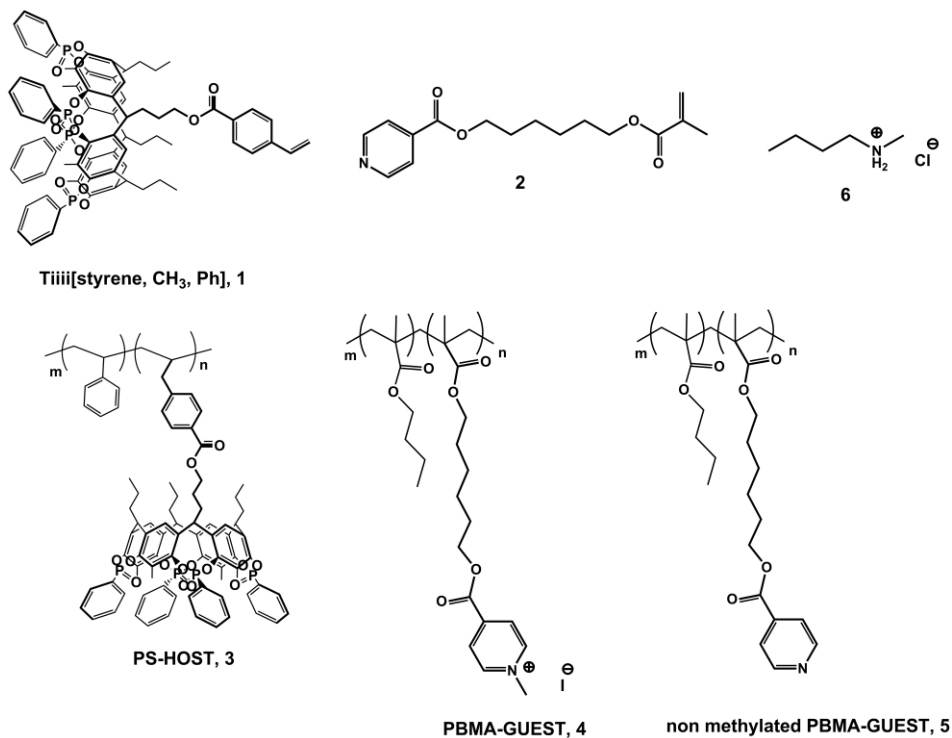
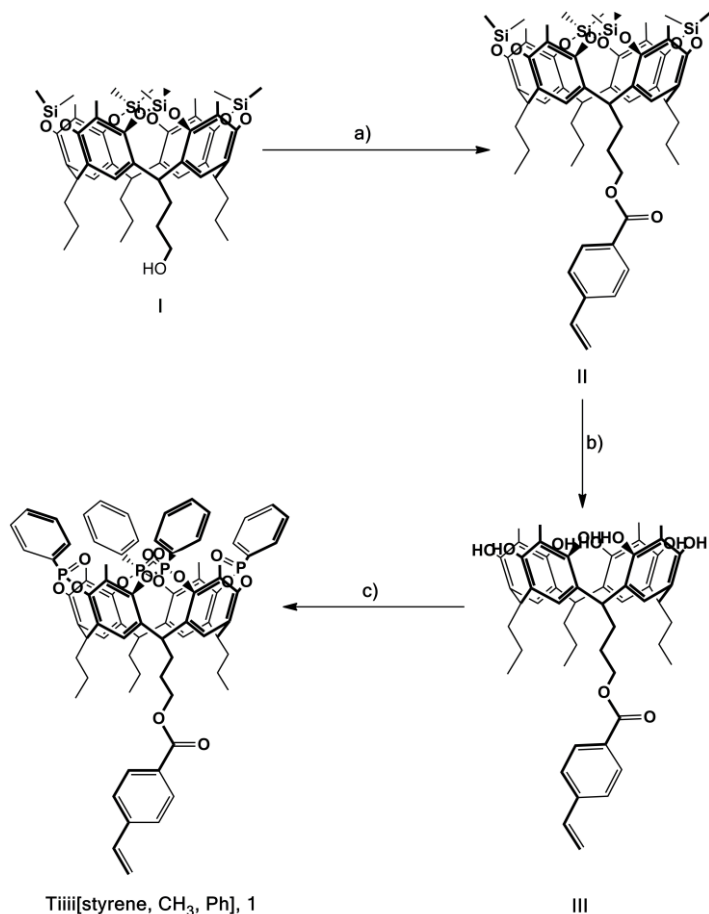


Chart 5.1 Molecules synthesized in this study

5.2.1 Design, Synthesis, Characterization of Monomers and Copolymers.

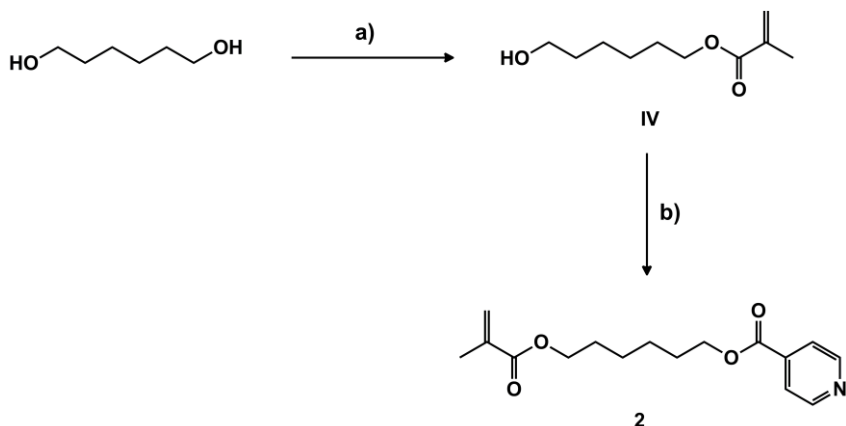
In order to achieve the polymer blending, we chose to functionalize the two polymers with two complementary host-guest counterparts, namely a tetraphosphonate cavitand and a pyridinium derivative, because their well documented interactions. We prepared a monostyrene footed tetraphosphonate cavitand **Tiiii[Styrene,CH₃,Ph]¹⁵ (1)** and **6-methacryloxy)isonicotinate (2)** (Chart 5.1). The molecule **1** was synthesized in three steps starting from monohydroxy-footed silylcavitand⁹ **I** (Scheme 5.4). The key step is the introduction of the styrene moiety at the lower rim of the resorcinarene skeleton, allowing

the incorporation of the host motif in the PS chain. The direct coupling between the monohydroxy-footed silylcavitand and the 4-vinyl benzoic acid, under Steglich conditions,¹⁶ led to the intermediate **II**. After removal of the silyl protecting group, the resorcinarene **III** was ready to react with dichlorophenylphosphine. This latter reaction gave rise to a tetraphosphonite intermediate which was *in situ* oxidized to give the tetraphosphonate cavitant **1**. Only the diastereoisomer with all the four PO groups facing inward the cavity was formed due to the stereospecificity of the bridging reaction.



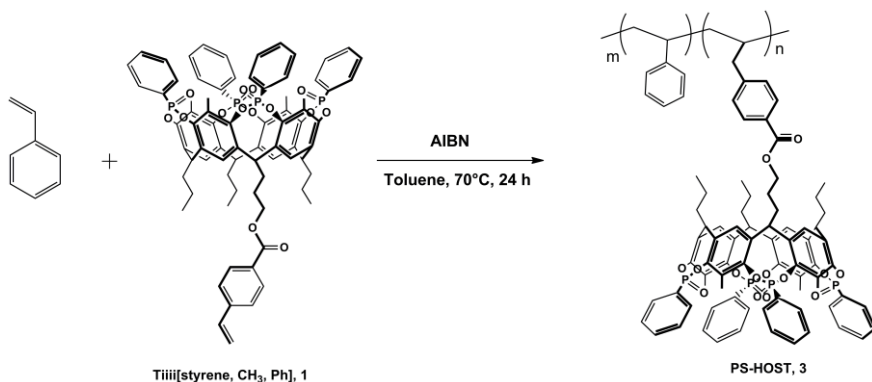
Scheme 5.4 Synthesis of **Tiiii[styrene, CH₃, Ph] 1**: a) 4-vinylbenzoic acid, DCC/DMAP, DCM dry, r.t. o.n., 42%; b) HF_{aq}, 36%, DMF, 50°C, 12h, quantitative; c) 1-PhPCl₂, py, 75°C, 3h, 2-H₂O₂, r.t., 1h 90% over two steps.

The pyridinium derivative **2** was prepared in two steps. A first mono esterification of hexandiol with methacryloyl chloride allowed the installation of a functional group for subsequent incorporation in PBMA. Then, the monoester derivative **IV** was reacted with isonicotinoyl chloride leading to **2** (Scheme 5.5).



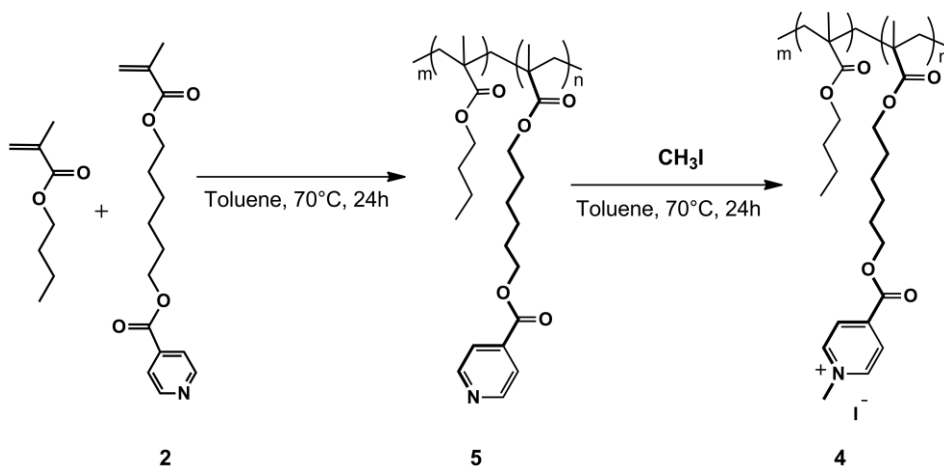
Scheme 5.5 Synthesis of monomer **2**: a) methacryloyl chloride, DMAP, Et_3N , DCM, r.t., 12h 48%; b) isonicotinoyl chloride, DMAP, Et_3N , DCM, r.t., 12h, 96%.

The free radical copolymerization of **1** with styrene introduced the HOST part in PS (from here inward PS-HOST, **3**) (Scheme 5.6). The ratio between styrene and **1** was 96 : 4 molar which is reflected in the polymer composition (see characterization below). Therefore, the reactivity of the styrene moiety in **1** is not affected by the presence of the bulky cavitand substituent in para position.



Scheme 5.6 Synthesis of functionalized PS-HOST **3**.

The installation of **2** (GUEST) in PBMA side chain led to a polybutyl methacrylate guest (from here inward PBMA-GUEST, **4** (Chart 5.1). In this case the copolymerization was carried out in two steps: first copolymerization between BMA and **2** followed by the N-methylation of pyridine residue with methyl iodide (Scheme 5.7). Also in this case the molar ratio between butylmethacrylate and **2** was 96 : 4.



Scheme 5.7 Synthesis of functionalized **PBMA-GUEST 4**

The constraint of molecular weight (between 15-20 KDa) and comonomer composition (HOST in PS-HOST and GUEST in PBMA-GUEST, respectively, of about 4 mol %) are important parameters for the successive molecular level mixing between PS-HOST and PBMA-GUEST. The relative low molecular weight of the copolymers allows the minimization of physical entanglement of polymer coils in semidilute solutions. The 4 mol % content of both host-guest counterparts assures a strong interaction that will lead to the copolymer blending, without altering the main features of the pristine polymers. Due to the low content of the functional monomers in the copolymers, comparable reactivity ratios between comonomers were assumed to determine the feed composition in copolymerizations experiments.

The two copolymers were fully characterized by several complementary techniques. In the case of PS-HOST, FT-IR and $^1\text{H-NMR}$ analyses confirm the formation of the desired product. From the comparison of integrals of the signals at 8.1 and 6.8-6.0 ppm of $^1\text{H-NMR}$ spectrum

(Figure 5.8) of PS-HOST, the amount of HOST in copolymer has been estimated in 4.3 mol %. This value was further confirmed by elemental analysis (Table 5.1).

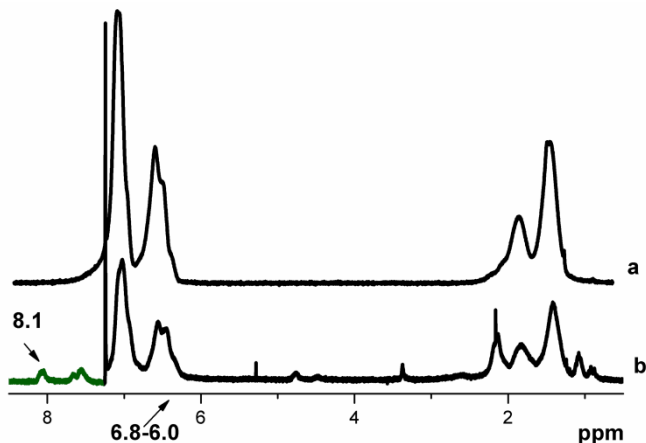


Figure 5.8 *Overlapping of $^1\text{H-NMR}$ spectra of PS (a) and PS-HOST, 3 (green trace : diagnostic cavitand signals) (b).*

PS-HOST, 3 (4% mol)		PBMA-GUEST, 4 (4 % mol)	
% P theoretical	% P experimental	% N theoretical	% N experimental
3.58	3.52	0.38	0.36

Table 5.1 *Elemental analysis results for diagnostic elements for PS-HOST, 3 and PBMA-Guest, 4 containing both 4% molar of functionalized monomers.*

The polymer was characterized by gel permeation chromatography (GPC), in order to determine the molecular weight (M_w) and the polydispersity index (I_d) of **3**. GPC analysis was performed in chloroform at room temperature. The M_w found was 28.1 kDa, and it is rather monodispers, indeed the I_d was 1.64, although a little shoulder is visible on the right end of the curve (Figure 5.9).

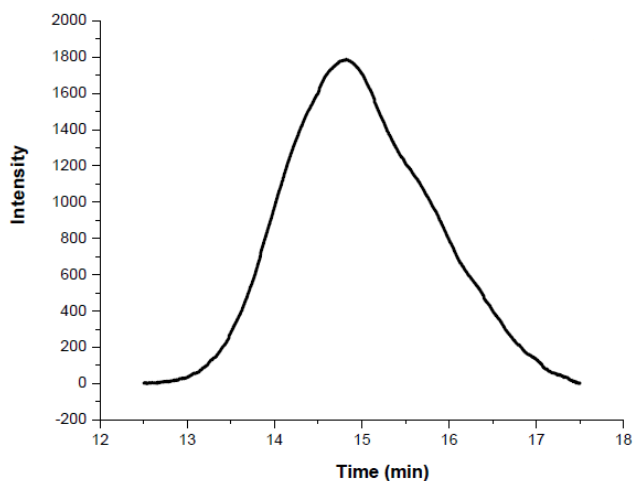


Figure 5.9 GPC curve of PS-HOST, 3.

The preparation of PBMA-GUEST was carried out in two steps. We first checked the incorporation of monomer **2** in the PBMA chain by ^1H NMR and FT-IR. Then methyl iodide was employed for the N-methylation of the pyridine groups. The progression of the reaction was monitored with UV-Vis spectroscopy, following the decreasing of the band at 273 nm (Figure 5.10)

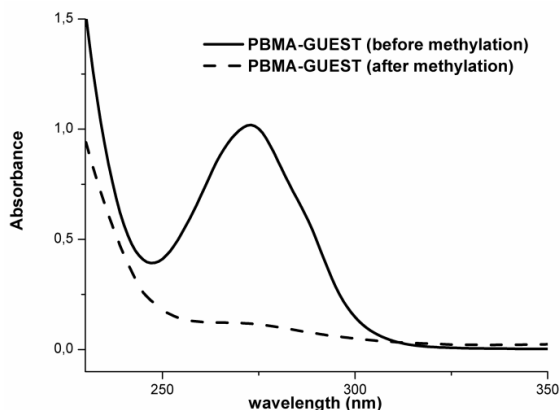


Figure 5.10 Overlapping of UV-Vis spectra of PBMA-GUEST before (continuous line) and after methylation (dashed line)

The ^1H -NMR analysis (in particular the singlet at 4.8 ppm of the methyl groups bound to nitrogen) confirms the results obtained by UV-Vis analysis. In ^1H -NMR spectrum, all aromatic signals of pyridine protons are shifted at lower fields with respect to no-methylated PBMA-GUEST. Therefore, all pyridine groups are N-methylated (Figures 5.11 and inset)

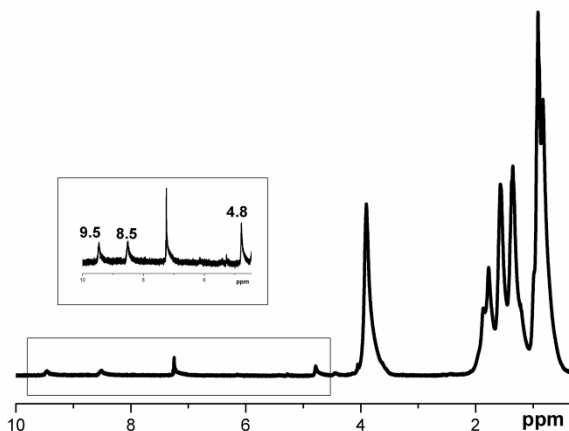


Figure 5.11 ^1H -NMR spectra of PBMA-GUEST after methylation.

The content of **2** incorporated in the polymer was estimated to be 4% molar by both proton NMR signals integration and elemental analysis (Table 5.1). For complete characterization, both Mw and ID of **4** were determinate by GPC. In this case the Mw was 27 kDa, with a Id equal to 1.5 (Figure 5.12). Both polymers have comparable Mw, so the introduction of modified monomers did not affect the whole reactivity in polymerization reaction, and, most importantly, the properties of the resulting polymers are similar.

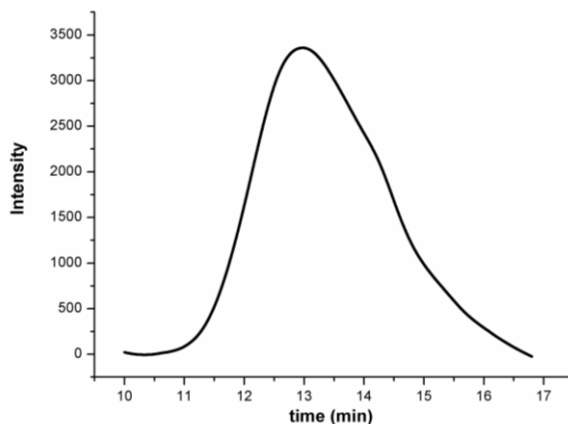


Figure 5.12 GPC curve of PBMA-GUEST, 4.

5.2.2 Complexation properties of copolymers in solution

Intermolecular association between PS-HOST and PBMA-GUEST was readily observed by ^{31}P – NMR spectroscopy (Figure 5.13). Free PS-HOST showed a broad peak at 6.5 ppm. After addition of 0.5 equivalent of PBMA-GUEST, a peak at 9.6 ppm was recorded. This was assigned to the complex formed between the tetraphosphonate cavitand residue and the N-methylpyridinium moiety, in agreement with previously observation.¹⁷ Moreover, the presence of both peaks (6.5 and 9.6 ppm) accounted for a slow exchange on the NMR time scale of the process. Further addition of 0.5 equivalent of PBMA-GUEST, led to complete complexation, as confirmed by the disappearance of the peak at 6.5 ppm. Interestingly, this demonstrated a 1:1 molar ratio between the two polymers in solution.

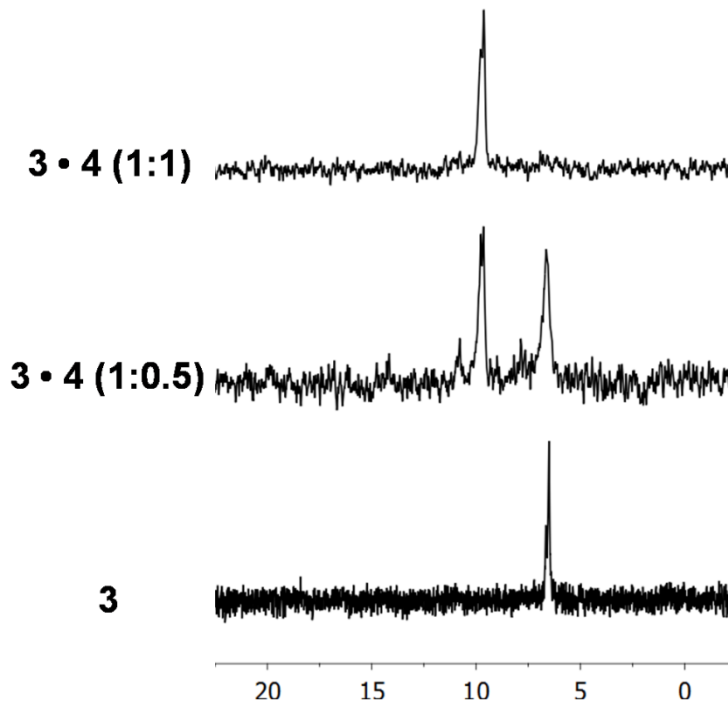


Figure 5.13 ^{31}P NMR in CDCl_3 monitoring of host-guest driven association between **3**•**4** (0.45 mM solution each) (stoichiometric ratio in brackets).

5.2.3 DSC Analysis

The miscibility of a polymer blend is often assessed by measuring its glass transition temperature (T_g), through Differential Scanning Calorimetry (DSC).¹⁸ We, thus, performed a systematic DSC analysis on a series of samples, including the functionalized polymers as well as different blends compositions. To erase any thermal history, the T_g was calculated at the second heating, after 3 min of isothermal stage at the lowest cooling temperature. For the PBMA-GUEST no differences were noted in comparison with the parent polymer. In the case of PS-HOST a slightly increase in T_g was observed up to 97.1°C. This might be due to the hindered side chain of the cavitands that stiffened the polymer. When a 1:1 molar mixture of **3** and **4** was submitted to a DSC analysis,

only one Tg is observed at about 40°C, consistent with the formation of an homogeneous blend (Figure 5.14).

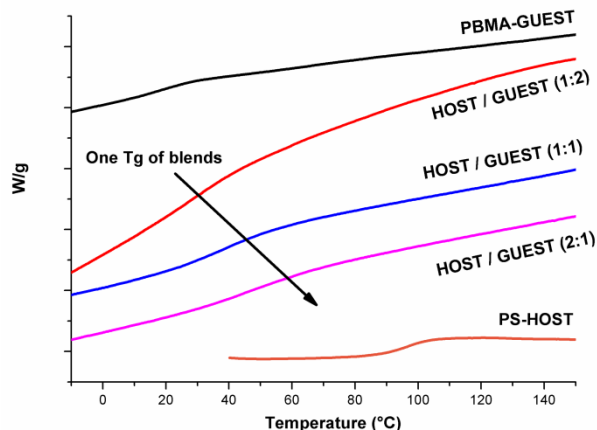


Figure 5.14 2° heating of DSC thermograms of PBMA-GUEST (black line), PS-HOST (orange line) and blends HOST / GUEST 1:2 (red line), 1:1 (blue line), 2:1 (magenta line).

Interestingly, when one of the two components exceeds the other, only one Tg is still observed, but it changed upon changing the composition. In particular when 2:1 PS-HOST and PBMA-GUEST molar mixture was prepared, the Tg raises to ca. 50°C; on the other hand, for 1:2 PS-HOST and PBMA-GUEST mixture the Tg falls to about 32°C. However, a 1:1 molar mixture of PS and PBMA showed two different Tgs: one at 25°C and the other at 95°C that correspond to the pristine polymers. This is in accordance with the immiscibility of the two homopolymers (Figure 5.15).¹⁹

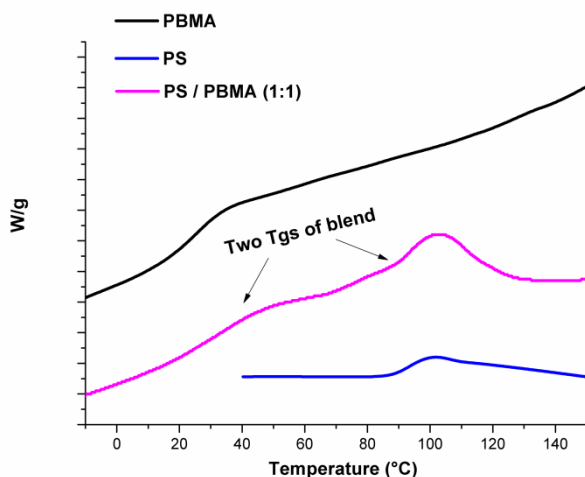


Figure 5.15 2° heating of DSC thermograms of PBMA (black line), PS (blue line), blend PBMA / PS (1:1) (magenta line).

In a control experiment carried out using a mixture of PS-HOST and non-methylated PBMA-GUEST (**5**), (Figure 5.14) two distinct Tgs are recorded (20°C and 97°C). Again, the system was not compatible, because the absence of the N-methyl pyridinium moiety does not allow the interaction with the tetraphosphonate cavitand contained in the **3**.

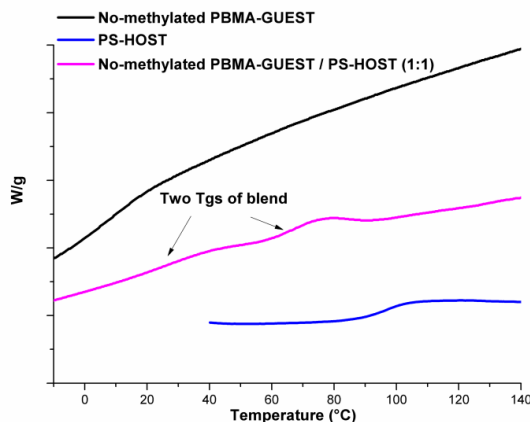


Figure 5.16 2° heating of DSC thermograms of no-methylated PBMA-GUEST (black line), PS-HOST (blue line) and blend PS-HOST / no-methylated PBMA-GUEST 1:1 (magenta line).

5.2.4 Solid state mixing.

In order to confirm the host-guest driven polymer blending, a series of AFM studies were engaged. Since the glass transition temperature (T_g) of the two polymers are completely different (PS ~ 100 °C, PBMA ~ 23 °C), it was necessary to work at 15 °C, in order to avoid the dewetting phenomena. We prepared a film from a 0.45 mM solution of a $1:1$ molar mixture of PS and PBMA which was deposited on silicon surface by spin coating. The AFM topography (Figure 5.17 a) shows a pitted surface and evident surface segregation. Careful analysis of the morphology of the film showed the presence of islands and depressions. The islands present a lateral dimension of the ranging from ca. 800 nm to 500 nm,²⁰ while the depth of the depressions were estimated 100 nm. Because of the higher mobility of PBMA molecules, they tend to “flow” around and are likely to enrich the bottom area, PS molecules tend to segregate forming the islands observed. The phase segregation is related to the low chemical affinity between the two polymers, but also to the great difference in terms of surface energy.^{20a} By contrast, the topographic image of $1:1$ molar mixture of **3** and **4** was quite flat, with few surface features and without phase separation (Figure 5.17 b). Moreover the topographical data supported an almost flat surface. These evidences demonstrate the mixing of the two copolymers at molecular level, hence their compatibilization.

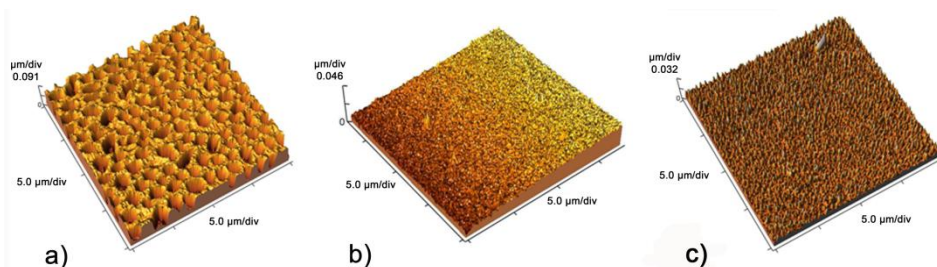


Figure 5.17 AFM images of the surface topography of PS•PBMA (a), PS-host•PBMA-guest (3•4) (b), PS-host•no-meth PBMA-guest (3•5) (c).

5.2.4.1 Control Experiments. The evidences gathered so far allowed us to conclude that the polymer blending is real, and it is related to the selective molecular recognition between the host-guest counterparts. However, more investigations were conducted to validate this statement. In a first set of experiments, a 1:1 molar mixture of **3** and **5** was spin coated on a silicon slice to study its morphology by AFM. The images recorded show a non homogeneous and pitted topography (Figure 5.17 c), as well as a mixture of a pristine polymers; the “defects” are smaller and shallower (compare Figure 5.17 a and c). Due to the absence of the N-methyl pyridinium moiety, the host-guest interactions do not take place; which proves that the molecular recognition drives the polymer blending. The introduction of a more competitive guest, such as N-methyl butyl ammonium chloride **6**,^{9,10} should trigger the segregation of the blend. Hence, we treated a 1:1 molar mixture of **3** and **4** with a N-methyl butyl ammonium salt solution. The disassembly process was followed by ³¹P – NMR spectroscopy. Addition of **6**, lead to the formation of peak at 10.4 ppm, attributed to the complex formed between the cavitand part of **3** and **6** (Figure 5.18). When one equivalent of **6** was added only the peak at 10.4 ppm was visible; accounting for fully displacement of **4** by the N-methyl butyl ammonium guest.

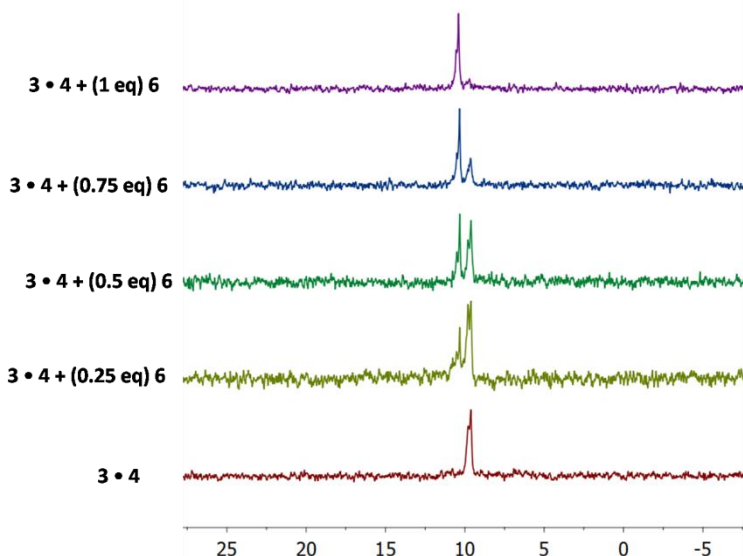


Figure 5.18 ³¹P NMR in CDCl₃ monitoring of guest induced segregation (N-methylbutyl ammonium chloride 6,9 μM) (stoichiometric ratio in brackets).

The AFM topography of an aliquot of this solution showed a heterogeneous surface with the same topography as PS and PBMA mixture (Figure 5.19). The depressions reached about 100 nm of depth, and the islands were still visible. The addition of a competitive guest clearly demonstrates that the molecular recognition drives the polymer blending and the reversibility of the system.

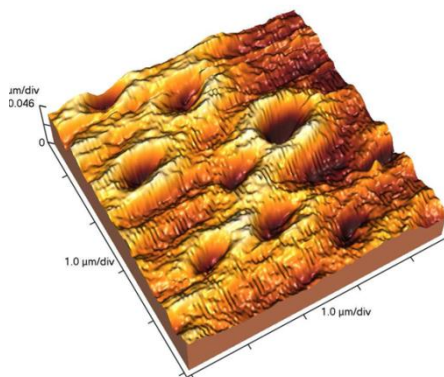


Figure 5.19 AFM images of the surface topography **3•4** after treatment with *N*-methylbutyl ammonium chloride (**6**).

5.2.5 Host-guest polymers as interphase compatibilizers.

Single phase polymer solution is obtained when the components are intimately mixed at molecular level. From thermodynamic point of view, for a known component composition, the *free energy of mixing* (ΔG_{mix}) must be negative, at given temperature and pressure.²¹ When ΔG_{mix} , at particular temperature, is plotted against composition for a blend of two polymers, a typical curve results, the so-called *diagram phase* (Figure 5.20). According to the Flory-Huggins theory (See experimental part), mixing two polymers A and B is limited by enthalpic reasons. Since entropic factors are rather small, the energetic gain of contacts between polymer chains is not sufficient to make the *free energy negative*. Hence, *compatibilisation* is achieved either by mechanical mixing followed by a lowering of temperature, or by incorporation of macromolecules, the *compatibilisers*, into the blend. The effect of the *compatibilisers* is to reduce the surface energy associated with the interface between the different phases. Another approach has been the

introduction of reactive groups to connect individual polymers within the blend.

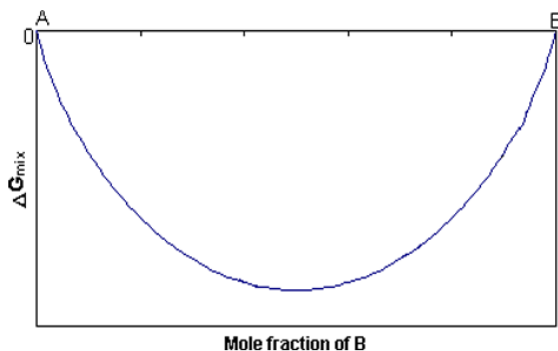


Figure 5.20 ΔG_{mix} plotted against composition for a partially soluble blend

In the reported simplest case, the curve is concave upwards, then all the points below the line represent a single phase system, whereas all the points above the line accounted for a two phase system. This because, below the curve the ΔG_{mix} value is always lower than the *free energy* of two phases. The shape of the curve is the result of how entropic and enthalpic parts of the free energy vary in a different manner with composition.²² Previously, we exploited the use of host-guest chemistry for polymer blending. The introduction of tetraphosphonate cavitand in polystyrene backbone (**PS-HOST, 3**) and *N*-methylpyridinium derivative in polybutylmethacrylate chain (**PBMA-GUEST, 4**) in a 4% molar lead to the polymer blending (Chart 5.1).

By introduction of molecular recognition units, the two immiscible polymers became compatible. Important technological fallout is the use of the functionalized polymers as a *compatibilisers*, but for this purpose it is mandatory knowing what is the minimum amount of **PS-HOST** and **PBMA-GUEST** to obtain the *compatibilisation* of PS and PBMA in bulk.

Herein, we will report on the polymer blending formation of PS and PBMA in bulk, changing the composition of **PS-HOST** and **PBMA-GUEST** as *compatibilisers*, trying to build up a phase diagram for the selected polymer mixture.

Polymer compatibility can be evaluated by different analytical tools, by determining the *glass transition temperature* (T_g), by differential

scanning calorimetry (DSC), or by light scattering, infra red spectroscopy or even viscosimetry. In any case, a change in a physical property of the blending is recorded, upon change in the components composition. Nevertheless, by these techniques it is not possible to visualize the morphology of polymer blending. For this reason we chose to follow the blending by AFM.

The samples were simply prepared by spincoating a dichloromethane solution of selected mixtures on a silicon slide. Importantly, since the PBMA T_g is 23°C, all the images were recorded at 12°C under nitrogen atmosphere, so humidity cannot affect the measurements outcome.

As a reference, we firstly recorded an AFM image of a 1:1 molar mixture of a PS-PBMA (Figure 5.21).

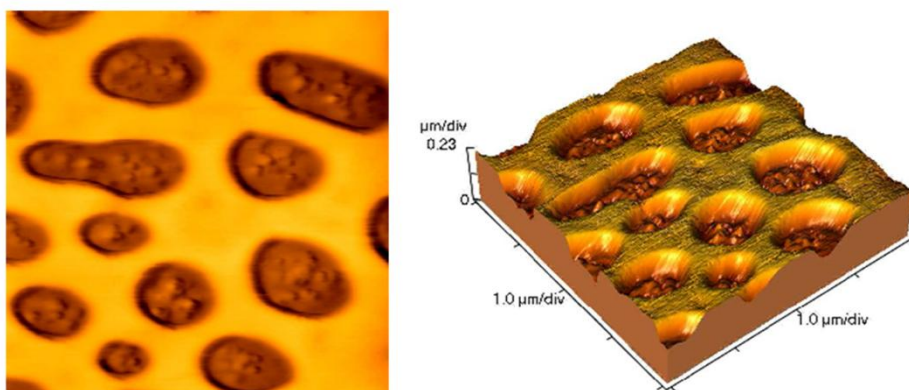


Figure 5.21 AFM image of 50:50 % mol,mol PS-PBMA

The AFM topography shows a pitted surface and evident surface segregation comparable to that of Figure 5.15 a.²⁰ From this starting point, we added an equimolar amount of **PS-HOST**, **PBMA-GUEST** solution to the PS-PBMA mixture.

After addition of 30% molar of the functionalized mixture, no evidences of miscibility were recorded. Indeed, the surface is heterogeneous with high degree of roughness, resembling the 1:1 PS-PBMA mixture (Figure 5.22).

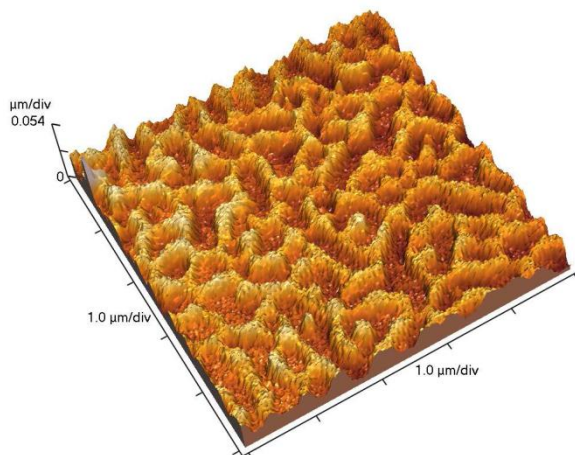


Figure 5.22 AFM image of PS-PBMA mixture after addition of 30% mol of **PS-HOST;PBMA-GUEST** solution

When the amount of **PS-HOST;PBMA-GUEST** reached 50 % molar, the morphology started to change. In fact the surface became flatter and smoother than the previous case, the depressions are shallower, but the system is still not completely homogeneous.

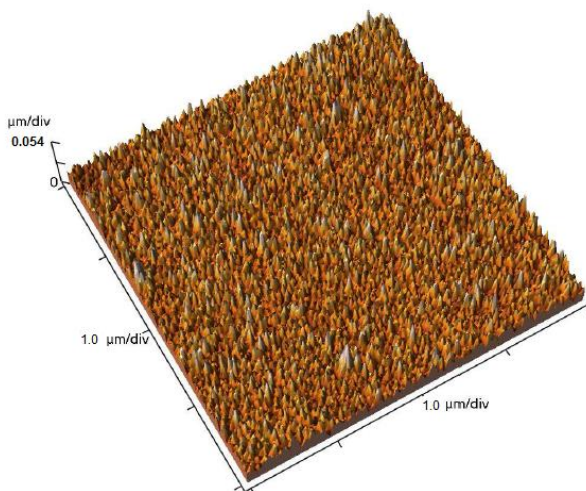


Figure 5.23 AFM image of PS-PBMA mixture after addition of 50% mol of **PS-HOST;PBMA-GUEST** solution

Only when the molar content of the functional constituents raised to 70% molar, a flat and homogeneous surface was recorded indicating complete blending.

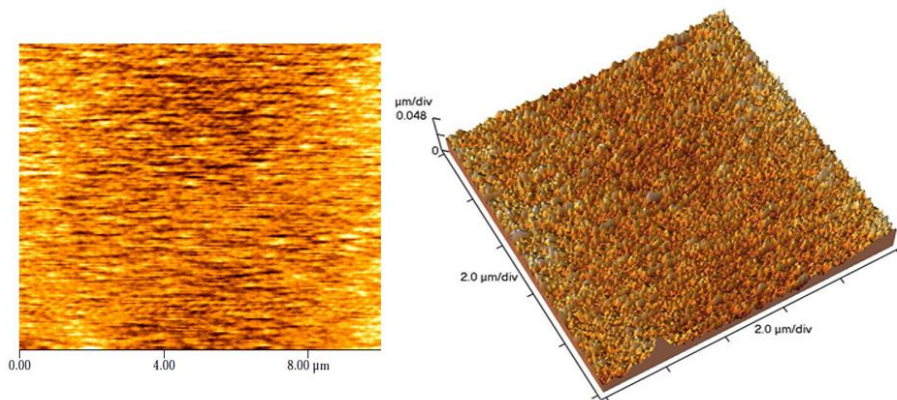


Figure 5.24 *AFM image of PS-PBMA mixture after addition of 70% mol of PS-HOST;PBMA-GUEST solution*

5.3 Reversible supramolecular cross-linking via molecular recognition

Stimuli responsive cross-linked polymers are highly desirable in many application fields from gels to structural polymers. An ideal material would be a polymer shifting from thermoplastic to thermosetting properties, under a given set of conditions.

As a first step in the direction of this goal, we explored the host-guest interactions of **PS-HOST, 3** toward ditopic guests **7** and **8** and monotopic guests **9** and **10** in solution (Chart 5.2).

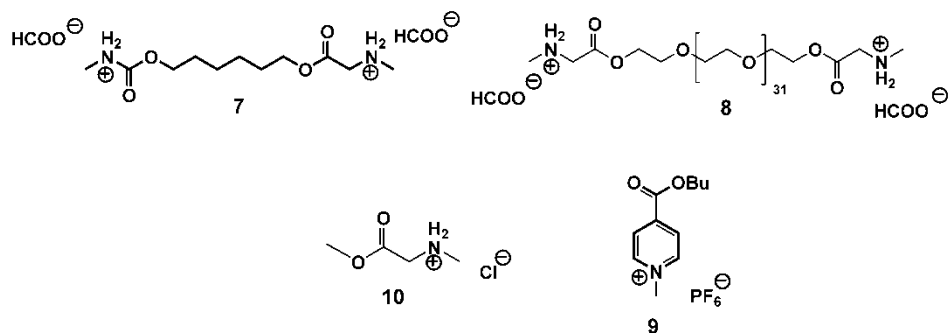


Chart 5.2 *Ditopic and monotopic cross linking guests.*

As terminal guest units in **7** and **8**, we chose *N*-methyl sarcosine because of its remarkable affinity for tetraphosphonate cavitands²⁴ as illustrated by the crystal structure of figure 5.25.

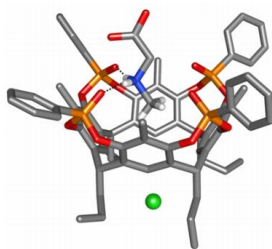
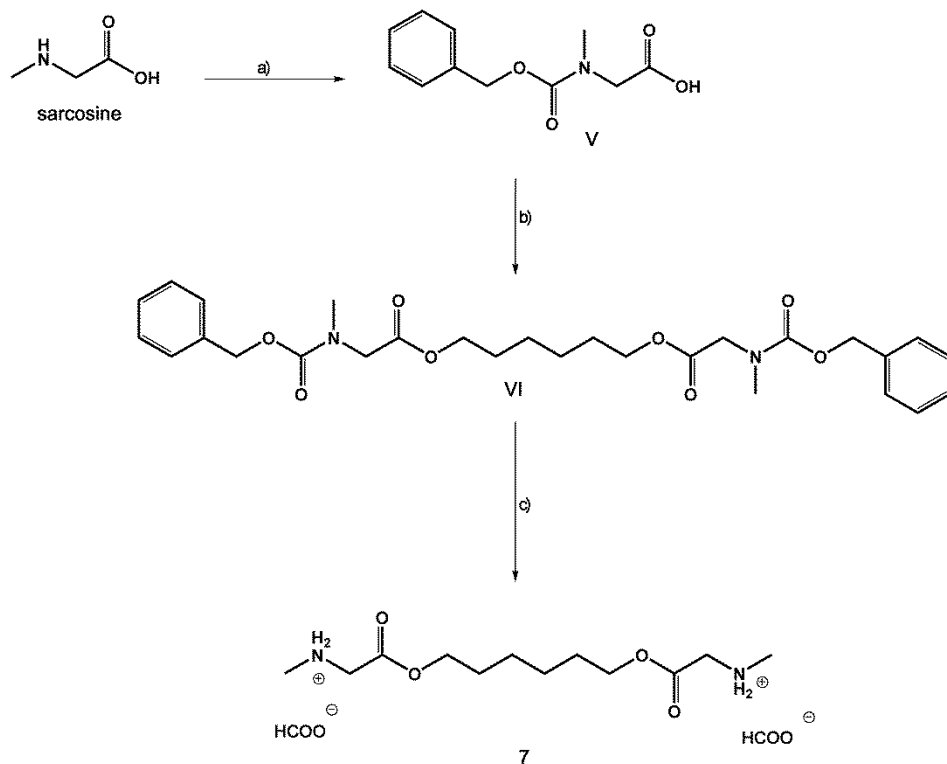


Figure 5.25 *X-Ray structure of the sarcosine-Tiui complex (chloride as a counterion).*

The two sarcosine units have been installed both on a guest chain tether **7** and on a polymeric PEG **8** to test the influence of the chain length on the cavitand-sarcosine interactions.

Post-functionalization of polymers is usually challenging, due to difficulties in controlling the regioselectivity of the reactions, and for the low reactivity of the polymers.²⁵ Therefore we first studied the reaction pathway using a simple model, such as **7**, for the similarity structure of PEG. Hence, hexandiol was esterificated with two equivalent of Cbz-protected sarcosine V under modified Steglich conditions, leading to intermediate VI (Scheme 5.8).¹⁶



Scheme 5.8 Synthesis of sarcosine derivative model **7**: a) CbzCl, H₂O (pH = 9), r.t., 2h, 64%; b) EDCCl, DMAP, DCM dry, r.t., 12 h, 50%; c) Pd/C, H₂, CHOOH 3%, r.t., 1h, quantitative.

Almost all the signals in the ¹H-NMR spectrum are splitted in a doubled (Figure 5.26 a). This is due to the well known C-N hindered rotation in amides. The free rotation is activated by heating at 80 °C, leading to a simplified spectrum (Figure 5.26b).

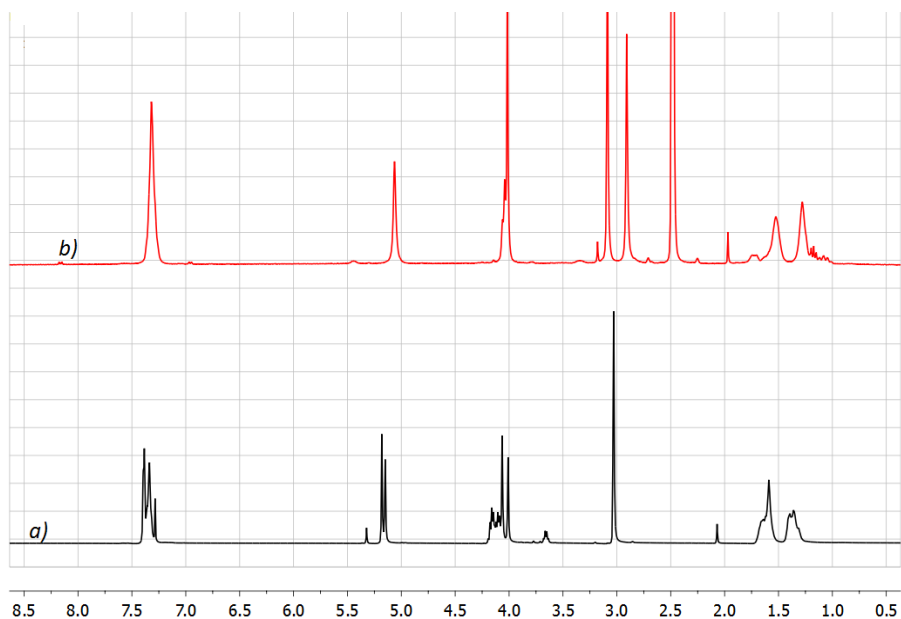


Figure 5.26 $^1\text{H-NMR}$ (DMSO-d_6) of sarcosine-derivative model **7** a) room temperature; b) 80°C .

The subsequent reductive cleavage of the benzoyl protecting group led to the desired product **7**, in almost quantitative yield (Scheme 5.8). The reaction was carried out under H_2 atmosphere in presence of Pd/C and formic acid, and complete in one hour.

Once the experimental conditions were set up, a monodisperse PEG (33 repeating units) was functionalized via the same route, affording *N*-methylsarcosine terminated PEG, **8** (Scheme 5.9). However, the reaction conditions were modified during the synthesis, due to the lower reactivity of the polymer chain. In fact, higher temperatures and longer reaction times are required in all three steps. Moreover the purification of the intermediates and the final product is rather difficult.

ppm, peak indicative of free Ti_{iii} a signal at 10.02 ppm appeared, in a slow exchange regime, diagnostic of the **PS-HOST@9** complex. After addition of 1.25 equivalents of guest **9** all the cavitand units were complexed.

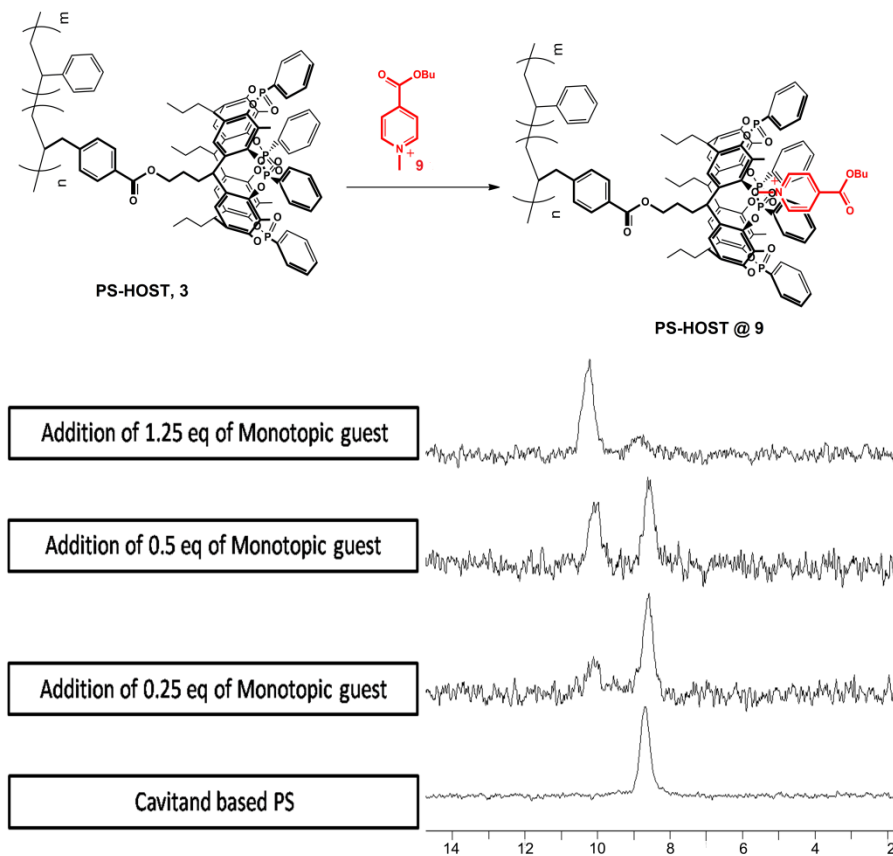


Figure 5.27 ^{31}P -NMR ($CDCl_3$) Titration of **PS-HOST, 3** with *N*-methylpyridinium guest **9**.

Subsequently, the complexation capability toward sarcosine methyl-ester hydrochloride **10** was tested in acetone, to mimic the sarcosine terminated PEG, **8**. The ester functionality prevents undesired self-association, whereas the hydrochloride ensures constant protonation of the nitrogen, with concomitant formation of ammonium cation. Addition of slight excess of guest led to complete disappearance of the peak at

7.27 ppm (free **PS-HOST 3**), with concomitant formation of a peak at 10.99 ppm, ascribed to the guest **10** inclusion (Figure 5.28).

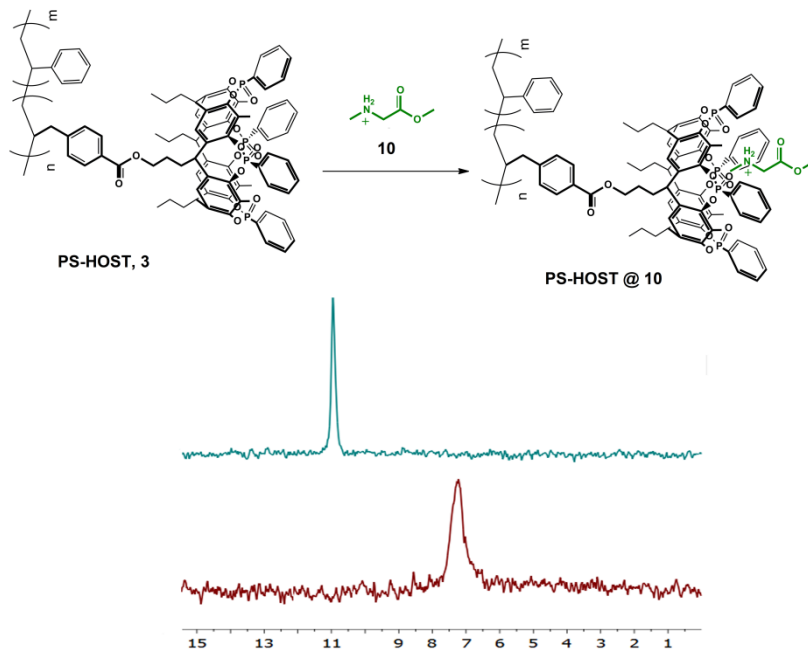


Figure 5.28 ^{31}P -NMR (Acetone d_6) spectra of free **PS-HOST 3** (red) and complexed polymer with sarcosine **10** (**PS-HOST@10**, light blue).

The results reported above, prompted us to explore the interaction between the **PS-HOST 3** and sarcosine-terminated PEG, **8**. In a qualitative experiment we added an equimolar amount of **8** to a solution of **3** in deuterated tetrachloroethane, and the outcome of the reaction was continuously monitored by ^{31}P -NMR spectroscopy (Figure 5.29).

Although the interactions between the host-guest partners are favorable, the expected complexation did not take place, at least at the beginning. Indeed, after either long period of time or imposing higher temperature, the expected upfield shift was not observed. However, when 0.1 mL of acetone were added at the mixture, a shift toward higher frequencies was recorded. In contrast with the previous observation, i.e. sarcosine addition, the peak attributed to the complex moved to ~ 14 ppm.

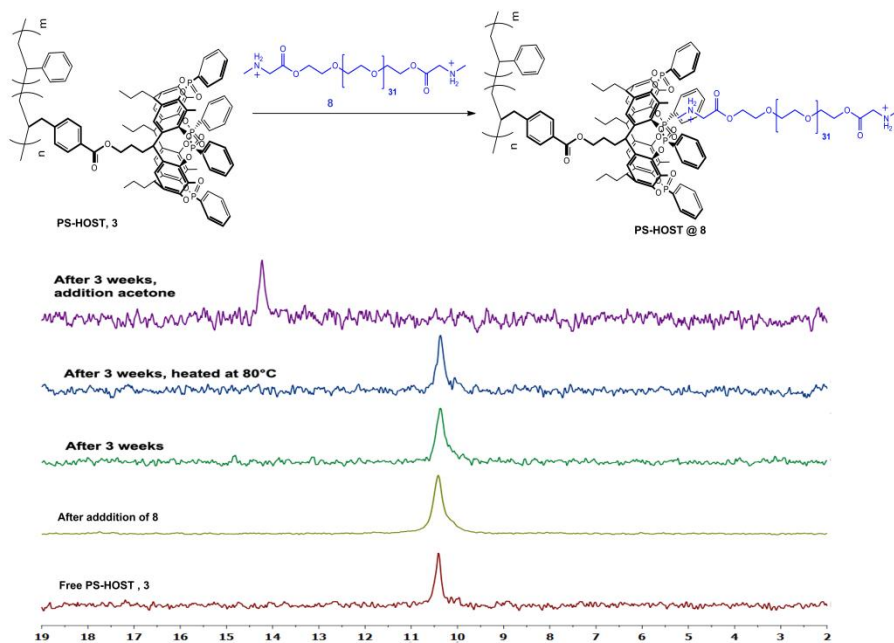


Figure 5.29 $^{31}\text{P-NMR}$ (CD₂Cl₄ and Acetone-d₆) monitoring of self-assembly of PS-HOST **3** and sarcosine terminated PEG, **8** under different reaction conditions.

The addition of acetone was necessary to fully solubilize PEG **8** in tetrachloroethane. In fact, the charged terminal residues highly reduce the solubility of PEG **8** in chlorinated solvents.

5.4 Conclusions.

The formation of polymer blending from a pair of immiscible polymers by host-guest chemistry has been exploited. Tetraphosphonate cavitand and methylpyridinium derivative were introduced in the back bone of PS, PBMA respectively, in 4% molar. The host-guest pair formation lead to polymer blending. The association between the polymers was unambiguously demonstrated by several and complementary analytical tools, namely NMR, DSC and AFM. We also demonstrated that the system responded to precise external stimuli: chemical segregation is triggered by addition of a competitive guest.

This result underscores the importance of high-affinity and high-fidelity heterocomplexation in the creating of new supramolecular polymer architectures.

Important technological fallout could be the use of the functionalized polymers as a *compatibilisers*. Specifically, to a 1:1 molar ratio solution of PS and PBMA we added increasing aliquots of **PS-HOST, 3** and **PBMA-GUEST,4** solution. As the percentage of the functionalized polymer solution raised up to 70% molar a flat and smooth surface appeared, although this value is too high for using our system as a real *compatibiliser* for PS and PBMA system.

Finally, reversible host-guest interactions between **PS-HOST 3** and PEG-guest **8** have been tested in solution as a first step in the direction of stimuli response cross-linking polymers.

5.5 Acknowledgments.

Special thanks to Dr G. Pecchini, Prof. L. Cristofolini from University of Parma and to Dr. Lucia Ricci Prof. Giacomo Ruggeri from the Department of Industrial Chemistry at Pisa University.

5.6 Experimental Section.

Synthesis of monomers

Styrene – based silylcavitand (II).

To a solution of monohydroxy footed silylcavitand (1.23 g, 1.29 mmol) in dry dichloromethane (20 mL) DCC (0.53g, 2.58 mmol), DMAP (0.32 g, 2.62 mmol) and 4-vinylbenzoic acid (0.19 g, 1.29 mmol) were added. The resulting suspension was stirred overnight at room temperature. After an aqueous work up, the organic phase was purified by column chromatography (hexane : ethyl acetate 95:5) to give pure **II** as a white solid (0.64 g, 0.59 mmol, yield 42%). **¹H-NMR (CDCl₃, 400 MHz):** δ = 8.03 (d, 2H, ³J=8.0 Hz, (C=O)ArH_o); 7.48 (d, 2H, ³J=8.0 Hz, (C=O)ArH_m); 7.22 (s, 4H, ArH); 6.78 (dd, 1H, ³J₁=17.4 Hz, ³J₂=11.0 Hz, ArCH=CH₂); 5.88 (d, 1H, ³J=17.6 Hz, ArCH=CH_{trans}); 5.40 (d, 1H, ³J=10.8 Hz, ArCH=CH_{cis}); 4.66 (m, 4H ArCH); 4.43 (m, 2H, CH₂CH₂O(C=O)); 2.39 (m, 2H, CH₂CH₂CH₂O(C=O)); 2.21 (m, 6H, CH₂CH₂CH₃); 1.95 (s, 12H, ArCH₃); 1.81 (m, 2H, CH₂CH₂O(C=O)); 1.34 (m, 6H, CH₂CH₂CH₃); 0.99 (t, 9H, ³J=7.4 Hz, CH₂CH₂CH₃); 0.54 (s, 12H, SiCH_{3,out}); -0.65 (s, 12H, SiCH_{3,in}). **ESI-MS:** *m/z* calcd. for C₆₁H₇₈O₁₀Si₄ (1083.61), [M+Na]⁺ 1106.6. Found: 1106.2 [M+Na]⁺.

Styrene – based resorcinarene (III).

An aqueous 36% HF solution (160 μ L) was added to **II** (0.400g, 0.37 mmol) dissolved in DMF (15 mL). The suspension was stirred overnight at 55 °C. The solvent was removed in vacuo and the solid was suspended in water. Vacuum filtration afforded **III** as a white solid (0.318 g, 0.37 mmol, quantitative yield). **¹H-NMR (Acetone-d₆, 300 MHz):** δ = 8.01 (m, 10H, ArOH + (C=O)ArH_o); 7.61 (d, 2H, ³J=8.4 Hz, (C=O)ArH_m); 7.51 (s, 2H, ArH); 7.45 (s, 2H, ArH); 6.85 (dd, 1H, ³J₁=17.7 Hz, ³J₂=10.8 Hz, ArCH=CH₂); 5.98 (d, 1H, ³J=17.7 Hz, ArCH=CH_{trans}); 5.41 (d, 1H, ³J=11.1 Hz, ArCH=CH_{cis}); 4.41 (m, 6H, ArCH + CH₂CH₂O(C=O)); 2.50 (m, 2H, CH₂CH₂CH₂O(C=O)); 2.28 (m, 6H, CH₂CH₂CH₃); 2.08 (s, 12H, ArCH₃); 1.77 (m, 2H, CH₂CH₂CH₂O(C=O)); 1.30 (m, 6H, CH₂CH₂CH₃); 0.93 (t, 9H, ³J=7.4 Hz, CH₂CH₂CH₃). **ESI-MS:** *m/z* calcd. for C₅₃H₆₂O₁₀ (859.1), [M+Na]⁺ 882.1. Found: 882.6 [M+Na]⁺.

Monostyrene footed tetraphosphonate cavitand (Tiii[styrene, CH₃, Ph])(1).

To a solution of **III** (0.318g, 0.37 mmol) in freshly distilled pyridine (10 mL), dichlorophenylphosphine (210 μ L, 1.55 mmol) was added slowly, at room temperature. After 3 hours of stirring at 70 °C, the solution was allowed to cool at room temperature and 2 mL of aqueous 35% H₂O₂ was added. The resulting mixture was stirred for 1 h at room temperature, then the solvent was removed in vacuo. Addition of water resulted in the precipitation of a white powder, which is filtered to give pure **1** (0.45 g, 0.33 mmol, 90 %). **¹H-NMR (CDCl₃, 400 MHz):** δ = 8.11 (m, 8H, P(O)Ar**H_O**); 8.03 (d, 2H, ³J=7.6 Hz, (C=O)Ar**H_O**); 7.70 (m, 4H, P(O)Ar**H_P**); 7.60 (m, 8H, P(O)Ar**H_M**); 7.47 (d, 2H, ³J=8.0 Hz, (C=O)Ar**H_M**); 7.28 (bs, 4H, Ar**H**); 6.76 (dd, 1H, ³J₁=18 Hz, ³J₂=10.8 Hz, Ar**CH=CH₂**); 5.87 (d, 1H, ³J=17.2 Hz, Ar**CH=CH_{TRANS}**); 5.41 (d, 1H, ³J=10.8 Hz, Ar**CH=CH_{CIS}**); 4.81 (m, 4H, Ar**CH**); 4.52 (m, 2H, CH₂**CH₂O**(C=O)); 2.59 (m, 2H, CH₂**CH₂CH₂O**(C=O)); 2.41 (m, 6H, CH₂**CH₂CH₃**); 2.16 (s, 12H, Ar**CH₃**); 1.93 (m, 2H, CH₂**CH₂CH₂O**(C=O)); 1.45 (m, 6H, CH₂**CH₂CH₃**); 1.09 (m, 9H, CH₂**CH₂CH₃**). **³¹P{¹H} NMR (CDCl₃, 161.9 MHz):** δ = 8.30 (bs, P(O)). **HR ESI-MS:** calcd. for C₇₇H₇₄O₁₄P₄ (1346.40290) [M+Na]⁺: 1369.39212. Found:1369.39212.

6-hydroxyhexyl methacrylate (IV).

To a solution of 1,6-hexanediol (5.6 g, 48 mmol) in dry dichloromethane (20 mL), DMAP (0.46 g, 4 mmol), triethylamine (3.96 ml, 29 mmol) were added. The mixture was cooled at 0 °C and methacryloyl chloride was added slowly (1.85 mL, 20 mmol). The solution was warmed at room temperature and stirred overnight. After an aqueous workup, the organics were collected and purified by column chromatography (hexane : dichloromethane 7 : 3) to give **IV** as a colorless oil (1.86 g, 9.7 mmol, 48 %). **¹H NMR (CDCl₃ , 400 MHz):** δ = 6.05 (s, 1H, **H_{TRANS}**HC=C); 5.51 (s, 1H, **H_{CIS}**HC=C); 4.10 (t, 2H, ³J=6.6 Hz, (C=O)O**CH₂CH₂**); 3.58 (t, 2H, ³J=6.6 Hz, CH₂**CH₂OH**); 2.39 (s, 1H, CH₂**OH**); 1.90 (s, 3H, **CH₃**); 1.65 (m, 2H, (C=O)O**CH₂CH₂**); 1.54 (m, 2H, CH₂**CH₂OH**); 1.37 (m, 4H, CH₂**CH₂CH₂CH₂**). **ESI-MS:** *m/z* calcd. for C₁₀H₁₈O₃ (186.25), [M+Na]⁺: 209.2 Found: 209.3 [M+Na]⁺.

6-(methacryloxy)hexyl isonicotinate (2).

To a solution of **IV** (0.572 g, 3.08 mmol), in dry dichloromethane (20 ml), DMAP (40 mg, 0.31 mmol) and, triethylamine (0.86 ml, 6.16 mmol) were added. The mixture was cooled at 0 °C and isonicotinoyl chloride was added (1.92 g, 10.8 mmol). The solution was warmed at room temperature and stirred overnight. After aqueous workup, the organics were collected and the solvent was removed to afford pure **2** as a yellowish oil (0.86 g, 2.97 mmol, 96%). **¹H-NMR (CDCl₃, 400 MHz):** δ = 8.79 (d, 2H, ³J=5.6 Hz, ArH_o); 7.85 (d, 2H, ³J=6.0 Hz, ArH_m); 6.01 (s, 1H, H_{TRANS}HC=C); 5.55 (s, 1H, H_{CIS}HC=C); 4.37 (t, 2H, ³J=7.2 Hz, CH₂CH₂O(C=O)Ar); 4.17 (t, 2H, ³J=6.6 Hz, (C=O)OCH₂CH₂); 1.94 (s, 3H, CH₃); 1.81 (m, 2H, (C=O)OCH₂CH₂); 1.73 (m, 2H, CH₂CH₂O(C=O)Ar); 1.50 (m, 4H, CH₂CH₂CH₂CH₂). **HR ESI-MS:** calculated for C₁₆H₂₁NO₄ (291.14796) [M+H]⁺: 292.15433. Found:292.15530.

Synthesis of copolymers**Copolymer between styrene and monostyrene footed tetraphosphonate cavitand (PS-HOST) 3.**

In a shlenk, 0.45 mL of styrene, 220 mg of **1** and AIBN (33.3 mg) were dissolved in 4 ml of toluene under inert nitrogen atmosphere. The solution was degassed with freeze – pump procedure (three times). Afterwards, the mixture was heated at 70°C and kept for 24 h in these conditions under stirring. At the end of the reaction, the copolymer was recovered by twice precipitation in 500 ml of cold methanol (0°C) and dried under vacuum at room temperature (yield 76.2 % of PS-HOST). **¹H-NMR (CDCl₃, 300 MHz):** δ = 8.05 (2H, (C=O)ArH_o); 7.7 (4H, P(O)ArH_P); 7.6 (8H, P(O)ArH_M); 7.0-6.8 (2H, ArH_{PS}); 6.8-6.0 (3H, ArH_{PS} + 2H, ArH_o); 4.8 (4H, ArCH); 4.5 (2H, CH₂CH₂O(C=O)); 2.2 (12H, ArCH₃); 1.8 (1H, CH_{PS}); 1.4 (2H, CH_{2PS}); 1.1 (6H, CH₂CH₂CH₃); 0.9 (9H, CH₂CH₂CH₃). **IR** (solution casting on KBr plate): 3060, 3027, 3027 (aromatic νC–H); 2923 (asym νC–H CH₂); 2850 (sym νC–H CH₂); 1718 (νC=O); 1602 (ring stretching); 1275 (νP=O); 1134 (sym νC–O–R); 1077 (asym νC–O–R); 952 (νP–O–Ar) cm⁻¹. **Elemental analysis:** C 78.77, H 7.01, N 1.55, P 3.52 %. **GPC** (CHCl₃): Mn = 21 KDa, Mw = 27 KDa, Id = 1.30.

Copolymerization between n-butyl methacrylate and 6-(methacryloxy)hexyl isonicotinate ester (5) and successive N-methylation (PBMA-GUEST) (4).

In a schlenk with magnetic stirrer, 2.3 g of n-butyl methacrylate (BMA) and 0.2 g of isonicotinic acid 6-(2-methyl-acryloyloxy)-hexyl ester were dissolved in 15 mL of toluene under inert nitrogen atmosphere. The solution was purged with nitrogen for 30 minutes and heated to 70 °C, then AIBN was added (55.0 mg) and the polymerization mixture kept for 24 h in these conditions. At the end of the reaction, the copolymer was purified by twice precipitation in 500 mL of cold methanol and after filtration, copolymer was dried under vacuum at room temperature (yield 63.5 %).

IR (solution casting on KBr plate): 2960 (asym ν C-H CH₃); 2936 (asym ν C-H CH₂); 2875 (sym ν C-H CH₃); 1728 (ν C=O); 1599 (ν C=N-); 1563 (ν -C-C-aromatic ring); 1466 (asym δ CH₃), 1385 (sym δ CH₃); 1268, 1242, 1177, 1154 (ν C-O-C); 735 (ρ CH₂); 709 (oop bending aromatic C-H); 677 (in-plane vibration Py ring) cm⁻¹.

¹H-NMR (CDCl₃, 300 MHz): δ = 8.8 (-CH-N-CH-); 7.8 (-CH-CH-N-CH-CH-); 4.4 (Py-COO-CH₂-); 4.0 (-COO-CH₂-CH₂-); 1.9-1.8 ([-CH₂-C(CH₃)(COOC₄H₉)-]n); 1.6 (-COO-CH₂-CH₂-); 1.4 (-CH₂-CH₂-CH₃); 0.9 (-CH₂-CH₂-CH₃); 0.8 ([-CH₂-C(CH₃)(COOC₄H₉)-]n). Elemental analysis: C 65.10, H 9.42, N 0.36 %. **GPC (CHCl₃):** Mn = 14 KDa, Mw = 35 KDa, Id = 2.50. **UV-Vis (CH₂Cl₂):** λ_{\max} = 273 nm.

N-Methylation reaction for synthesis of PBMA-GUEST (4).

N-Methylation reaction was carried out using iodomethane in toluene. In a three neck flask equipped with magnetic stirrer, dropping funnel and dropping cooling, 2.0 g of copolymer (5) were dissolved in 20 ml of anhydrous toluene under inert nitrogen atmosphere. The solution was heated at 70 °C and then 0.25 ml of methylene iodide was added. The mixture was stirred for 24 hours at 70 °C and then the methylated copolymer (PBMA-GUEST) was recovered by precipitation in methanol, and after filtration the solid washed with diethyl ether and dried (yield 69.6 %).

¹H-NMR (CDCl₃, 300 MHz): δ = 9.5 (-CH-N+(CH₃)-CH-); 8.5 (-CH-CH-N+(CH₃)-CH-CH-); 4.8 (-N+(CH₃)-); 4.3 (Py-COO-CH₂-); 3.9 (-COO-CH₂-CH₂-); 1.9-1.8 ([-CH₂-C(CH₃)(COOC₄H₉)-]n); 1.6 (-COO-CH₂-CH₂-); 1.4 (-CH₂-CH₂-CH₃); 0.9 (-CH₂-CH₂-CH₃); 0.8 ([-CH₂-C(CH₃)(COOC₄H₉)-]n). **UV-Vis (CH₂Cl₂):** λ_{\max} = 265 nm. Elemental analysis: C 65.10, H 9.42, N 0.36%.

Surface topography was examined using an atomic force microscopy Thermomicroscope Autoprobe CP Research. All measurements were performed in contact mode with a tapping silicon probe (MPP-12100-10). In order to preserve the initial structure, the films were not annealed. All samples were cooled down at 15°C using a Peltier cell. The collected images were flattened using Image Processing (IP) 2.1NAME. The samples were prepared by spincoating on silicon slide from 0.45 mM solution of the polymer blend in dichloromethane.

Mixing experiments among PS, PBMA, PS-HOST, **3 and PBMA-GUEST, **4**.**

All solutions were 0.45 mM in dichloromethane each. Starting from 1:1 molar ratio of PS, PBMA solution increasing amount of **3** and **4** were added: 0.3 eq., 0.5 eq. and 0.7 eq.. Each solution was spincoated on silicon slide and submitted to AFM analysis.

2-(((benzyloxy)carbonyl)(methyl)amino)acetic acid (V**).**

N-methyl sarcosine (500 mg, 5.61 mmol) was dissolved in water (15 mL; pH= 9). At 0°C benzyl chloroformate (4,00 mL; 28 mmol) was slowly added. After two hours, ethyl acetate (40 mL) was added, and the aqueous layer was separated, and acidified to pH = 1. Dichloromethane was added (40 ml), and the organic layer was separated, solvent removal afforded pure **V** as a yellowish oil (750 mg; 3,59 mmol, 64%).

¹H-NMR (CDCl₃, 300 MHz): δ = 10.99 (s, 1H, COOH); 7.31 (m, 2H, **H_o**); 7.28 (m, 3H, **H_p**+**H_m**); 5.11 (s, 2H, ArCH₂O); 4.02 (s, 2H, NCH₂C(O)OH); 2.97 (s, 3H, NCH₃). **ESI-MS:** *m/z* calcd. for C₁₁H₁₃NO₄ (223,08 Da) [M+Na]⁺ 246.07. Found: 246.06.

Hexane-1,6-diylbis(2-(((benzyloxy)carbonyl)(methyl)amino)acetate) (VI**).**

To a solution of **V** (0.57 g., 2.71 mmol) in dichloromethane (10mL), EDC chloride (519 mg, 2,71 mg), DMAP (330 mg, 2,71) and hexandiol (160 mg, 1.36 mmol) were added and stirred for twelve hours. The mixture was diluted with water (pH = 1) and the organic layer was separated,

and washed with water (pH = 9). Solvent evaporation afforded **VI** as a colorless oil (714 mg, 1.36 mmol, 50%).

¹H-NMR (CDCl₃, 400 MHz): δ = 7.38 (m, 2H, **H_o**); 7.34 (m, 3H, **H_p+H_m**); 5.16 (s, 2H, Ar**CH₂O**); 4.10 (m, 2H, C(O)**OCH₂CH₂**); 4.02 (s, 2H, N**CH₂C(O)OH**); 3.03 (s, 3H, N**CH₃**); 1.63 (m, 2H, O**CH₂CH₂CH₂**); 1.35 (m, 2H O**CH₂CH₂CH₂**). **ESI-MS:** *m/z* calcd. for C₂₈H₃₆N₂O₈ (528.25 Da) [M+2Na]²⁺ 287.11. Found: 287.36.

2,2'-(hexane-1,6-diylbis(oxy))bis(N-methyl-2-oxoethanaminium) (7).

To a solution of **VI** (350 mg, 0.66 mmol) in methanol (20 mL), 3% of formic acid, Pd/C were carefully added. The suspensions was stirred under H₂ atmosphere for one hour. Then, the mixture was filtered over celite, and the solvent was removed affording **2** as colorless oil (220 mg, 0.63 mmol, quantitative)

¹H-NMR (CDCl₃, 400 MHz): δ 4.14 (m, 2H, C(O)**OCH₂CH₂**); 4.03 (s, 2H, N**CH₂C(O)OH**); 3.03 (s, 3H, N**CH₃**); 1.65 (m, 2H, O**CH₂CH₂CH₂**); 1.38 (m, 2H O**CH₂CH₂CH₂**). **ESI-MS:** *m/z* calcd. for C₁₂H₂₆N₂O₄ (262.19 Da) [M²⁺]. Found: 262.23.

Bis-Cbz-sarcosine-PEG (VII).

V (754 mg, 3.60 mmol) was dissolved in pyridine (30 mL), then PEG (Mw = 1500 Da, 1.35 g, 0.9 mmol), DCC (741 mg, 3.60 mmol) and DMAP (110 mg, 0.9 mmol) were added. The mixture was heated up to 70 °C for two days. The solvent was removed under reduce pressure, then the crude was dissolved in dichloromethane and washed with water. The organic layers were separated, the solvent evaporated and triturated with toluene. The removal of the solvent afforded **VII** as white solid. (525 mg 30%)

¹H-NMR (CDCl₃, 400 MHz): δ = 7.28 – 7.23 (m, 10H, **H_{arom}**); 5.00 (s, 4H, Ar**CH₂O**); 4.21 (m, 4H, C(O)**OCH₂CH₂**); 4.00 (s, 4H, N**CH₂C(O)OCH₂**); 3.74 (m, 4H, C(O)**OCH₂CH₂**); 3.53 (m, 116H, O(**CH₂CH₂O**)₂₉); 2.94 (s, 3H, N**CH₃**).

Bis-sarcosine-PEG (8).

VII (525 mg) was dissolved in methanol (20 mL), 5% of formic acid, Pd/C were carefully added. The suspensions was stirred under H₂ atmosphere for twelve hours. Then, the mixture was filtered over celite,

and the solvent was removed affording **8** as white soli (465 mg, quantitative).

¹H-NMR (DMSO-d₆, 400 MHz): δ 4.28 (m, 4H, C(O)O**CH₂**CH₂); 4.10 (s, 4H, N**CH₂**C(O)OCH₂); 3.85 (m, 4H, C(O)OCH₂**CH₂**); 3.44 (m, 116H, O(**CH₂CH₂**O)₂₉); 2.94 (s, 3H, N**CH₃**).

Flory-Huggins theory for polymer blending

By thermodynamic consideration, polymeric blend can be obtained only if at equilibrium, the *free energy change*, upon mixing reaches a minimum:

$$\Delta G_m < 0$$

At given temperature and pressure, ΔG_m is related to the enthalpy and entropy change by:

$$\Delta G_m = \Delta H_m - T\Delta S_m$$

Using a statistical thermodynamic approach, Flory and Huggins proposed the equation for the free energy of polymer solution, as

$$\frac{\Delta G_m}{RT} = \frac{\Delta G_m}{RT} \frac{V_r}{V} = \frac{\Phi_A}{M_A} \ln \Phi_A + \frac{\Phi_B}{M_B} \ln \Phi_B + \Phi_A \Phi_B \chi$$

ΔG_m is the free energy of mixing per mole.

V_r is the reference molar volume; for a polymer system A, B it could be equal to the molar volume of one of the chemical repeat units.

V is the total molar volume of the system.

M_i is the "degree of polymerization" of the i component.

Φ_i is the volume fraction of the i component.

χ is the solubility factor.

The equation containing both the entropy and enthalpy terms associated to the polymer blending, in fact the term

$$\frac{\Phi_A}{M_A} \ln \Phi_A + \frac{\Phi_B}{M_B} \ln \Phi_B$$

accounted for the entropic term, whereas

$$\Phi_A \Phi_B \chi$$

accounted for the enthalpic term. This because the *solubility factor*, χ factor can be deduced by

$$\Delta H_m = RT \chi n_i \Phi_i$$

where $n_A \Phi_A$ represent the number of molecules of the polymer i .

When A, B are two distinct polymers the value of M_A and M_B should be quite high, the entropy would be quite small. So only the enthalpic factor controls the mixing. It depends, in turn, on the *solubility factor*, χ which is usually positive for most polymers. This means that the *free energy change* is positive and no polymer blending occurs.

5.7 References and notes.

- 1 Whitesides, G.M.; Boncheva, M. *Proc. Natl. Acad. Sci. U.S.A.* **2002**, *99*, 4769 - 4774.
- 2 Brunsveld, L.; Folmer, B.J.B., Meijer, E.W; Sijbesma, R.P. *Chem. Rev.* **2001**, *101*, 4071 - 4097.
- 3 *Supramolecular Polymer Chemistry*, Edt. Arada, H.,**2011**, Wiley-VCH.
- 4 Wojtecki, R.J.; Meador, M.A.; Rowan, S.J. *Nature Mat.* **2011**, *10*, 14 - 27.
- 5 Sijbesma, R.P.; Beijer, F.H.; Brunveld, L.; Folmer, B.J.B.; Hirschberg, J.H.K.K.; Lange, R.F.M.; Lowe, J.K.L.; Meijer, E.W. *Science* **1997**, *278*, 1601 - 1604.
- 6 Groger, G.; Meyer-Zeika, W.; Bottcher, C.; Grohn, F.; Ruthard, C.; Schmuck, C. *J. Am. Chem. Soc.* **2011**, *133*, 8961 - 8971.
- 7 Ustinov, A.; Weissman, H.; Shirman, E.; Pinkas, I.; Zuo, X.; Rybtchinski, B. *J. Am. Chem. Soc.* **2011**, *133*, 16201 - 16211.
- 8 Tancini, F.; Dalcanale E. in *Supramolecular Polymer Chemistry*, Chapter 4 editor Arada, H., **2011**, Wiley-VCH.
- 9 Yabeutchou, R.M.; Tancini, F.; Demitri, N.; Geremia, S.; Mendichi, R.; Dalcanale, E. *Angew. Chem. Int. Ed.* **2008**, *47*, 4504 - 4508.
- 10 Menozzi, D.; Biavardi, E.; Massera, C.; Schmidtchen, F.-P., Cornia, A.; Dalcanale, E. *Supramol. Chem.* **2010**, *22*, 768-775.
- 11 Tancini, F., Yebeutchou, R. M., Pirondini, L., De Zorzi, R., Geremia, S., Scherman, O. A. and Dalcanale, E. *Chem. Eur. J.* **2010**, *48*, 14313 - 14321.
- 12 Harada, A.; Kobayashi, R.; Takashima, Y.; Hashidzume, A.; Yamaguchi, H. *Nature Chem.* **2011**, *3*, 34 - 37.
- 13 Park, T.; Zimmerman, S.C. *J. Am. Chem. Soc.* **2006**, *128*, 11582 - 11590.
- 14 Li, Y.; Park, T.; Quansah, J.K.; Zimmerman, S.C. *J. Am. Chem. Soc.* **2011**, *133*, 17118 - 17121.
- 15 For the nomenclature adopted for phopshonate cavitand see: Pinalli, R.; Suman, M., Dalcanale, E. *Eur. J. Org. Chem.* **2004**, 451 - 462.
- 16 B. Neises and W. Steglich *Angew. Chem, Int. Ed.*, **1978**, *17*, 522.
- 17 Dionisio, M.; Maffei, F.; Rampazzo, E.; Prodi, L.; Pucci, A.; Ruggeri, G.; Dalcanale E. *Chem. Commun.* **2011**, *47*, 6596 - 6598.

- 18 Aubon, M; Prud'homme, R.E. *Macromolecules* **1988**, *21*, 2945-2949.
- 19 a) Chuai, C., K. Almdal *J. App.Polym. Sci.* **2004** *91*, 609-620; b) Ton-That, C., A. G. Shard *Macromolecules* **2000**, *33*, 8453-8459; c) Chuai, C. Z., K. Almdal, *Polymer* **2002**, *44*, 481-493.
- 20 a) Chen, C.; Wang, J., Woodcock, S. E.; Chen, Z. *Langmuir* **2002**, *18*, 1302-1309. (b) Affrossman, S.; Jerome, R.; O'Neil, S. A.; Schmitt, T.; Stamm, M. *Colloid Polym. Sci.* **2000**, *278*, 993-999.
- 21 *Polymer Chemistry*, 6th Edt. Seymour, C. Marcel Dekker, **2005**.
- 22 *An introduction to polymer physics*, Bower, D.I., Cambridge University Press, **2002**.
- 23 a) Jiang, G.; Wu, H.; Guo, S. *Polym. Eng. Sci.*, **2010**, *50*, 2273 - 2286; b) Park, Y.; Veytsman, B.; Coleman, M.; Painter, P. *Macromolecules*, **2005**, *38*, 3703 - 3707.
- 24 Biavardi, E.; Todisco, C.; Maffei, F.; Motta, A.; Massera, C.; Condorelli, G.G.; Dalcanale, E. *Proc. Natl. Acad. Sci., U.S.A.* **2012**, *in press*.
- 25 *Handbook of polymer synthesis*, Kricheldorf, H.R.; Nuyken, O.; Swift, G. *Marcel Dekker*, 2005.

Appendix A

Materials and Methods.

A.1 Materials

All reagents and chemicals were obtained from commercial sources and used without further purification. Dry pyridine was distilled from KOH before use or purchased from Aldrich and used as received (Pyridine absolute, over molecular sieves, $H_2O \leq 0.005\%$). CH_2Cl_2 was dried by distillation over CaH_2 according standard procedures. Dry DMF (DMF purissim. $\geq 99.5\%$ (GC), over molecular sieves) was provided by Aldrich and used as received; dry diethyl ether (Diethyl ether purum $\geq 99.8\%$ (GC), over molecular sieves) was purchased from Fluka and used as received.

Silica column chromatography was performed using silica gel 60 (Fluka 230-400 mesh ASTM), or silica gel 60 (MERCK 70-230 mesh).

A.2 Methods

- **NMR Measurement**

1H NMR spectra were obtained using a Bruker AVANCE-300 (300 MHz) or a Bruker AVANCE 400 (400 MHz) spectrometer. All chemical shifts (δ) were reported in ppm relative to the proton resonances resulting from incomplete deuteration of the NMR solvents. ^{31}P NMR spectra were obtained using a Bruker AVANCE-400 (162 MHz) spectrometer. All chemical shifts (δ) were recorded in ppm relative to external 85% H_3PO_4 at 0.00 ppm.

(Ch. 4): ^{31}P MAS NMR. NMR experiments were conducted on a home-built 360 ($B_0 = 8.4T$) spectrometer (courtesy of Dr. David Ruben) with a

4 mm triple-channel chemagnetics MAS probe. Samples were ground using a mortar and pestle, and placed within ZrO₂ rotors (60 μ l volume). Spectral acquisition included Bloch and Hahn-echo experiments, using between 128 and 4096 co-added transients, spinning frequency (ω_r) between 0 and 12 kHz and high power ¹H decoupling (ν_{rf} = 83 kHz) when required. Recycle delays were optimized for each sample and were typically 35 seconds. All ³¹P data were referenced using 85% H₃PO₄ (0.0 ppm).

- **MS Studies**

Electrospray ionization ESI-MS experiments were performed on a Waters ZMD spectrometer equipped with an electrospray interface. Exact masses were determined using a LTQ ORBITRAP XL Thermo spectrometer equipped with an electrospray interface.

- **Fluorescence Measurements**

Fluorescence spectra in solution were obtained with a modular UV/Vis visible NIR spectrofluorimeter, Edinburgh, equipped with a 450 W Xe lamp. All solvent employed are CHROMASOLV[®], for HPLC grade.

- **Atomic Force Microscopy**

Atomic force microscopy was carried out using a Thermomicroscope Autoprobe CP Research. All measurements were performed in contact mode with a tapping silicon probe (MPP-12100-10). In order to preserve the initial structure, the films were not annealed. All samples were cooled down at 15°C using a Peltier cell. The collected images were flattened using Image Processing (IP) 2.1NAME.

- **DSC Measurements**

DSC thermograms were recorded by using a Mettler Toledo Stare System, model DSC 822e differential scanning calorimeter equipped with a Stare software.

- **IR Measurements**

FT-IR spectra were recorded on a Perkin Elmer FT-IR Spectrum One Spectrometer on films obtained by solution casting onto KBr windows of polymers diluted CHCl_3 solution.

- **GPC Measurements**

GPC System apparatus equipped with Jasco PU-2089 Plus pump, Jasco RI 2031 Plus as Refractive Index Detector, Jasco CO_2063 Plus column oven (set at 30 °C) and 2 polymer laboratories PLgel MIXED D columns and PL gel guard column poly(styrene-co-divinylbenzene) (linear range 100 - 600000 Da), was used for determination of Molecular Weight of chloroform diluted solutions of samples (eluted at 1 ml/min). The calibration curve was made with polystyrene standards and calculations were carried out with software Borwin 1.21.61 (JMBS DEVELOPMENT).

- **Light Scattering Measurements**

(Ch. 2): Nanoparticles (NPs) hydrodynamic diameter distributions were obtained through Dynamic Light Scattering (DLS) measurements employing a Malvern Nano ZS instruments with a 633 nm laser diode. Samples were housed in semi-micro (1400 μL volume) quartz cell of 1 cm optical path length, using chloroform as solvent (CHROMASOLV® Plus for HPLC, $\geq 99.9\%$, amylene stabilized). All DLS measurements were carried out on 400 μL solutions. NPs suspensions were prepared through sonication in chloroform at room temperature (10 min). solvent and suspensions used were thoroughly filtered (PTFE membrane syringe filter, 0.20 μm) before DLS measurements.

The width of DLS hydrodynamic diameter distribution is indicated by PDI (polydispersion Index). In case of a mono-modal distribution (Gaussian) calculated by means of cumulant analysis, $PDI = (\sigma/Z_{avg})^2$, where σ is the width distribution and Z_{avg} is average diameter of the particles population respectively.

(Ch. 3): The dynamic light scattering (DLS) measurements were carried out using a Malvern PCS 100 spectrometer, equipped with an Ar⁺ laser (Coherent Innova 70 C) operating at the wavelength $\lambda=647$ nm which is well outside the gold nanoparticles absorption band (peak at $\lambda = 522$ nm). The sample cell, a glass round cuvette of 10 mm diameter, is immersed in a index matching bath, where the temperature is controlled through an external thermal bath with an accuracy of 0.1 °C. The spectrometer includes a photomultiplier tube, operating in photon counting mode, mounted on a rotating arm provided by a goniometer spanning in an angles range of 10-150°. A computer equipped with an acquisition board (NI PCI-6602E) has been employed for the acquisition of the photon pulses and for computation of the signal autocorrelation function on a logarithmic scale spanning on 6 decades of time (10⁻⁵-10 sec). The photons arrival times have been continuously acquired and stored during the experiments with 100 ns resolution. The DLS autocorrelation functions have been calculated from the data acquired at different time intervals to characterize the processes kinetics.

Curriculum Vitae



- 08/1983 Born, Trani (Ba), Italy
- 07/2002 *High School Diploma*: Istituto Tecnico Industriale “V. Volterra”, Ancona, Italy
- 10/2005 *Bachelor in Industrial Chemistry*, University of Bologna, Italy. Referent Prof. P. Righi
- 07/2007 *Master in Industrial Chemistry*, University of Bologna, Italy. Referent Prof. V. Zanotti
- 09/2007-12/2007 *Post-graduate Research*, University of Zaragoza, Spain, Advisor Prof. M.A. Esteruelas
- 01/2008-12/2008 *Post-graduate Research*, University of Bologna, Italy, Advisor Prof. M.A. Cassani
- 01/2009-12/2011 *Doctoral Research* with Prof. E. Dalcanale. University of Parma, Italy
- 01/2001-07/2011 *Research Exchange* with Prof. T.M. Swager, MIT, Boston, USA.